High-speed Optical Transmission System Using Coherent Optical Orthogonal Frequency-Division Multiplexing

by

Yan Tang

Submitted in total fulfilment of

the requirements of the degree of

Doctor of Philosophy

Department of Electrical and Electronic Engineering

The University of Melbourne

Australia

June 2010

Printed on archival quality paper.

Abstract

High-speed Optical Transmission System Using Coherent Optical Orthogonal Frequency-Division Multiplexing

by **Yan Tang**

Recently, Coherent Optical Orthogonal Frequency-division Multiplexing (CO-OFDM) has been considered as a promising technology for high-speed optical transmission due to its easiness of dispersion compensation, high optical spectral efficiency and superior scalability over the channel dispersion and data rate. In this thesis, we conduct analysis on the transceiver nonlinearity impact on a coherent optical Orthogonal Frequency-division Multiplexing (OFDM) system and the feasibility of transmitting up to 1 Tb/s per channel data rate over CO-OFDM WDM systems.

We investigate the optimum design for a CO-OFDM transmitter using an optical In-phase/Quadrature (I/Q) modulator and show by simulation that in contrast to the direct-detected system, the optimal modulator bias point for the coherent system is π, or the null point of the modulator. We also propose and demonstrate through simulation a transmitter side digital signal processing technique including digital clipping and digital pre-distortion to compensate the nonlinearity induced by the OFDM peak-to-average power ratio effect and Mach–Zehnder modulator (MZM). Furthermore, we conduct analysis on the study of nonlinearity and dynamic range for a CO-OFDM receiver induced by the imbalance between the two ports of a balanced receiver. The input power dynamic range and tolerance to the relative-intensity-noise (RIN) are analyzed for the coherent balanced-receiver.

We then explore the transmission performance for high speed wavelength-division multiplexing (WDM) CO-OFDM systems with up to 1Tb/s per channel data rate under the impact of fiber nonlinearity. We find that the optimum fiber launch power increases almost linearly with the increase of data rate. A 7 dB optimum launch power difference is observed between 107-Gb/s and 1.07-Tb/s CO-OFDM systems. We also investigate the

dispersion compensation fiber impact and filter concatenation effect issues when upgrading the 10-Gb/s to the future 100-Gb/s CO-OFDM systems. We identify three contributions to the Q degradation for the inline dispersion compensated WDM systems. We show that due to the high spectral efficiency, 100-Gb/s CO-OFDM signals have very high tolerance to the filter narrowing effect, and are resilient to the group ripples from the filter concatenation effect.

This is to certify that

(i) the thesis comprises only my original work,

(ii) due acknowledgement has been made in the text to all other material used,

(iii) the thesis is less than 100,000 words in length, exclusive of table, maps, bibliographies, appendices and footnotes.

Signature_____

Date_____

Declaration

I hereby declare that this thesis comprises only my original work. No material in this thesis has been previously published and written by another person, except where due reference is made in the text of the thesis. I further declare that this thesis contains no material which has been submitted for a degree or diploma or other qualifications at any other university. Finally, I declare that the thesis is less than 100,000 words in length, exclusive of tables, figures, bibliographies, appendices and footnotes.

Acknowledgments

The work described in this thesis was conducted with the kind help and support of many people to whom I would like to express my thanks.

Firstly, I would like to express my deepest gratitude to my supervisor Associate Professor William Shieh, and co-supervisor Professor Rob Evens, for the high quality of their academic advice and direction, and for their generous help and constant support throughout my Ph.D study. I would also like to acknowledge Dr. Fred Buchali at Alcatel-Lucent Research and Innovation in Germany, for giving me the opportunity to undertake an internship.

I feel grateful to the Victoria Research Laboratory, National ICT Australia, for providing my PhD scholarship, conference trips and internship travel expenses. I also appreciate the support I have received from the University of Melbourne through MIFRS scholarship. Many thanks go to my colleagues around me for providing a friendly and entertaining working environment.

My special thanks to my research partners within Associate Professor William Shieh's research group. We had many productive and insightful discussions. I am grateful to Associate Professor Xingwen Yi for guidance in different aspects of the experimental studies. I appreciate the collaboration opportunities with Mr. Yiran Ma and Mr. Qi Yang on several projects.

On a personal level, I am forever indebted to my parents for the support they provided me through my entire life. Their love, encouragement and support make my life beautiful.

Contents

List of Figures

List of Tables

Chapter 1

Introduction

1.1 Overview

The use of optical fibers for information transmission has become widespread during the decade of 1980s. The earliest commercial systems operated near 0.8 μm, at a bit rate of 45 Mb/s and allowed repeater spacing up to 10 kilometers (km) [1]. With the introduction of single mode fiber (SMF), the operation wavelength region was shifted to 1.3μm by the end of the 1980s. During the 1990s, the invention of broadband optical amplifiers around 1.5 μm and wavelength division multiplexing (WDM) led to rapid advances in optical fiber transmission systems. Nowadays, 40-Gb/s WDM networks are being deployed and systems operating at 100-Gb/s or beyond have been experimentally demonstrated in research labs and actively developed by all the major equipment vendors [2-3].

Based on the number of carriers used in each wavelength, optical fiber communication systems can be generally grouped into two categories, signal-carrier and multi-carrier optical systems. For single-carrier systems, the data is carried with a single main carrier. This has been the dominant optical communication system for over three decades. Nowadays, with the advent of new internet applications such as Youtube and Internet Protocol (IP) TV, the internet traffic is projected to maintain the phenomenal growth and will not de-accelerate in the long seeable future [4]. To cope with the tremendous growth of internet traffic and new services, the optical system that was dominated by a low-speed, point-to-point transmission a decade ago needs to be upgraded to support massive WDM and multi-point-to-multi-point reconfigurable networking capabilities with a transmission speed approaching 100 Gb/s. With the increase of network data rate and transparency, the optical signal is extremely sensitive to the chromatic dispersion (CD), polarization mode dispersion (PMD), reconfigurable optical add-drop multiplexer (ROADM) filtering effects, and imperfections of the electric-optics components. These place significant challenges on the conventional single-carrier system.

The multi-carrier optical system is proposed in response to the above-mentioned modern optical system. Multi-carrier systems use the multi-carrier modulation (MCM) scheme by which the transmitted data stream is divided into several parallel lower bit rate sub-carriers [5]. Orthogonal Frequency-Division Multiplexing (OFDM) is a special form of MCM in the sense that the sub-carriers are partially overlapped in the frequency domain but yet orthogonal to each other incurring no inter-carrier-interference.

1.1.2 Coherent Optical Orthogonal Frequency-Division Multiplexing

OFDM has been emerged as the leading physical-layer interface in wireless communications in the last decade. It has been widely studied in mobile communications to combat the hostile frequency-selective fading and has been incorporated into wireless network standards (802.11a/g WiFi, HiperLAN2, 802.16 WiMAX) and digital audio and video broadcastings (DAB and DVB-T) in Europe, Asia, Australia, and other parts of the world. Coherent Optical Orthogonal Frequency-Division Multiplexing (CO-OFDM) [6] combines the advantages of 'coherent detection' and 'OFDM modulation' and posses many merits that are critical for future high-speed fiber transmission systems.

i) The CD and PMD of the transmission system can be effectively estimated and mitigated.
ii) The spectra of OFDM subcarriers are partially overlapped, resulting in high optical spectral efficiency.
iii) By using the direct up/down conversion, the electrical bandwidth requirement can be greatly reduced for the CO-OFDM transceiver, which is extremely attractive for the high-speed circuit design, where electrical signal bandwidth dictates the cost.
iv) The signal processing in the OFDM transceiver can take advantage of the efficient algorithm of Fast Fourier Transform (FFT)/Inverse Fast Fourier Transform (IFFT), which suggests that the OFDM has superior scalability over the channel dispersion and data rate.

Due to the superior advantages offered by CO-OFDM, it has been considered to be a promising technology for the high speed optical transport system.

1.2 Thesis Motivation

As prominent as its advantages, OFDM has many disadvantages. One of the major problems associated with OFDM is its large peak-to-average power ratio (PAPR) [7-9]. It has been shown that the OFDM signal may exhibit high instantaneous amplitude peak with respect to the average amplitude level, thus results in high PAPR. The high PAPR of OFDM makes the system performance very sensitive to the nonlinear devices introduced distortion. In the radio frequency (RF) OFDM system, the main problem induced by high PAPR resides on the power amplifiers (PAs) at the transmitter end where the output power gain will saturate at the high input power. Thus, in order to mitigate nonlinear distortion, linear PAs with a wide power dynamic range are required. Therefore, large PAPR cause severe power penalty at the transmitter. Such problem does not exist in the optical systems, since the optical power amplifier (predominately an Erbium-doped-amplifier today) is ideally linear as long as the nonlinearity is faster than microseconds.

However, in order to make a successful transmission of OFDM signal, other system devices such as transmitter or receiver must be linear over a wide range of signal levels. Therefore, it is important to investigate the linear performance of optical modulator and receiver in the CO-OFDM system. Furthermore, optical fiber is a well-known nonlinear device [10]. It can be expected that large PAPR will enhance the fiber nonlinearity and finally degrade the system performance.

In Chapter 4 and Chapter 5 of this thesis, we will focus on the analysis of CO-OFDM transceiver nonlinearity impact and the optimum design scheme. In chapter 6, we will concentrate on the transmission performance for the high speed CO-OFDM WDM system up to 1-Tb/s line data rate including the impact of the fiber nonlinearity and the network impairment induced by the dispersion compensation fiber and ROADM filter concatenation effect.

1.2.1 CO-OFDM Transceiver Nonlinearity Impact

For the CO-OFDM transmitter, Mach–Zehnder modulator (MZM) is used for the

Electro-Optic (E/O) conversion. It has been shown that the MZM has a *sine* shape transfer function which results in two issues: (i) With a high PAPR, the OFDM signal is severely distorted by MZM especially at high modulation index, which increases the system penalty. (ii) To operate the MZM in the linear region, a small modulation index of the input RF signal is required, thus causing large excess modulation insertion loss. The nonlinearity of MZM on the system performance in the direct-detected systems has been extensively studied in [11-12].

Optical coherent detection is adopted for the CO-OFDM receiver. In a coherent receiver, the received optical signal is mixed coherently with a local oscillator (LO) before feeding into the photodetector. With coherent receivers, the complex optical signal (including amplitude and phase) can be linearly down-converted to a base-band electrical signal with homodyne or heterodyne detection. Compared with the direct-detection optical OFDM (DDO-OFDM) [13], The CO-OFDM receiver comprises two pairs of balanced receivers and is more costly and complex than the DDO-OFDM [13-15]. It is desirable to reduce the cost and complexity of the CO-OFDM receiver using balanced receivers that are tolerant of imbalance, or using simpler single-ended receivers. Furthermore, as the linear transformation in modulation, transmission, and demodulation is the most critical assumption for the CO-OFDM system. The receiver imperfections such as the imbalance between the two ports of a balanced receiver will increase the system nonlinearity especially under the impact of high PAPR.

Therefore, we are interested in the following questions related to the CO-OFDM transceiver nonlinearity:

- How can we characterize the nonlinearity performance of the CO-OFDM optical transceiver?
- How much impact caused by the transceiver nonlinearity will be introduced into the system?
- Is there any method to compensate the transceiver induced nonlinearity impact?

1.2.2 High-speed CO-OFDM Transmission

As we mentioned earlier, CO-OFDM has emerged as an attractive modulation format to

realize the high speed optical transparent network and has been considered as the upgrade solution from today's 10-Gb/s to the future 100-Gb/s systems.

However, optical fiber is a well known nonlinear medium that limits the practical power launched for a given received signal quality or bit error ratio (BER). When a light wave transverses through the optical fiber, the light intensity can reach or exceed a mega-watt/cm^2. At such high intensity, the fiber's refraction index is affected by the presence of optical signals through the optical Kerr effect and refractive index changes lead to the change of the signal's optical phase which finally results in the waveform distortion that increases with signal power. Fiber nonlinearity is always considered as a limiting factor for high speed optical transmission systems. Furthermore, it can be expected that large PAPR will enhance the fiber nonlinearity and degrade the overall system performance. Thus it is very important to evaluate the feasibility of transmitting high speed CO-OFDM signal under the impact of fiber nonlinearity.

Besides, there is huge interest to reuse the existing infrastructure for the high-speed upgrade. There is two problems need to be investigated.

i) For optical OFDM, no optical dispersion compensation is need as the dispersion can be compensated for in the electrical domain. However, a periodic inline dispersion compensation fiber (DCF) is widely used in the existing 10-Gb/s transmission systems and when a 40-Gb/s or 100-Gb/s OFDM channel would be used to upgrade such a link, a periodic dispersion map is inevitable for the OFDM signal. DCF obviously increases the amplified spontaneous emission (ASE) noise due to the adoption of double-stage amplifiers. DCF also introduces additional nonlinearity degradation due to its large nonlinear coefficient. What is more intriguing is the dispersion map impact on the nonlinearity performance [16] for CO-OFDM systems [17].

ii) For the current optical fiber communication system, dense wavelength division multiplexed (DWDM) transmission with 10-Gb/s wavelength channels at 50-GHz channel spacing is an International Telecommunication Union (ITU) standard for long-haul and metropolitan networks. As 100-Gb/s technology has become increasingly a commercial reality, it is desirable to design current

10-Gb/s based DWDM systems ready for the future 100-Gb/s upgrade. One of the main limitations for the transparent networks with large number of nodes is the signal degradation due to transmission through multiple ROADMs. Therefore, it is critical to study the feasibility of transmitting 100-Gb/s CO-OFDM signals over present transparent DWDM systems with the impact of the cascaded ROADMs.

Consequently, for the high speed WDM CO-OFDM system, the following questions need to be answered.

- What is the CO-OFDM transmission performance at a data rate up to 1Tb/s including the impact of fiber nonlinearity? Is it feasible to transmit high speed data over CO-OFDM systems?
- How to implement high speed CO-OFDM transmitter/receiver under the impact of Digital-to-Analog Converter (DACs)/ Analog-to-Digital Converter (ADC) electrical bandwidth bottleneck?
- What is the DCF and ROADM impact on high speed CO-OFDM system?

1.3 Thesis Outline

The remainder of this thesis is laid out as follows:

Chapter 1: Overview of the coherent optical OFDM system and introduction of the thesis.

Chapter 2: Literature Review This chapter reviews the relevant literature on high-speed optical transmission technologies and electronic dispersion compensation techniques including the optical OFDM scheme.

Chapter 3: Theoretical Fundamentals for CO-OFDM Systems In this chapter, the OFDM fundamentals including its basic mathematical formulation, discrete Fourier transform implementation and cyclic prefix are first presented. The coherent optical OFDM technique including the system architecture, optical spectral efficiency, coherent

optical MIMO-OFDM models and signal processing will also be discussed.

Chapter 4: Optimum Design for CO-OFDM Transmitter This chapter conduct analysis on the optimum design for a coherent optical OFDM up-converter using an optical In-phase/Quadrature (I/Q) modulator. The closed-form expressions for the nonlinearity in the optical I/Q modulator is derived. Additionally, a numerical simulation is conducted to identify the Q penalty and excess modulation insertion loss under various transmitter conditions. Digital predistortion is then introduced to the transmitter to compensate the I/Q modulator nonlinearity. The transmitter optimum design is presented in terms of clipping ratio, I/Q modulator excess insertion loss, and DAC resolution.

Chapter 5: Study of Nonlinearity and Dynamic Range of Coherent Optical OFDM Receivers This chapter conducts analysis on the study of nonlinearity and dynamic range for a coherent optical OFDM receiver induced by the imbalance between the two ports of a balanced receiver. The theory for the I/Q coherent detection including the OFDM signal, nonlinearity, and noise is first formulated. Additionally, a numerical simulation is employed to identify Q penalty and signal power dynamic range for the CO-OFDM system with both balanced and single-ended receiver under the impact of imbalance.

Chapter 6: Coherent Optical OFDM Transmission up to 1 Tb/s Per Channel Data Rate This chapter investigates the feasibility of CO-OFDM transmission up to 1-Tb/s line data rate. Then the CO-OFDM performances on the upgrade of 10-Gb/s base system to 100-Gb/s CO-OFDM system under the dispersion map nonlinearity influence and ROADM concatenation impact are discussed. A comparison of CO-OFDM system performance under different data rate of 10.7 Gb/s, 42.8 Gb/s, 107 Gb/s and 1.07 Tb/s is also presented. Orthogonal-Band-Multiplexed OFDM is proposed to solve the electrical bandwidth bottleneck of ADC/DAC when implementing the high speed (100 + Gb/s) CO-OFDM system.

Chapter 7: Conclusions summarize the main results of this thesis.

1.4 Contributions of the Thesis

The contributions of the thesis are listed as follows.

Chapter 4

- We propose two CO-OFDM system architectures, the direct up/down conversion architecture and intermediate frequency architecture.
- We derive closed-form expressions for the nonlinearity in the optical I/Q modulator, represented by two-tone intermodulation products as a function of the bias point and modulation index and perform a numerical simulation to identify the Q penalty and the excess modulation insertion loss under various transmitter conditions.
- We find that in contrast to the direct-detected system, the optimal modulator bias point for the coherent optical OFDM system is null-point where the Q penalty and excess loss are minimized.

For the first time, we introduce the digital clipping and digital pre-distortion processes to the RF OFDM transmitter to compensate the nonlinearity effect introduced by the optical I/Q modulator.

- We find that for 4-Quadrature Amplitude Modulation (QAM) a 4-bit DAC resolution is sufficient for the CO-OFDM transmitter to incur only 0.3 dB Q penalty while maintaining the excess modulation insertion loss less than 6.0 dB.

Chapter 5

- We formulate the theory for the I/Q coherent detection including the OFDM signal, nonlinearity, and noise.
- We perform a numerical simulation to identify the Q penalty and signal power dynamic range for the CO-OFDM system with both balanced and single-ended receiver under the impact of imbalance.

- We find that the 0.5-dB Q penalty dynamic range for the double-ended receiver (single-ended receiver) is 26 dB (12dB) with -160 dBc/Hz laser relative-intensity-noise (RIN) and 4dBm LO power.

Chapter 6

- Transmission performances for 100-Gb/s WDM systems with CO-OFDM are simulated. The simulation shows that the system Q of the WDM channels at 100 Gb/s is over 15.0 dB for a transmission up to 1000 km of SSMF without dispersion compensation.

- We conduct the simulation analysis and experimental demonstration on the dispersion map nonlinearity influence on 107-Gb/s CO-OFDM systems.

- Through numerical simulation, we assess the performance of 107-Gb/s per channel CO-OFDM signal over transparent DWDM systems with 50-GHz channel spacing under the filter concatenation impact.

- A numerical simulation is carried out to investigate the feasibility of 1 Tb/s per channel CO-OFDM transmission.

We find that the optimum fiber launch power increases almost linearly with the increase of data rate. 7 dB optimum launch power difference is observed between 107-Gb/s and 1.07-Tb/s CO-OFDM systems.

1.5 Publications

Journal Papers

1. Y. Ma, Q. Yang, Y. Tang, S. Chen and W. Shieh, "1-Tb/s Single-Channel Coherent Optical OFDM Transmission With Orthogonal-Band Multiplexing and Subwavelength Bandwidth Access," *J. Lightwave Technol.*, vol.28, pp.308-315, 2010

2. Y. Tang and W. Shieh, "Coherent Optical OFDM Transmission up to 1-Tb/s per Channel," *J. Lightwave Technol.*, vol.27, pp.3511-3517, 2009.

3. Y. Ma, Y. Tang and W. Shieh, "107 Gbit/s transmission over multimode fibre with coherent optical OFDM using centre launching technique," *Electronics Letters* , vol.45, no.16, pp.848-849, July 30 2009

4. Y. Tang, Y. Ma and W Shieh, "Performance Impact of Inline Chromatic Dispersion Compensation for 107-Gb/s Coherent Optical OFDM," *Photonics Technology Letters, IEEE* , vol.21, no.15, pp.1042-1044, Aug.1, 2009.

5. Q. Yang, Y. Tang, Y. Ma and W. Shieh, "Experimental Demonstration and Numerical Simulation of 107-Gb/s High Spectral Efficiency Coherent Optical OFDM," *J. Lightwave Technology* , vol.27, no.3, pp.168-176, Feb.1, 2009.

6. Y. Tang, K.O Ho and W. Shieh., "Coherent Optical OFDM Transmitter Design Employing Predistortion," *Photonics Technology Letters, IEEE* , vol.20, no.11, pp.954-956, June1, 2008

7. Y. Tang and W. Shieh, "Transmission of 100 Gbit / s WDM Systems with Coherent Optical OFDM," *Electronics Letters* , vol. 44, pp. 588-589, 2008.

8. W. Shieh, H. Bao, and Y. Tang, "Coherent optical OFDM: theory and design," *Opt. Express*, vol. 16, 841-859 (2008)

9. Y. Tang; W. Shieh,; X. Yi; R Evans., "Optimum Design for RF-to-Optical Up-Converter in Coherent Optical OFDM Systems," *Photonics Technology Letters, IEEE* , vol.19, no.7, pp.483-485, April1, 2007

10. W. Shieh, X. Yi, Y. Ma, and Y. Tang, "Theoretical and Experimental Study on PMD-supported Transmission using Polarization Diversity in Coherent Optical OFDM Systems, " *Opt. Express*, vol. 15, Issue 16, pp. 9936-9947, 2007

11. W. Shieh, X. Yi, Y. Tang, "Transmission experiment of multi-gigabit coherent

optical OFDM systems over 1000km SSMF fibre," *Electronics Letters* , vol.43, no.3, pp.183-184, Feb. 1 2007

12. X. Yi, Shieh, W. Shieh, Y. Tang, "Phase Estimation for Coherent Optical OFDM," *Photonics Technology Letters, IEEE* , vol.19, no.12, pp.919-921, June15, 2007.

Conference Papers

13. Y. Ma, Y. Tang and W. Shieh, "107 Gb/s Transmission over Multimode Fiber with Coherent Optical OFDM Using Center launching Technique, " accepted for oral presentation at the 35th *Europ. Conf. Optical Commun. (ECOC 2009)*.

14. Y. Ma, Q. Yang, Y. Tang, S. Chen and W. Shieh, "1 - Tb/s per Channel Coherent Optical OFDM Transmission with Subwavelength Bandwidth Access, " *Conf. Optical Fiber Communication (OFC)*, paper PDP C1, San Diego, USA (2009).

15. Y.Tang and W. Shieh, "Filter Concatenation Impact on 107-Gb/s Coherent Optical OFDM System," *Optoelectronics and Communications Conference (OECC)*, Hong Kong, 2009.

16. Y. Ma, Y. Tang and W. Shieh, "107 Gb/s Transmission over Multimode Fiber with Coherent Optical OFDM Using Center launching Technique," 35th *Europ. Conf. Optical Commun.* (ECOC 2009), Vienna, Austria, 2009.

17 Y. Tang, Y. Ma, and W. Shieh, "107 Gb/s CO-OFDM Transmission with Inline Chromatic Dispersion Compensation," *Conf. Optical Fiber Communication (OFC)*, San Diego, California, USA, 2009.

18. Y. Tang, C. Wei, and W. Shieh, "Study of Nonlinearity and Dynamic Range of Coherent Optical OFDM Receivers," *Conf. Optical Fiber Communication (OFC)*, San Diego, California, USA, 2008, pp. 1-3.

19. B. S. Krongold, Y. Tang, and W. Shieh, "Fiber Nonlinearity Mitigation by PAPR Reduction in Coherent Optical OFDM Systems via Active Constellation Extension,"

34th *Europ. Conf. Optical Commun.* (ECOC), 2008, pp. 1-2.

20. Y. Tang, X. Yi, W. Shieh, and R. Evans, "Optimum Design for Coherent Optical OFDM Transmitter," *Conf. Optical Fiber Communication (OFC)*, Anaheim, California, USA, 2007, pp. 1-3.

21. W. Shieh, X. Yi, and Y. Tang, "Experimental Demonstration of Transmission of Coherent Optical OFDM Systems," *Conf. Optical Fiber Communication (OFC)*, Anaheim, California, USA, 2007, pp. 1-3.

22. Y. Tang, K.-P. Ho, and W. Shieh, "Optimal Design for Coherent Optical OFDM Transmitter Employing Pre-distortion," 33th *Europ. Conf. Optical Commun. (ECOC)*, 2007, pp. 1-2.

23. X. Yi, W.Shieh, and Y. Tang, “Phase Estimation for Coherent Optical OFDM Transmission,” in *Joint Conference on Optical Internet and Australian Conference on Optical Fiber Technology (COIN−ACOFT)*, June, 2007, paper TuA1-4.

Chapter 2

Literature Review

2.1 Introduction

Due to the growth of internet traffic together with an increase in the number and range of new services, the transmission data rate per channel has been fast increasing and rapidly approaching 100 Gb/s. New emerging applications such as internet video-to-TV and video communications will further triple the bandwidth demand in the year of 2011, requiring IP link capacity scalable to 1 Tb/s [18]. Therefore, finding a way to realize high capacity transmission is the target of many studies. WDM technology is a very common approach to increase the per fiber capacity which uses several wavelengths per fiber to transmit data simultaneously. For example, a 20-Tb/s transmission capacity is realized in 2007 using 204 wavelength channels. Besides, Optical Time Division Multiplexing (OTDM) is proposed to enable transmission of higher channel data rate [19]. OTDM is a time domain multiplexing technology which is realized by multiplexing a set of N tributary channels at a low bit rate on to a single multiplexed channel at a high bit rate of N times of that of individual tributary channels. Recently, OTDM transmission technology was successfully demonstrated in the transmission of a Time Division Multiplexing (TDM) data rate of 160 Gb/s over a record fiber length of 4320 km [20] and of a TDM data rate of 2.4 Tb/s over a fiber link length of 160 km [21]. In the meantime, coherent system for fiber-optic transmission is also considered as a promising technique to increase transmission speed. In coherent optical communications, as the information is encoded onto the electrical field of the light signal [22], the transmission of advanced modulation formats in which multiple bits per symbol transmission [23-25] can be realized.

With the increase of the network transmission speed, signal dispersion arises as one of the most important challenges. For high-speed optical communication systems, the signal becomes extremely sensitive to the chromatic and polarization-mode dispersion. The

conventional meticulous per-span optical dispersion compensation becomes too costly and time-consuming. Electronic Dispersion Compensation (EDC) techniques have emerged as a technology of great promise for high-speed networks. This is because: 1) It can be readily made adaptive to compensate for temporal variations in dispersion. Such self-adapt ability is useful for dynamic and remote network reconfiguration. 2) It eliminates optical dispersion compensators thus reduces total optical loss and amplification requirements.

Recently, optical OFDM has been proposed as a promising technology to realize high-speed channel transmissions. Optical OFDM is an optical equivalent of RF OFDM. Optical OFDM offer many advantages that are critical for future high-speed fiber transmission systems such as high optical spectral efficiency and scalability over the channel dispersion and data rate. Furthermore, the CD and PMD of the transmission system can be effectively estimated and mitigated. Since OFDM uses substantial electronic processing at the transmitter and receiver, it can be considered as an EDC technique.

This chapter undertakes the literature review on the topics of (i) techniques for high-speed transmission systems, (ii) electronic dispersion compensation and (iii) optical OFDM. The organization of this chapter is laid out as follows. Section 2.2 reviews the various high-speed optical transmission technologies including WDM, OTDM and optical coherent detection. The existing EDC techniques for optical dispersion are presented in Section 2.3. Section 2.4 illustrates various optical OFDM techniques in terms of their architecture, design and performance.

2.2 High-speed Optical Transmission Technologies

2.2.1 WDM Transmission Systems

The concept of WDM has been proposed in 1970s, by which multiple optical channels can be simultaneously transmitted at different wavelengths through a single optical fiber to increase the transmission capacity. ITU standardizes WDM channel grid in either multiple or fraction of 100 GHz. Typical WDM systems would use 40 channels at 100

GHz spacing or 80 channels with 50 GHz spacing. The basic configuration for WDM transmission systems can be found in Figure 2.1, in which N WDM channels are multiplexed in a single fiber and amplified with the same Erbium Doped Fiber Amplifier (EDFA) chain. The EDFA have a very wide gain bandwidth (up to 35nm in C band alone) which is capable of amplify many channels at the same time. EDFA generally operated in the C-band from 1.53nm to 1.56nm, and can be extended to the L-band of 1600nm. A multiplexer (MUX) is used to combine all WDM channels at transmitter and a de-multiplexer (DEMUX) is used at the receiver to de-multiplex each channel. The WDM MUX can be implemented as a passive combiner with a loss of at least $10log_{10}N$ in decibel (dB) unit. Both intensity modulation/direct detection (IM/DD) channels and coherent modulated channels can be transmitted in the same WDM system. For the coherent systems, the LO laser selects the target WDM channel. Only the channel which has a central frequency close to the LO laser frequency gives a beating frequency within the bandwidth of the receiver.

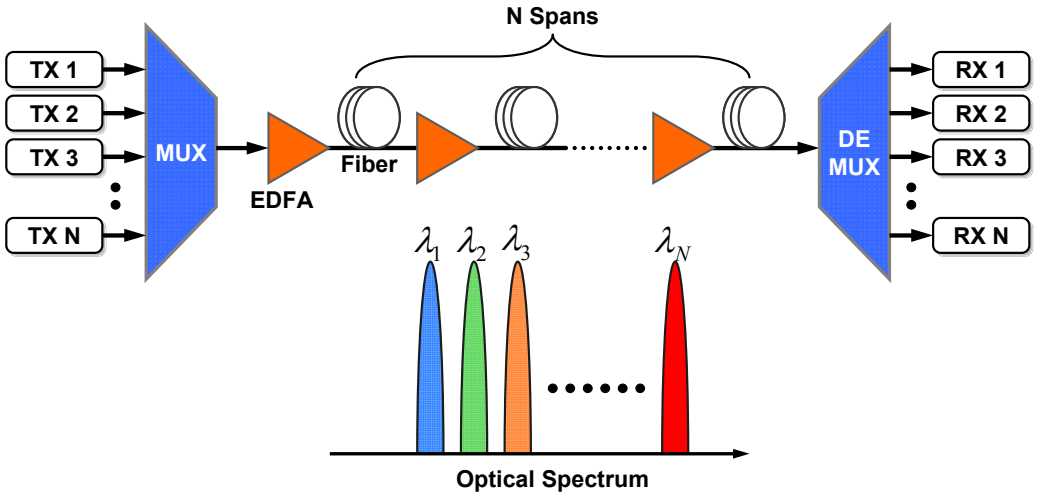

Figure 2.1 Configuration for WDM transmission.

WDM systems offer advantages of transmission capacity increase per fiber, system cost reduction, simultaneous transmission of different modulation-scheme signals, and service channel expandability after fiber installation. However, for WDM systems with large number of wavelength channels, wavelength management, power consumption and footprint probably limit the usefulness of increasing the number of WDM channels.

Besides, as WDM channels are usually transmitted on a fixed frequency grid, adding more and more low-speeds channels limits the overall transmission capacity due to the low spectral efficiency. Therefore, there is a great incentive to deliver high-capacity data pipe with minimum number of wavelengths, i.e., increasing the line rate per wavelength would expect to bring cost advantage.

2.2.2 OTDM Transmission systems

OTDM is realized by multiplexing a set of *N* tributary channels at low bit rate onto a single multiplexed channel at *N* times of the bit rate of the individual tributary channels. Figure 2.2 shows a schematic depiction of a 160-Gb/s OTDM transmission system [26]. The essential component at the transmitter side is an optical pulse source. The repetition frequency of a pulse train depends on the base data rate. The system shown in Figure 2.2 has a base data rate of 40 Gb/s, thus a 40-GHz optical pulse train is used. The pulse train is first coupled into four optical branches, in which modulators (MODs) are driven by 40-Gb/s electrical data signal generate 40 Gb/s optical return to zero (RZ) signal. The modulation format of OTDM system depends on the modulation format of the electrical data signal and the appropriate modulator. The modulation format can be on-off keying (OOK), differential phase shift keying (DPSK), and differential quadrature phase shift keying (DQPSK). The four optical OTDM tributary channels are bit-interleaved by a multiplexer to generate a multiplexed 160-Gb/s optical data signal. The multiplexed data signal can have the same polarization (SP) or the alternating polarization (AP). On the receiver side, optical DEMUX is used to separates the four tributary signals for subsequent detection and electrical signal processing. The transmission link of OTDM sustem requires compensation for CD and PMD.

For OTDM systems, the pulse source must provide a well-controlled repetition frequency and wavelength. For example, the pulse width should be significantly shorter than the bit period of the multiplexed data signal and the timing jitter should be much less than the pulse width [26]. The Lithium-Niobate (LiNbO3) modulators are the most commonly used modulators in the OTDM system due to their broad bandwidth and

wavelength independence in the 1.3–1.6 mm range. For OTDM systems, different data signals are combined with a delay which serves as a MUX. An OTDM receiver typically consists of three sub systems: the optical gate, the timing extraction device (clock recovery) for de-multiplexing, and the optoelectronic receiver at the tributary symbol rate.

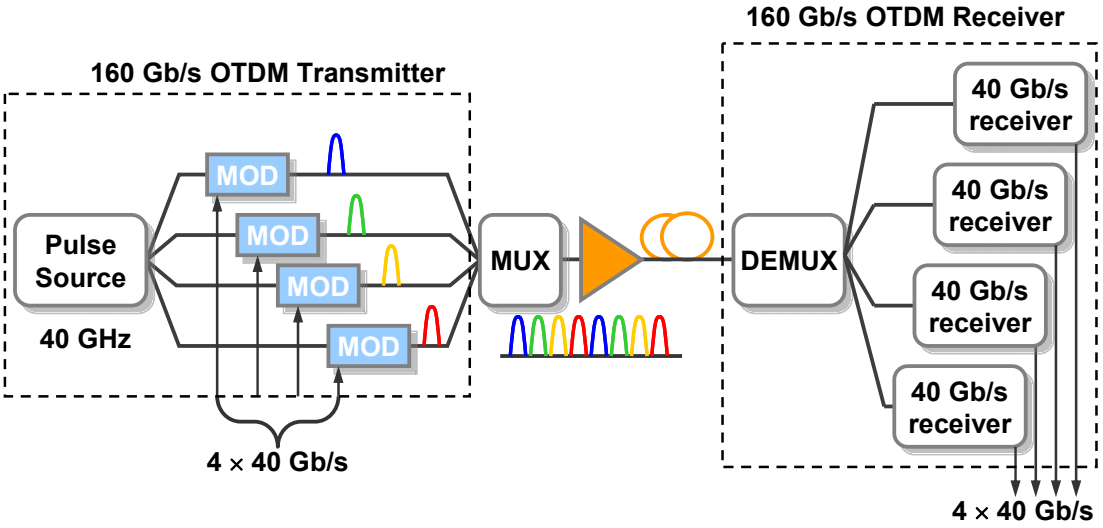

Figure 2.2 Schematic of a 160-Gb/s OTDM transmission system

2.2.3 Coherent Optical Systems

Most of commercial optical communication systems use IM/DD schemes in which the intensity of semiconductor lasers is modulated to carry the information and the optical signal is detected directly by a photodiode. In contrast to IM/DD scheme, a coherent optical communication system with the detection of the transmitted signal using homodyne or heterodyne detection schemes conveys information by modulating the intensity, phase and polarization of the optical carrier. Coherent optical communication systems were extensively studied in 1980s [27-29]. Compared with direct detection, coherent detection offers the advantages :

(i) improved receiver sensitivity. With a sufficient LO power, the shot-noise limited receiver sensitivity can be achieved using coherent detection for non-repeated systems, and ASE limited sensitivity for optical amplified systems.

(ii) improved spectral efficiency for high-capacity transmissions, which is particularly attractive for high speed transmission systems.

However, with the invention of EDFAs, direct detection systems could achieve the

receiver sensitivity within a few decibels of that of coherent receivers which made the shot-noise limited receiver sensitivity of the coherent receiver less significant. Besides, the technical difficulties of coherent detection also make it less attractive. The coherent detection also requires sophisticated management of the phase and polarization. Since the state of polarization (SOP) of the incoming optical signal is scrambled in the fiber, a dynamic polarization controller is needed to match the SOP of the signal and LO. The dynamic polarization controller is usually a bulky and expensive device [30]. The difficulty in carrier phase locking also prevents the practical application of the coherent detection. For these reasons, further research of coherent optical communications had been almost abandoned for nearly 20 years.

Coherent detections have emerged to attract a large interest over recent years, which are highlighted by the remarkable theoretical and experimental demonstrations from various groups around the world [31-36]. The drive behind using the coherent communication techniques nowadays is two-fold. First, current coherent detection systems are heavily entrenched in silicon-based digital signal processing (DSP). By taking the advantages of the high-speed DSP, both polarization and phase management can be easily realized, thus, a free running laser can be used as a local oscillator. Optical coherent detection in conjunction with high-speed DSP has the potential to increase the spectral efficiency and the ability to compensate linear transmission impairments such as CD and PMD in the electrical domain [37-39]. Second, in contrast to the optical network that was dominated by a low-speed, point-to-point, and single-channel system a decade ago, modern optical communication systems have advanced to massive WDM and reconfigurable optical networks with a transmission speed per channel approaching 100 Gbits/s. The primary aim of coherent communications has shifted toward supporting these high-speed dynamic networks by simplifying the network installation, monitoring, and maintenance.

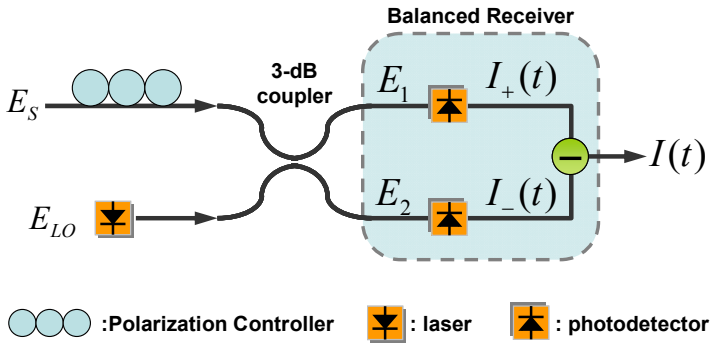

Figure 2.3 Configuration of a coherent receiver with a balanced detector

The basic idea behind coherent detection is to mix the received signal with another continuous (CW) light wave emitted from the LO before feeding into the photodetector. For coherent detection, a balanced receiver is generally used to suppress the common mode component such as to suppress the direct current component and minimize the laser RIN. Figure 2.3 shows the block diagram of a coherent receiver with a balanced detector. The optical signal and the LO are mixed with a 3-dB coupler that adds a 180^0 phase shift to either the signal or the LO field and split into two equal parts which are detected by two photodetectors.

Based on whether the LO frequency is set close to the signal frequency, coherent receiver can be divided into homodyne receiver and heterodyne receiver. The optical signal-to-noise-ratio (SNR) sensitivity of the homodyne receiver is the same as the heterodyne counterpart. Homodyne receiver requires optical hybrid to recover inphase (I) and quadrature (Q) components of the signal, and thus needs twice as much optical components. on the other hand, heterodyne needs an image rejection filter and twice as much photodetector bandwidth. Both homodyne receiver and heterodyne receiver need a polarization controller to align the SOPs of LO and signal, or preferably the polarization diversity detector which will be discussed below.

Without polarization controllers, because of the random changes resulted from the fiber birefringence, the polarization of the incoming signal is usually misaligned to the SOP of the LO. Thus, the receiver sensitivity of the coherent detection is highly dependent on the SOP of the incoming signal if no polarization controller is used. A coherent receiver with polarization diverse architecture can be employed to solve this

problem. The schematic of a phase and polarization diverse receiver is shown in Figure 2.4. The incoming signal with the arbitrary SOP is divided into two orthogonal linear polarization components by a polarization beam splitter (PBS) and fed into two homodyne I/Q receivers. A digital signal processing module performs the functionalities such as analog-to-digital conversion and polarization alignment. Therefore, coherent detection allows for the access of full information on the optical signal, i.e., signal amplitude, signal phase and signal SOP.

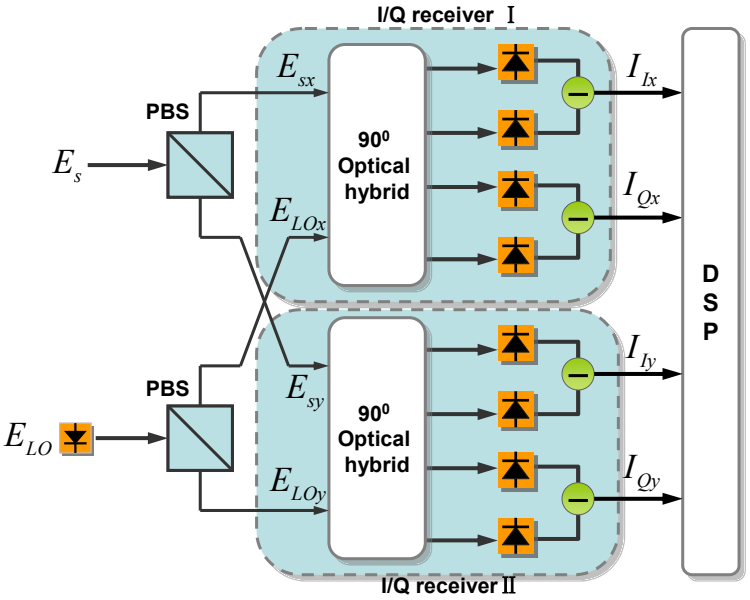

Figure 2.4 Configuration of a phase and polarization diversity receiver

2.3 Compensation of Optical Dispersion

EDC [40-42] is an alternative to optical dispersion compensation techniques such as DCF [42], Bragg gratings [43], and optical resonators [44]. The drive of EDC is twofold. First, the proposing of EDC is to meet the ever-increasing transmission bit rate per channel and transmission length in optical fiber networks. In the early days, the CD and PMD were not thought as limiting factor when the bit rate was at or below 2.5 Gb/s and the distance was about a few hundred kilometers. However, with the steady growth of bandwidth demand and the subsequent migration to 10-Gb/s and beyond transmission systems, dispersion has become quite problematic that needs to be overcome. Second, with the

rapid advancement of the semiconductor technology, DSP has emerged as a key technology to the development of low-cost, high-data rate optical communication systems.

The application of electronic signal processing to distortion equalization started in early 1990s [45]. At first, the application of DSP on the 10-Gb/s optical transmission system was actively studied. In DSP, the optical signal was first sampled by one ADC with a resolution of 3-4 bits. Then the digitized signal is processed with the Verterbi algorithm implemented in a complementary metal oxide semiconductor (CMOS) application specific integrated circuit (ASIC) [46-47]. However, the early demonstration showed limited performance in the range of dispersion that can be compensated. Besides, the polarization and phase information of the received signal could not be explored due to the single receiver photodiode. Around year 2004, DSPs based on the proposing of complex optical field started to be studied by a few groups [48]. These schemes depend on electronic pre-compensation and coherent or intradyne detection with electronic distortion compensation within the receiver [39,49-50]. In 2006, a new EDC scheme, optical OFDM was proposed [6, 13-14]. In the optical OFDM, DSP is used in both the transmitter and the receiver.

2.3.1 Optical Dispersion Compensation

Almost all the existing systems adopt optical approaches to compensate optical impairments. There are several approaches for optical dispersion compensation:

- ***Dispersion Compensation Fiber***

  The DCF is a special fiber designed to have opposite dispersion parameters to that of transmission fibers. DCF is capable of almost completely compensating the CD in transmission fibers in wide wavelength ranges. Up until now, DCF is the most mature technique in the presently deployed optical fiber networks. However, DCF suffers from high loss and high nonlinearity. Another important problem for DCF in WDM systems is the dispersion slop matching, or accurate CD compensation for multiple channels, especially for high-speed signal using conventional modulation formats.

- ***Fiber Grating for CD Compensation***

  A fiber Bragg grating is a versatile device where the grating can be designed to reflect different wavelengths at different points along its length, i.e., the linearly chirped Fiber Bragg grating (FBG) [51]. The chirped FBG introduces different delays at different wavelength and therefore compensates the CD. The CD parameter of the FBG can be tuned by changing the grating period, e.g., by the thermal change [52].

- ***Optical Equalizer***

  Optical equalizer is a discrete finite impulse response (FIR) filter which generates the inverse response of the channel response of CD [53-55]. The principle of optical equalizers is similar to that of electrical equalizers widely used in wireless communications [56].

- ***PMD compensator***

  The optical PMD compensation aims to perform the reverse of the PMD generation. The principle of PMD compensation is to split the received signal into its fast and slow polarization components, and to delay the fast component so that the Differential Group Delay (DGD) between two components can be compensated [52]. The challenge of PMD compensation is to track the fast variation of DGD which changes in the millisecond [57], and thus the PMD compensation must be carried out in real time. The PMD compensator can be classified in many different ways according to the control structure (feedback or feed-forward), the operating principle of the PMD emulator (e.g., piezo-electrical, electro-optical, thermal-optical) and the detection scheme (RF tones, degree of polarization, state of polarization, etc.) [58].

2.3.2 Electronic Dispersion Compensation

- ***Analog Equalizers: FFE, DFE***

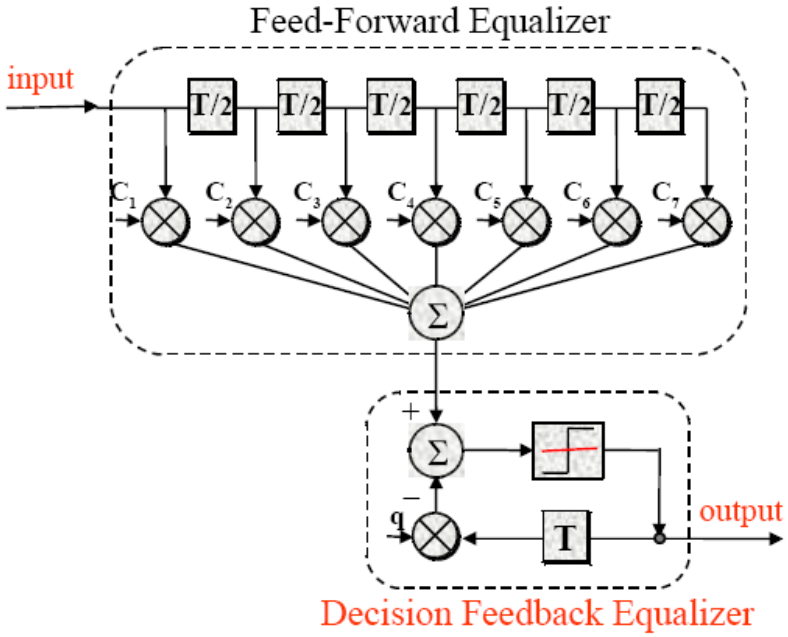

Figure 2.5 An example of the FFE and DFE equalizer.

The early research of electronic dispersion compensation focused on simple analog processing structures, such as feed-forward equalizer (FFE) and decision-feedback equalizer (DFE) [59] with a small number of taps. Figure 2.5 shows an example of FFE and DFE equalizer. The input signal is distorted electrical signals after O/E conversion. Within the FFE, the signal is delayed half-bit period by a tapped delay line with 7 taps. Then the delayed data signal is tapped and weighted by the tap coefficients *C1* - *C7* and summed together. The equalization is performed by tuning the tap coefficients. The DFE has a decision circuit and a feedback path. The feedback signal from the decision circuit is delayed by one bit period, weighted by *q* coefficient, and subtracted out from the input signal or the output of FFE. In this way, the DFE can remove post-cursors of previous decided bit. The FFE is a linear filter which compensates linear distortion while the DFE is a non-linear filter which eliminates post-cursors of distorted signals. For 10-Gb/s system, the FFE/DFE based products have been tested for emerging telecommunication standards [60].

- ***Electronic Pre-compensation***

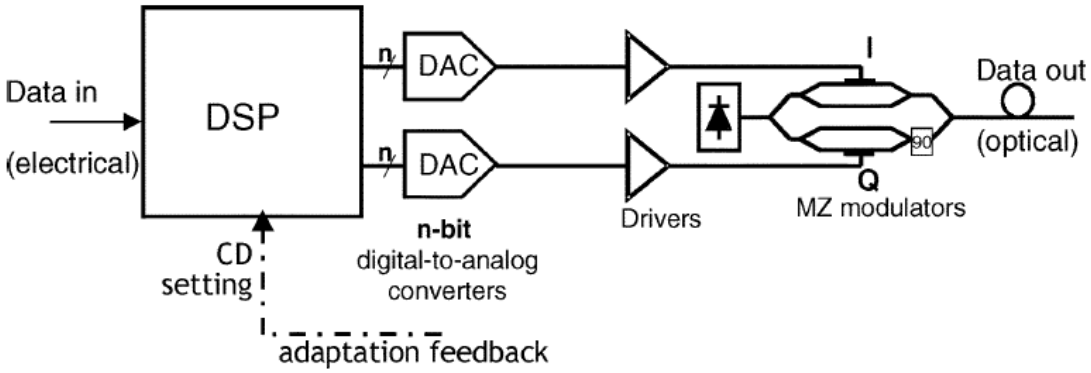

Figure 2.6 Electronic pre-compensation scheme with DSP. After Ref. [64]

Electronic pre-compensation (EPEC) [61-62] is a more developed EDC scheme where the signal at the transmitter use the channel to reconstruct the signal. A transmission length up to 5120 km [63] has been reported for such pre-compensation techniques. Figure 2.6 shows a typical transmitter architecture for EPEC. I and Q part of the predistorted field samples are calculated from the bit pattern in a DSP circuit [64]. Two real FIR filter are implemented in the DSP for binary modulation formats. The tap coefficients of the FIR filter are used to emulate field samples of the bit response of the inverse optical channel including CD. After DAC, I and Q components modulate the optical field with an optical I/Q modulator consisting two MZM and a 90^0 phase shifter. Besides, EPEC requires a reverse feedback path (see Figure 2.6) from receiver to transmitter. If the transmission length is 1000 km, the time delay from the feedback is about 5 ms which means that the rapid variations caused by the thermal drift, vibration, optical network switching, and polarization rotation cannot be compensated for. Thus, transmitter based EDC is only a semi-static solution. Furthermore, this technique is sensitive to finite laser linewidth for large transmission distances [65].

- ***Electronic post-compensation***

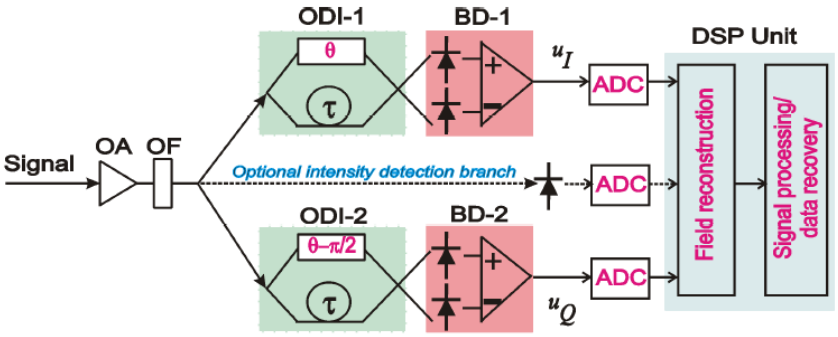

Figure 2.7 Schematic of digital self-coherent detection architecture based on orthogonal differential direct-detection followed by ADC and DSP. OA: optical pre-amplifier; OF: optical filter; ODI: optical delay interferometer; BD: balanced detector; ADC: analog-to-digital converter. After Ref. [66]

Electronic post compensation (EPOC) is another compensation method by which the dispersion compensation is conducted at the receiver. For EPOC, it is possible to access the optical field without a local oscillator by using digital self-coherent detection (DSCD). With the help of high-speed ADC and DSP following orthogonal differential direct detection, the phase and even the field of a received optical signal can be digitally reconstructed [66]. Figure 2.7 shows the architecture of a DSCD receiver. The receiver signal is first spitted into two branches that are connected to a pair of optical delay interferometers (ODIs) with quadrature phase. Two ADCs digitizes the two detected analog waves u_I, u_Q which are the phase rotation angle of the received field. Meanwhile, the field amplitude of the received field can be obtained with intensity detection branch as shown in Figure 2.7. In such way, the received optical field information can be fully reconstructed and adaptive equalization of transmission impairments such as nonlinear phase noise, CD, and PMD could then be performed with DSP. However this scheme suffers from phase ambiguity when the field amplitude is small due to the nature of its non-linear operation and noise accumulation.

- ***Coherent Detection***

The coherent detection with DSP enables digitally processing the sampled optical field in the receiver. As shown in Figure 2.8, coherent detection uses one local laser

to beat with the incoming optical signal to generate optical field components I and Q. A PBS is used to separate two polarization fields. Outputs from the coherent receiver are processed by DSP circuits, restoring the complex amplitude of the signal in a stable manner.

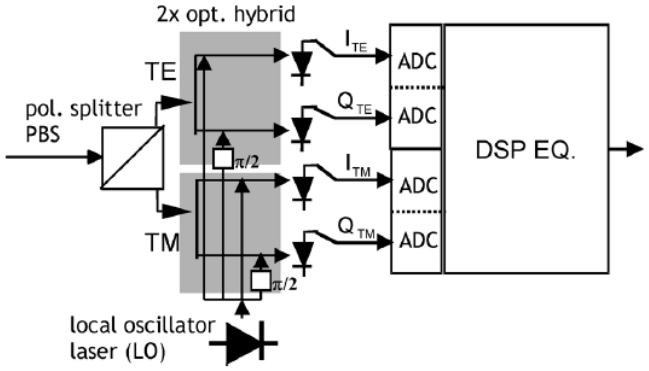

Figure 2.8 Coherent receiver with polarization and phase diversity front end with a local oscillator laser, four ADCs, followed by a digital equalizer (DSP EQ). After Ref. [64]

- ***Optical OFDM***

  Electronic compensation of optical distortion can resort to advanced modulation formats, such as optical OFDM. Recently, optical OFDM together with DSP is being actively pursued as another transmission scheme for multi-Gb/s data rate over SMF. Due to the long subcarrier symbol period (>> nanosecond), CD only results in a simple subcarrier- dependent complex phase rotation, which can be simply compensated by a multiplication with a complex coefficient. A detailed introduction of different flavors of optical OFDM will be presented in the next section.

2.4 Optical OFDM

OFDM is a widely used modulation/multiplexing technology in broadband wired and wireless communication systems because it is an effective solution to inter symbol interference (ISI) caused by a dispersive channel. Another major advantage of OFDM is that it allows for adaptation of signal data rate as well as format depending on the characteristics of the transmission channel. The basic concept of OFDM is quite simple [67-70]: the signal data is transmitted on a number of different frequencies, and as a result

the symbol period is much longer than that for a serial system with the same net data rate. Both modulation and multiplexing of the OFDM signal can be achieved digitally using FFT algorithms and as a result, the signals can be generated in a very computationally efficient way.

The concept of OFDM was first proposed by Chang in 1966 [71] for dispersive fading channels. The employment of the DFT to replace the banks of sinusoidal generators and the demodulators was suggested by Weinstein and Ebert [72] in 1969, which significantly reduces the implementation complexity of OFDM modems. The Cyclic Prefix (CP) was proposed in 1980 [73]. OFDM began to be considered for practical wireless applications in the mid–1980s. Cimini of Bell Labs [74] published analytical and early seminal experimental results on the performance of OFDM modems in mobile communications channels. In 1987, Lassalle and Alard [75] considered the use of OFDM for radio broadcasting. OFDM is now widely applied in radio systems for digital audio and video broadcasts, wireless local area networks (WLAN), wireless wide area networks (WWAN, Worldwide Interoperability for Microwave Access, or WiMAX), and wire line access systems via Asynchronous Digital Subscriber Line (ADSL).

The application of OFDM to long-haul optical communications for both coherent detection [6] and direct detection [13, 14] was introduced in 2006. Soon after that, there are an increasing number of papers on the theoretical and practical performance of optical OFDM transmission [76-77], 100-Gb/s [14,78-79] and 1-Tb/s channel data rate [80-82] transmissions. Novel optical OFDM schemes such as no-guard interval transmission [83], all-optical OFDM [84] and multi-mode fiber transmission [15,85-87] were also reported.

2.4.1 OFDM for Optical Communications

Despite the fact that the OFDM has been extensively studied in the RF domain, OFDM has only recently been applied to optical communications. The first application of Optical OFDM (O-OFDM) appeared in 1998 by Pan et al. [88] where a detailed analysis for OFDM-QAM signals in hybrid AM/OFDM subcarrier-multiplexed fiber-optic systems is presented. The recent increase of interests in optical OFDM is due to the following reasons:

i) The continuous increase in demand for network capacity across dispersive optical media.

ii) The development in silicon DSP technology enables the sophisticated OFDM signal processing.

For an OFDM system to work successfully, the most critical assumption is the linearity in modulation, transmission and demodulation. In other words, the system must be (approximately) linear between the transmitter IFFT input and the receiver FFT output. Consequently, ignoring the fiber channel nonlinearity, a linear transformation for the optical transmitter and the optical receiver is the key goal for the optical implementation of OFDM.

In single mode optical fiber systems, the best way to achieve linearity is to map each discrete OFDM subcarrier frequency in the baseband electrical domain to a single discrete frequency in the optical domain. There are two methods to linearly convert a complex valued electrical data signal into the optical domain. First, upon applying a complex electrical I/Q mixer, the signal can be electrically up-converted with an electrical intermediate frequency (IF) carrier. The resulting up-converted electrical OFDM data signal can be E/O converted using an optical amplitude modulator [6, 14] as shown in Figure 2.9 (a). Alternatively, a complex E/O I/Q modulator can be driven directly by the complex electrical OFDM signal and thus converted into the optical domain directly [6,78-79].

Instead of the direct detection of the optical OFDM subcarriers, an optical carrier must be delivered either by a transmitter as in DDO-OFDM [89] shown in Figure 2.10 (a) or by a local oscillator in the receiver as in CO-OFDM [6] where the OFDM signal beats with the LO signal in an optical 90° hybrid to obtain the real and imaginary components of the signal.

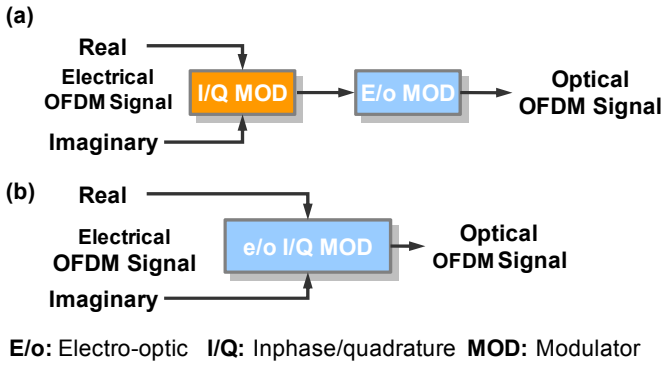

Figure 2.9 Optical OFDM optical up-converter with (a) IF architecture and (b) direct conversion architecture

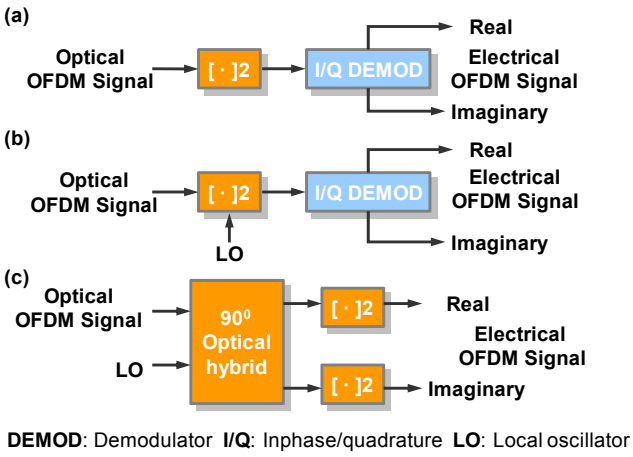

Figure 2.10 O-OFDM optical receiver architecture with (a) direct-detection, (b) heterodyne detection and (c) intradyne detection

Both techniques have advantages. CO-OFDM has the highest performance in receiver sensitivity, spectral efficiency and robustness against polarization dispersion. However, it requires a local laser at the receiver, and is more sensitive to phase noise. DDO-OFDM has simpler optical receiver architecture, but a frequency guard band is needed to prevent the interference from mixing products which reduces the electrical and optical spectral efficiency. Besides, as some power is allocated to the transmitted carrier, DDO-OFDM also requires more transmitted optical power. Currently, there is extensive research into the performance of both systems and on techniques to mitigate the disadvantages.

2.4.2 Direct Detection Optical OFDM

The common feature of DDO-OFDM is using the direct-detection in the receiver end. Due to its lower cost, the DDO-OFDM has many variants which can be divided into two groups as linearly mapped DDO-OFDM and nonlinearly-mapped DDO-OFDM. For the linearly mapped DDO-OFDM, there is a linear mapping between the optical field of the transmitted signal and the OFDM baseband signal. Nonlinearly mapped DDO-OFDM aims to obtain the linear mapping between the baseband OFDM and optical intensity even though there is no linear mapping between the baseband OFDM and the optical field. Since the OFDM signal is encoded in the amplitude not the field, and subsequently nonlinearly mapped DDO-OFDM do not have the same capability of the dispersion resilience as linearly mapped DDO-OFDM therefore it is not fit for long-haul transmission. However, because of its simple implementation, it has become a very attractive option for the short-reach single-mode fiber application [15,90], multimode fiber [91] and optical wireless systems [92-93]. In this thesis we focus our work on long-haul SSMF transmission, thus only linearly mapped DDO-OFDM will be discussed.

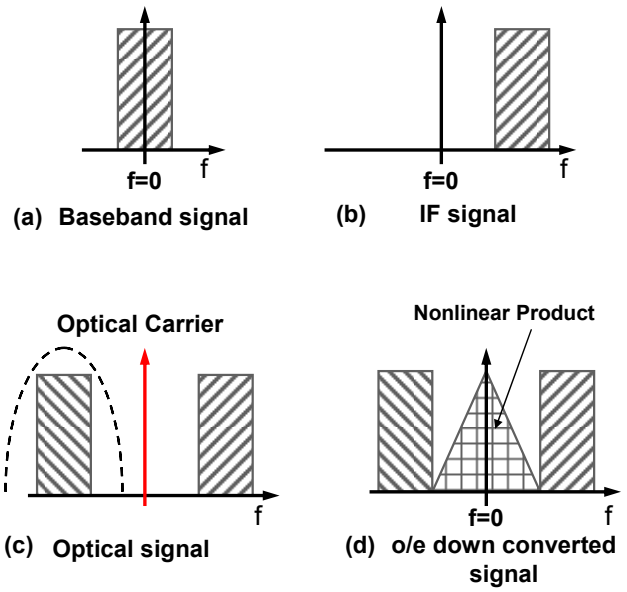

Figure 2.11 The spectra of DDO-OFDM signal

Direct detection optical OFDM system has been investigated in detail in [14,94-95]. A typical DDO-OFDM system uses real valued electrical OFDM signal after IF up-conversion to directly drive the E/O modulator. An optical filter is used to select one

of the signal sideband. The spectra of the electrical and IF up-converted OFDM signals are plotted in Figure 2.11 (a)-(b). After E/O modulation, an optical filter is used to select one of the signal bands to generate single side band (SSB) optical OFDM signal (Figure 2.11 (c)). Then the optical spectrum will be a linear copy of the RF signal. The position of the main optical carrier can be one OFDM spectrum bandwidth away [13] or right at the end of the OFDM spectrum [96-97]. In the receiver, a single photo-detector is used where the optical carrier mixes with the optical subcarriers to regenerate the electrical OFDM signal. The output of the optical receiver consists of three terms: the first term is a Direct Current (DC) component that can be easily filtered out. The second term is the fundamental term consisting linear OFDM subcarriers that are to be retrieved. The third term is the second-order nonlinearity product of the optical carrier and the OFDM subcarriers as shown in Figure 2.11 (d) that needs to be removed. If the optical OFDM band is located close to the optical carrier in the frequency domain, the second-order nonlinearity product located in the same frequency range as the electrical OFDM signal, leading to a performance degradation. Based on the approach used to minimize the second-order nonlinearity induced penalty, DDO-OFDM can be divided into the offset optical SSB-OFDM, baseband optical SSB-OFDM, RF-tone assisted OFDM and Virtual SSB-OFDM.

- ***Offset Optical SSB-OFDM***

For the offset optical SSB-OFDM, a guard band is resided between the second-order nonlinearity components and the OFDM band such that their spectra are non-overlapping. As a result, the second-order nonlinearity can be easily removed with a RF filter in [13,98-99]. Figure 2.12 shows the proposed system of offset OFDM with 10 Gb/s per channel data rate and 4-QAM modulation. The OFDM signal is first up-converted to a 7.5 GHz RF carrier which gives an RF OFDM band from 5 GHz to 10 GHz. After the optical modulation, an optical filter is used to remove the lower sideband. The power of optical carrier is set to be equal to the power within the OFDM sideband to achieve the best receiver sensitivity. The third inset in Figure 2.12 shows that the second-order nonlinearity components is from DC to 5 GHz and falls outside the OFDM band which

gives insignificant penalty. A noiseless photodiode is used in simulation to produce the electrical signal. Figure 2.13 shows the system Q for 8×10-Gb/s WDM transmission under the different fiber input power and transmission distances. It can be shown that for all transmission distance the optimum input power is around -7 dBm. At lower input power, the Q is limited by the ASE noise and at high input power, the Q is limited by fiber nonlinearity.

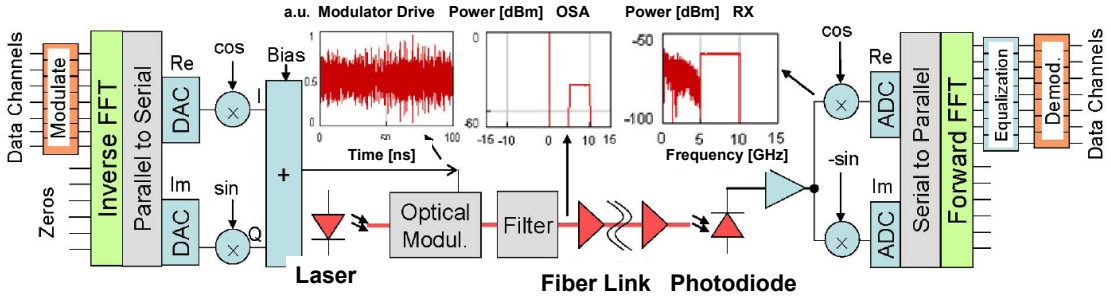

Figure 2.12 DDO-OFDM system block diagram, including modulator drive waveform, optical spectrum after filter, and RF spectrum after the photoreceiver. After Ref. [98]

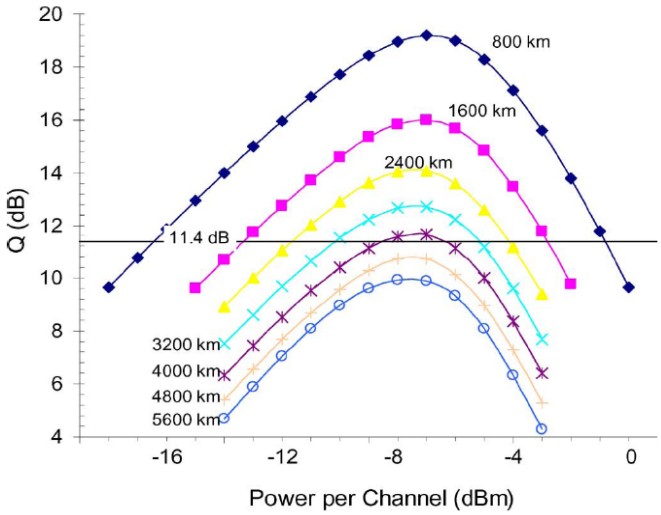

Figure 2.13 Q versus input power for a number of fiber lengths, showing the definition of the minimum and maximum Q-values and the optimum power for each length. After Ref. [98].

- ***Baseband Optical SSB-OFDM***

Baseband optical SSB-OFDM [96] is proposed to improve the electrical and optical spectral efficiency. Figure 2.14 shows the proposed baseband SSB DDO-OFDM system. Unlike the offset SSB DDO-OFDM, no IF up-conversion to the RF frequency is needed

for the baseband SSB-OFDM. The real-valued electrical signal can be obtained by adding the conjugate form of the complex data and applying IFFT. The optical SSB is generated by applying the electrical signal to a dual MZM optical modulator with 90-degree phase difference between the dual driving signals. The received baseband spectrum is shown in Figure 2.15. Since the signal is essentially intensity modulated, a photodiode is used to perform the O/E conversion. Because the second-order nonlinearity components is a product of the optical carrier and the OFDM subcarriers, for the baseband SSB DDO-OFDM approach, the second-order nonlinearity is suppressed by decrease the power of optical OFDM signal

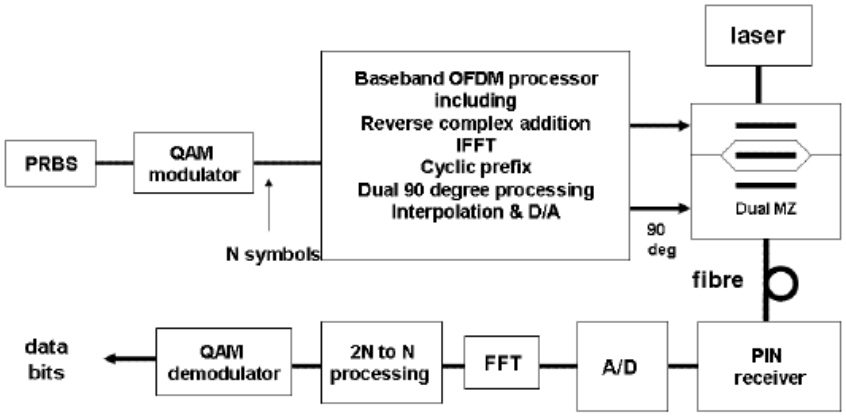

Figure 2.14The Baseband SSB DDO-OFDM system. After Ref.[96].

- ***RF-tone Assisted OFDM***

As mentioned in last section, the baseband optical SSB-OFDM scheme does not need IF up-conversion thus has a better spectral efficiency than the offset optical SSB-OFDM scheme. However, there is a trade-off between the high modulation depth and robustness to chromatic dispersion. Peng et al. [100] proposed a RF-tone assisted OFDM scheme to increase the receiver sensitivity while keeping the same spectral efficiency. In such an approach, the optical OFDM signal is generated coherently and detected directly and an RF-tone is inserted in to the OFDM band to replace the optical main carrier. Based upon the location of the RF-tone, RF-tone assisted OFDM schemes is divided into two groups as OFDM-A and OFDM-B as shown in Figure 2.16. For OFDM-A, a gap with the same width as the signal badwidth is used between the RF tone and the signal. For OFDM-B,

odd subcarriers relative to the RF-tone are used for the data and the even subcarriers are left unused. For both scheme, complex base band OFDM signal is generated and its real and imaginary parts are fed into the two arms of an optical I/Q modulator. The electrical spectrum after the square-law detector is shown in Figure 2.16. For the OFDM-A scheme, the second order nonlinearity components fall on the subcarriers within the gap. That is similar to the offset optical SSB-OFDM. However OFDM-A does not need electrical RF up conversion and requires smaller electrical bandwidth for the modulator. For OFDM-B, the nonlinearity components will fall on those subcarriers interleaved with the data subcarriers. Thus the data of the two schemes can be extracted without suffering from nonlinearity components.

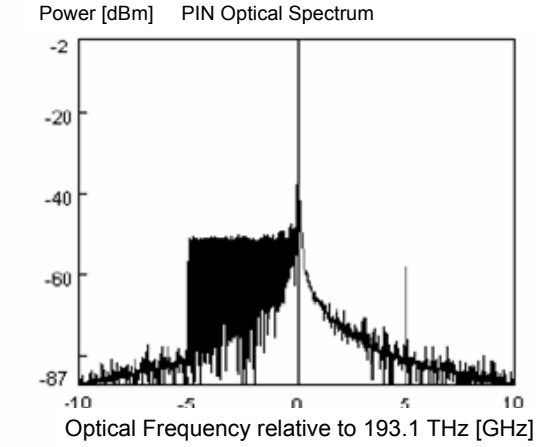

Figure 2.15 Optical spectrum of the baseband optical SSB-OFDM. After Ref. [96]

Experiment was conducted to test the proposed RF-assisted OFDM system where 8-QAM was used to generate 10-Gb/s data rate signal. Figure 2.17 shows the BER performance for both the proposed RF-assisted OFDM system and the conventional baseband optical SSB-OFDM system at 10 Gb/s data rate with 8-QAM modulation. It can be shown that the back-to-back optical signal to noise ratio (OSNR) sensitivity for the OFDM-A and OFDM-B are similar and has 5 dB better sensitivity than the conventional scheme. After 260 km SSMF transmission, neglected penalty is observed for the proposed system.

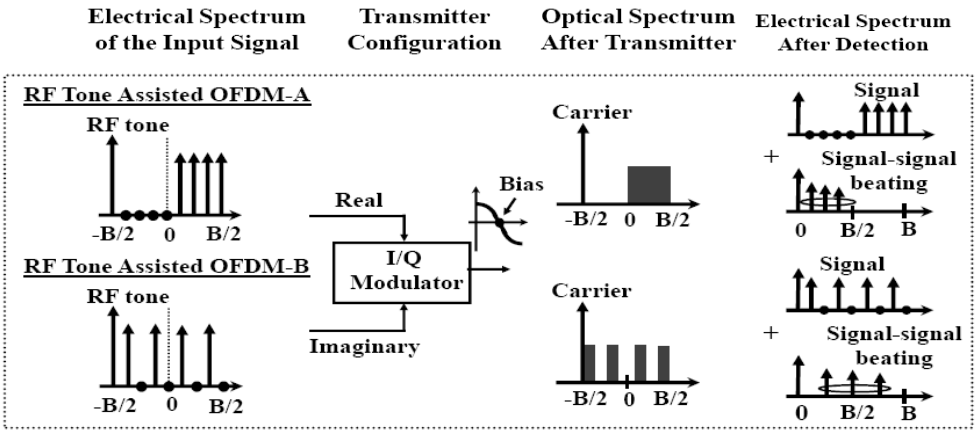

Figure 2.16 The proposed RF-tone assisted OFDM-A and OFDM-B. After Ref. [100]

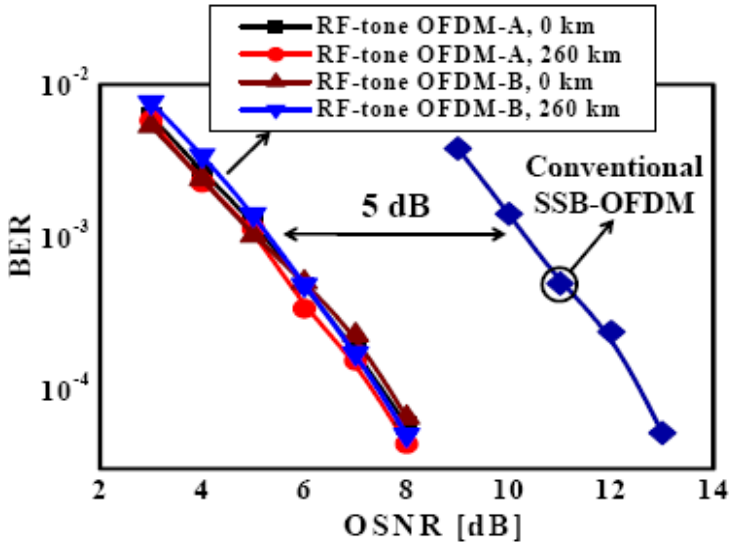

Figure 2.17 Experimental results of BER versus OSNR. The OSA resolution is 0.2 nm. After Ref. [100]

- ***Virtual SSB-OFDM***

Peng et al. propose a virtual SSB-OFDM direct-detection technique [97] by employing an RF tome insertion and interactive detection to increase the electrical spectral efficiency yet still preserves a high sensitivity and chromatic dispersion tolerance. Figure 2.18 shows the transmitter architecture for the proposed system. A RF tone is inserted at the left most subcarrier. The RF-tone together with the data subcarriers are transferred into a complex baseband OFDM signal by IFFT. No redundant subcarriers are allocated thus this scheme only requires half of electrical bandwidth that is used by the conventional

baseband optical SSB-OFDM. The real and imaginary parts of the complex signal are feed into the two ports of the I/Q modulator where the original optical carrier is suppressed and RF-tone is used as the main carrier. The second order nonlinearity components generated by the square-law photo-detector is removed by an iterative cancellation process [97] as shown in Figure 2.19. The principle of this technique is: (i) The photocurrent is firstly stored in the memory and is used to made decisions. (ii) Using the decisions to reconstruct the second-order nonlinearity components. (iii) Subtract the rebuilt second-order nonlinearity components from the stored photocurrent and make decisions. (iv) Repeat (ii)-(iii) until the constellation converges. However, such iterative cancellation process greatly increases the computation efficiency and makes this scheme impractical.

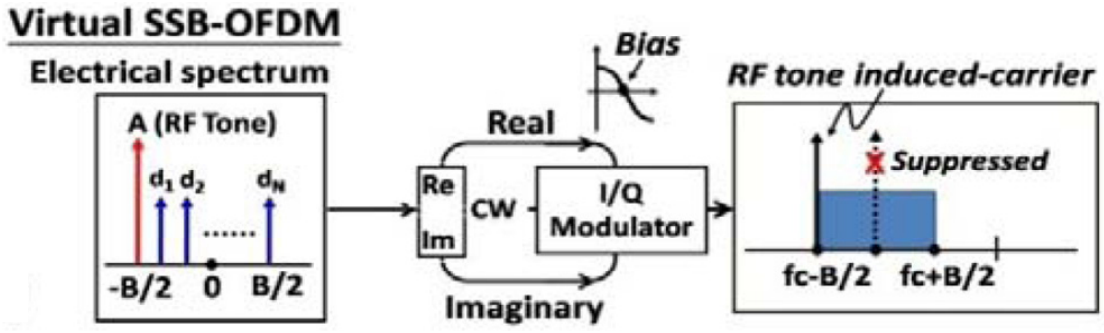

Figure 2.18 Transmitter architectures for the proposed virtual SSB-OFDM. After Ref. [97].

Figure 2.20 shows the BER performance for both conventional baseband SSB DDO-OFDM system and the proposed virtual SSB-OFDM system. Due to the decreased requirement on the electrical bandwidth (i.e., the sampling rate of Waveform Generator) of the proposed system, the minimum constellation size for 10 Gb/s data is decreased from 8-QAM to 4-QAM. It can be seen that the proposed system has 5 dB better sensitivity than the conventional SSB scheme and 340km SSMF transmission introduces almost zero penalty. The 5-dB gain is attributed to the optimum optical carrier to signal power ratio and the smaller constellation size used in virtual SSB-OFDM.

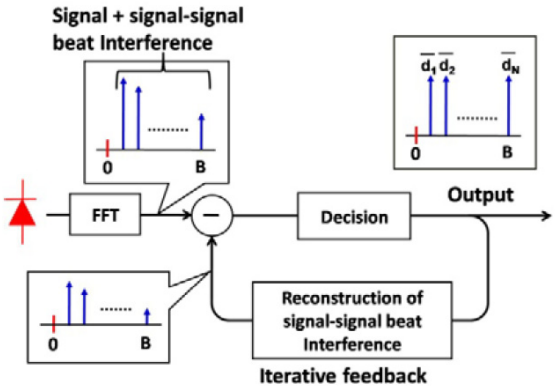

Figure 2.19 Iterative detection for the virtual SSB-OFDM. After Ref. [97].

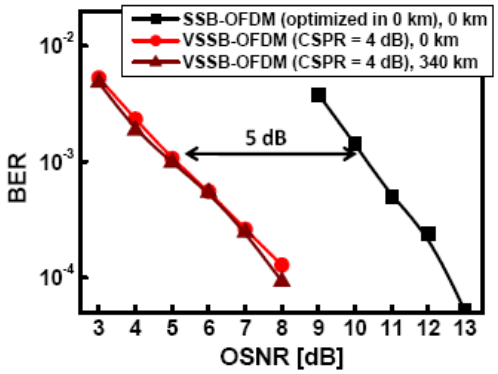

Figure 2.20 Measured bit error rate versus the optical signal to noise ratio for the conventional and the virtual SSB-OFDM. The OSA resolution is 0.2 nm. After Ref. [97].

2.4.3 Coherent Optical OFDM

CO-OFDM was first proposed by Shieh et.al. [6], and the first proof of concept of CO-OFDM experiments were carried out by Shieh et. al. for a 1000 km SSMF transmission at 8 Gb/s [101]. In such CO-OFDM system, a digital transmitter/coherent receiver with DSP is preferred to implement both Inverse Discrete Fourier Transform (IDFT) and Discrete Fourier Transform (DFT). L. Xu proposed a LO free CO-OFDM architecture using self optical carrier extraction to reduce the complexity of the required DSP. Another group of CO-OFDM called no-guard interval (No-GI) CO-OFDM proposed and demonstrated by Yamada et. al. in [102]. Unlike the conventional CO-OFDM where signal subcarriers are generated electrically with IDFT, No-GI CO-OFDM is constructed using optical subcarriers without a need for the cyclic prefix. Despite all the verities, the fundamental principle of CO-OFDM remains the same, which is to achieve high spectral

efficiency by overlapping subcarrier spectrum yet avoiding the interference by using coherent detection and signal set orthogonality. In this section, we describe the detailed principle for above mentioned CO-OFDM schemes. .

- ***FFT Based Coherent Optical OFDM***

Figure 2.21 (a), and (b) shows respectively the transmitter and receiver configuration of a FFT based CO-OFDM system. A detailed discussion of such system will be presented in Chapter 4. At the Transmitter (Figure 2.21 (a)), the electrical OFDM signal is generated by DACs after IFFT operation performed by DSP block. This electrical OFDM signal is then up-converted to the optical domain by using carrier-suppressed optical I/Q modulation. At the receiver (Figure 2.21 (b)), the received optical signal is detected by a phase-diversity receiver, and demodulated by FFT operation after sampling at ADCs.

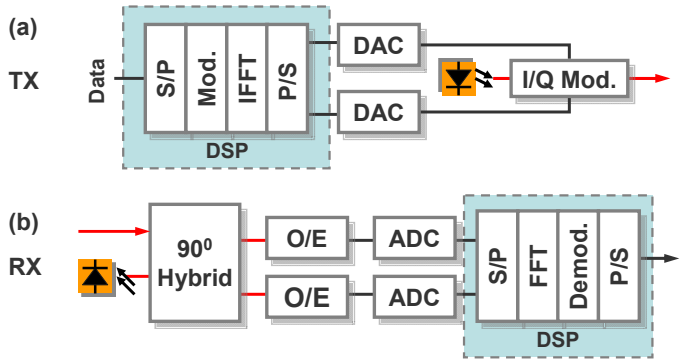

Figure 2.21 The transmitter and receiver configurations of CO-OFDM systems.

Figure 2.22 shows the optical spectrum of a 10-Gb/s OFDM signal with single polarization transmission. The spectra of conventional intensity modulation (IM) signal and the optical duobinary signal with the same average power are shown for reference. The 20 dB bandwidth of 10 Gb/s OFDM signal is around 6.8 GHz in contrast with 18 GHz for conventional IM, and 12 GHz for optical duobinary signal. This signifies that CO-OFDM has potential to achieve high spectral efficiency.

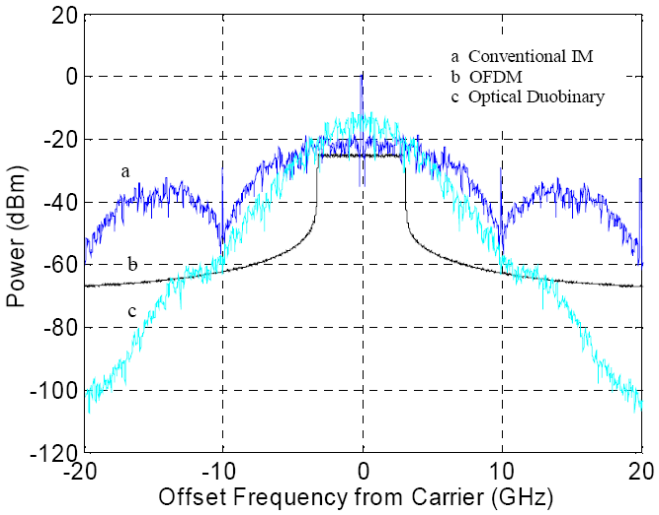

Figure 2.22 Optical Spectra for 10 Gbit/s CO-OFDM, optical duobinary and conventional IM signal with the same average power. After Ref [76].

- ***CO-OFDM System with Self Optical Carrier Extraction***

The CO-OFDM system performance heavily relies on the digital signal processing to perform FFT/IFFT, channel equalization, synchronization, ADC/DAC and so on. Although there has been a significant progress in the implementation of high speed DSP, the requirement of practical implementation of real time CO-OFDM at 40 Gb/s and beyond exceeds the processing capability of current DSP. CO-OFDM using self optical carrier extraction is proposed to reduce the complexity of DSP of a CO-OFDM system. In such architecture, no local laser is needed at the receiver, the optical carrier is extracted from the incoming signal behaves as a local laser and is used to beat with the incoming signal for coherent detection. Since the two interfering signals come from the same source, they have the same polarization states and their phase noise can be minimized. Figure 2.23 shows the proposed scheme for optical carrier extraction. At the receiver side, the incoming signal is spitted into two branches with coupler 'A', one passes through an optical band pass filter (OBPF) for carrier extraction for coherent interference while the other branch goes directly to coupler 'B'. The output of 'B' will be fed into a coherent detector. To assist carrier extraction, the carrier should not be suppressed and the carrier component should be separable which can be realized by using a RF carrier or zero padding.

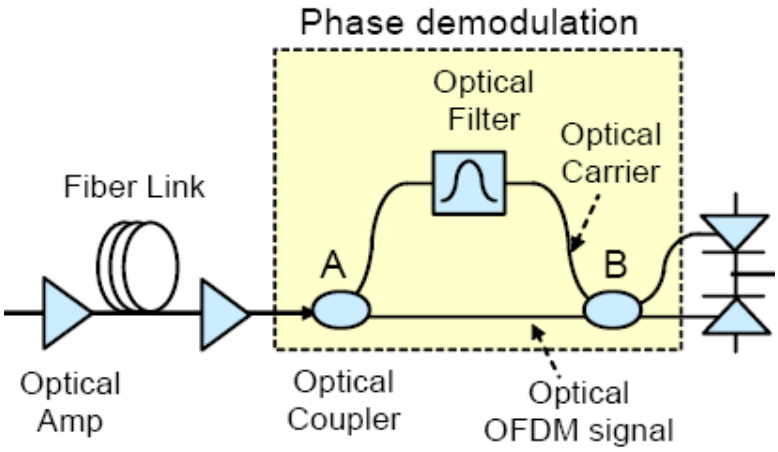

Figure 2.23 Coherent optical OFDM system using self optical carrier extraction. After Ref. [103]

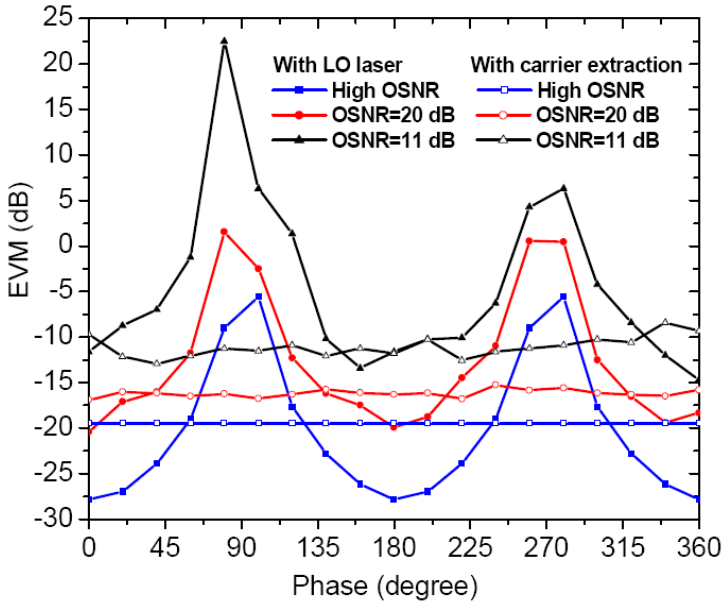

Figure 2.24 Signal EVM under different phases of incoming optical OFDM signal. After Ref. [103]

Figure 2.24 compares the signal Error Vector Magnitude (EVM) for conventional CO-OFDM system and the proposed systems. No phase estimation is included in the receiver. It can be seen that the performance of the new scheme does not have fluctuations under random phases of the incoming signal. Therefore, phase estimation can be avoided by using self carrier extraction which simplifies the ASE requirement.

- ***Principle of No-guard Interval Coherent Optical OFDM***

Conventional CO-OFDM using FFT/IFFT and high CD and PMD tolerance is achieved by the use of guard-interval (GI) which also introduces excess overhead and increases the redundant line rate. To address this issue, Yamada et. al. proposed a No-GI CO-OFDM scheme [102] where the linear distortion caused by CD and PMD is equalized by fixed-tap linear equalizers and adaptive FIRs with blind channel estimation at the receiver.

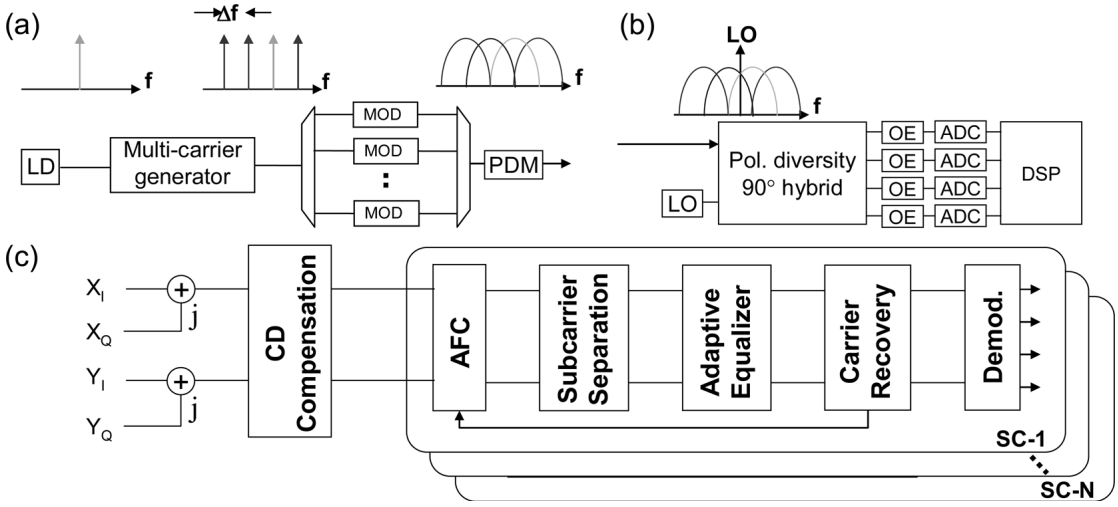

Figure 2.25 Tx configuration (a), Rx configuration (b), and DSP block diagram (c) of No-GI CO-OFDM. PDM: polarization division multiplexing, AFC: automatic frequency control. After Ref. [102]

The configuration of No-GI CO-OFDM system is shown in Figure 2.25. At the transmitter (Figure 2.25 (a)), a multi-carrier generator consists external intensity /phase modulator is used to generate multiple optical subcarriers. Each subcarrier is encoded with a data stream as conventional single-carrier modulation and finally coupled to create an OFDM signal [104]. The optical subcarrier spacing is equal to the baud rate of each subcarrier. At the receiver, a DSP-based polarization-diversity intradyne coherent receiver is used to detect both I and Q components of the received signal for each polarization (Figure 2.25 (b)). The functionalities of the DSP are similar to that for the single carrier coherent receiver which include: automatic frequency control, subcarrier separation, adaptive equalizer, carrier recovery, and data demodulation.

2.5 Conclusion

Supporting high capacity data transmission and easy of dispersion compensation are two necessary functions for future optical networks. In this chapter, we have explored the literature pertinent to these two research areas.

In Section 2.2, we have reviewed the available techniques relating to high capacity optical transmission including WDM, OTDM, and coherent optical detection. WDM technology is a very common approach to increase the per fiber capacity which uses several wavelengths per fiber to transmit data simultaneously. OTDM is designed to increase the network capacity through using higher per wavelength transmission data rate. Coherent detection is considered as a promising solution to achieve high spectral efficiency transmission.

In Section 2.3, we have reviewed the available techniques of electronic dispersion compensation. Electronic compensation has become feasible due to the fast advances of microelectronics. On the other hand, the evolution of optical fiber networks requires adaptive and cost-effective compensation solutions. Electronic approaches are promising to satisfy the requirements. The structure and performance of electronic compensator vary vastly. It depends on the application to choose an appropriate electronic compensator.

Recently, Optical OFDM has attracted large attention as another transmission scheme which supports high speed data transmission and easiness of dispersion compensation. Section 2.4 reviewed the various optical OFDM techniques including direct-detection optical OFDM and coherent optical OFDM.

Chapter 3

Theoretical Fundamentals for CO-OFDM Systems

3.1 Introduction

With the continuous increase in demand for network capacity, both the installed optical transmission links as well as new deployed "green field" needs to operate at the highest possible data rates. The increase in overall network capacity can be achieved by an increase in the number of applied fibers, the number of DWDM channels per fiber, or the data rate per wavelength channel. From the cost effective pint of view, the increase in data rate is the most important means to increase the network capacity.

Coherent Optical OFDM takes advantage of the recent advances in DSP and has become one of the promising solutions for the high data rate optical transmission. OFDM has been widely studied in mobile communications to combat hostile frequency-selective fading and has been incorporated into various wireless network standards. OFDM is a special form of a broader class of MCM. It has an important property that the carriers are partly overlapped since each of its subcarrier frequency is orthogonal with every other subcarrier frequencies. CO-OFDM is an optical equivalent of RF OFDM which combines the technique of 'optical coherent detection' and 'OFDM' [105]. The coherent detection brings OFDM a much needed linearity in RF-to-optical (RTO) up-conversion and Optical-to-RF (OTR) down conversion. OFDM brings coherent system computation efficiency and ease of channel and phase estimation. CO-OFDM was first proposed to combat fiber chromatic dispersion [6]. It was soon extended to polarization-diversity detection, and has been shown to be resilient to fiber PMD [106]. The first CO-OFDM transmission experiment has been reported for 1000 km SSMF transmission at 8 Gb/s [101], and more CO-OFDM transmission experiments using off-line signal processing [34-36] have been demonstrated. The CMOS ASIC chip

recently demonstrated for single carrier coherent systems [107-108] signify that the current silicon speed can support 40 Gbit/s OFDM transmission systems. Real-time CO-OFDM system with 3 Gb/s data rate [109] has also been demonstrated recently. Because of its superior scalability over the bit rate of the transmission systems, CO-OFDM is well-positioned to be an attractive choice of modulation format for the next generation of ultra-high speed optical networks.

In this chapter, we first provide an introduction to the OFDM fundamentals in Section 3.2, including basic mathematical formulations of OFDM, discrete Fourier transform implementation and cyclic prefix. Section 3.3 introduces the principle of CO-OFDM from the aspect of system architecture, CO-MIMO-OFDM model and signal processing. A comparison between single carrier and multicarrier systems is presented in Section 3.5.

3.2 Principle of OFDM

Conventional single carrier systems as shown in Figure 3.1 (a) use one frequency to carry all the data. An alternative approach is to use MCM techniques when single carrier is not desirable for performance or costs. The principle of MCM is to transmit data by dividing the stream into several parallel lower bit rate streams, and using each of sub-streams to modulate several carriers as shown in Figure 3.1 (b). Because different carriers share the same transmission media, conventional MCM system has to use frequency spacing between each carrier to minimize the interference which greatly reducing the spectral efficiency. OFDM (Figure 3.1 (c)) is a special form of MCM. It has an important property that carrier spacing is minimized since each of its frequency is orthogonal with every other frequency. For OFDM system, each sub channel can be considered non-dispersive. Thus, no channel equalizer is required. Besides, instead of implementing a bank of sub-channel modems, OFDM system can be conveniently implemented with the aid of a single FFT, as it will be outlined in Section 3.2.2. The fundamental principle of orthogonal multiplexing originates from Chang [110] in mid-1960s and many discussions on this technique can be found in [74,111-113]. OFDM has been widely studied in mobile communications to combat frequency-selective fading and has been incorporated into

wireless network standards and digital audio and video broadcastings.

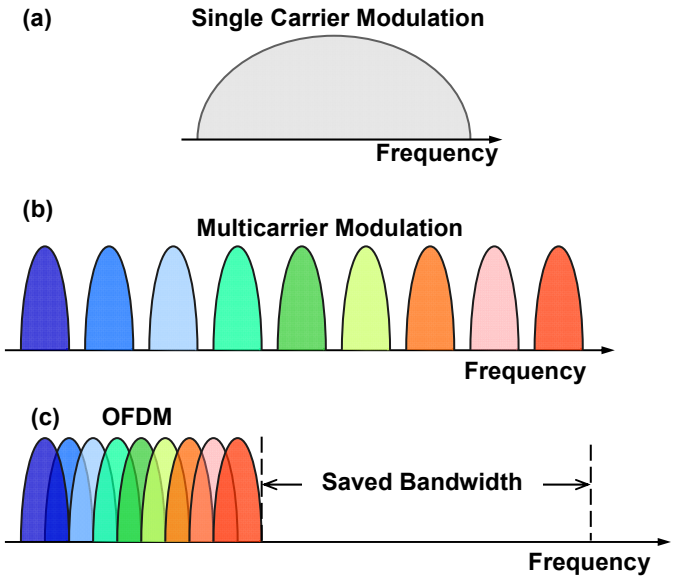

Figure 3.1 Comparison of (a) single carrier, (b) general frequency division multiplexing and (c) orthogonal frequency division multiplexing.

3.2.1 Mathematical Description of OFDM Signal

A simple multi-carrier system consisting of a transmitter and a receiver is presented in Figure 3.2, the serial data stream is first decided into a number of parallel channels with a serial-to-parallel converter. The data in each channel is applied to an electrical I/Q modulator. For N_{sc} channels there are N_{sc} modulators with carrier frequencies of $\{f_1, f_2, \ldots f_{Nsc}\}$. Each subcarrier signal can be represented as

$$s_k(t) = c_k(t)e^{j2\pi f_k t} \tag{3.1}$$

where $k = 1, 2, \ldots, N_{sc}$, $c_k(t)$ is a complex data at k_{th} subcarrier. For the sake of simplicity, the pulse shape term is dropped. The MCM transmitted signal $s(t)$ is the combination of all subcarriers which can be written as:

$$s(t) = \sum_{k=1}^{N_{sc}} c_k e^{j2\pi f_k t} \tag{3.2}$$

The orthogonality of the OFDM signal originates from the straightforward correlation between any two subcarriers. It can be seen that if the following condition

$$f_k - f_l = m\frac{1}{T_s} \quad k,l \in \{1,2,\ldots,N_{sc}\} \tag{3.3}$$

is satisfied, then the two subcarriers are orthogonal to each other over one OFDM symbol period T_s. This signifies that these orthogonal subcarrier sets, with their frequencies spaced at multiple of inverse of the symbol rate can be recovered without Inter-Carrier Interference (ICI) in spite of strong signal spectral overlapping. In reality, a number of OFDM symbols are grouped together as an OFDM frame, which might also include additional symbols for synchronization and channel estimation. For an OFDM frame with multiple OFDM symbols, the output is the summation of multiple Eq. (3.2), which can be expressed as

$$s(t) = \sum_{i=-\infty}^{\infty} \sum_{k=1}^{N_{sc}} c_{ki} s_k(t - iT_s) \tag{3.4}$$

$$S_k(t) = \prod(t) e^{j2\pi f_k t} \tag{3.5}$$

$$\prod(t) = \begin{cases} 1 & (0 < t < T_s) \\ 0 & (t \le 0, t > T_s) \end{cases} \tag{3.6}$$

where c_{ki} is the i_{th} information symbol at the k_{th} subcarrier, S_k is the waveform for the k_{th} subcarrier, N_{sc} is the number of subcarriers, f_k is the frequency of the subcarrier, and T_s is the symbol period.

3.2.2 Discrete Fourier Transform Implementation of OFDM

A fundamental challenge with the OFDM is that a large number of subcarriers are needed so that the transmission channel affects each subcarrier as a flat one. This leads to an extremely complex architecture involving many oscillators and filters at both transmit and receive end. Besides, the OFDM signal has overlapped frequency, although it can save the required bandwidth, it is difficult to recover subcarrier without inter-subcarrier interference by means of analog filter. The idea of using IDFT/DFT for OFDM modulation/demodulation was first presented in [114].

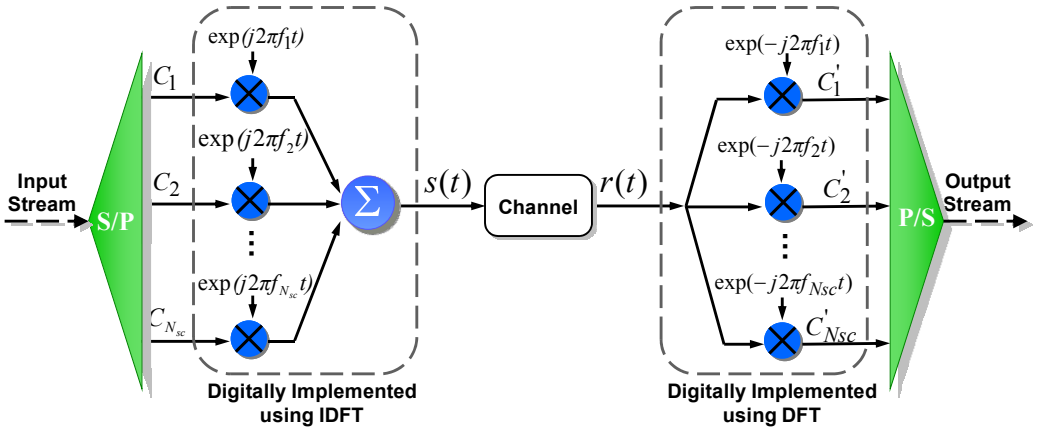

Figure 3.2 The conceptual diagram of a simple multi-carrier system and the discrete Fourier transform implementation of OFDM

For the sake of simplicity, only one OFDM symbol is considered. Sampling time domain OFDM signal is $s(t)$ with sampling rate of T_s/N_{sc}, the *mth* sample of $s(t)$ from Eq. (3.2) becomes

$$s_m = \sum_{k=1}^{N_{sc}} c_k \cdot e^{j2\pi f_k \frac{(m-1)T_s}{N_{sc}}} \tag{3.7}$$

Using orthogonality condition of Eq.(3.3)

$$f_k = \frac{k-1}{T_s} \tag{3.8}$$

and substituting Eq. (3.8) into Eq. (3.7) we have

$$s_m = \sum_{k=1}^{N_{sc}} c_k \cdot e^{j2\pi \frac{(m-1)(k-1)}{N_{sc}}} = F^{-1}\{c_k\} \tag{3.9}$$

In Eq. (3.9) F^{-1} stands for the N_{sc} points IDFT between the time domain discrete signal and its frequency domain signal representation. Similarly, at the receive end, we get

$$c_k' = F\{r_m\} \tag{3.10}$$

where r_m is the received value sampled at every interval of N_{sc}/T_s and F is Fourier

transform. Eq. (3.9) and Eq. (3.10) show that discrete value of the OFDM transmitted signal $s(t)$ is a N_{sc} point IDFT of the information symbol c_k, and received information symbol value c_k' is a simple N_{sc} point DFT of the receive sampled value.

3.2.3 Cyclic Prefix for OFDM

With the increase in channel data rate, the optical signal is more and more limited by transmission impairments in optical fibers such as CD and PMD. Chromatic dispersion is a deterministic distortion occurs in optical fiber when different spectral components of a pulse travel at different speeds [115-116]. CD causes pulse broadening and its effect on the transmitted signal scales quadratically with the bandwidth consumption or equivalently with the data rate. No CD compensation is need for a data rate less than 2.5 Gb/s even at long haul distances. At 10 Gb/s or higher data rate, consideration of the fibers' chromatic dispersion compensation becomes necessary. In optical fiber, small departures from the perfect cylindrical symmetry lead to birefringence, which results in two different polarization modes. If the input pulse excites both polarization modes, it becomes broader as the two modes disperse along the fiber because of their different transmission constants. This phenomenon is called the PMD, which is considered as a limiting factor in high-speed long-haul optical fiber communication systems

Both CD and PMD will destroy the orthogonality between subcarriers and causes ICI. Furthermore, a system may transmit multiple OFDM symbols in a series so that a dispersive channel causes ISI between successive OFDM symbols. One of the enabling techniques for OFDM is the insertion of CP [5,117] to mitigate the fiber induced dispersion. To prevent ISI, a cyclically extended GI is created. As shown in Figure 3.3, each OFDM symbol is preceded by a CP which is essentially an identical copy of the last portion of the data symbol appended to the front of the symbol during the guard interval. This CP preserves the orthogonality of the subcarriers and prevents the ISI between successive OFDM symbols. The condition for ISI-free OFDM transmission is given by

$$t_d < \Delta_G \tag{3.11}$$

where t_d is the time delay introduced by channel. The corresponding time-domain

OFDM symbol is illustrated in the Figure 3.3 that shows one complete OFDM symbol comprised of observation period and cyclic prefix. The waveform within the observation period is used to recover the frequency-domain information symbols.

The cyclic prefix introduces overhead into the system as it contains redundant information, therefore, a short guard time is preferable to minimize such overhead. It has been shown that the condition for ISI-free OFDM transmission is given by Eq. (3.11). Thus, the minimum guard time can be expressed as,

$$\frac{c}{f_c^2}|D|\,N_{sc}\Delta f + DGD_{MAX} \le \Delta_G \tag{3.12}$$

where f_c is the optical carrier frequency, c the speed of light, D the accumulated chromatic dispersion, DGD_{MAX} the maximum budgeted DGD, N_{sc} the number of subcarriers and Δf is the subcarrier spacing.

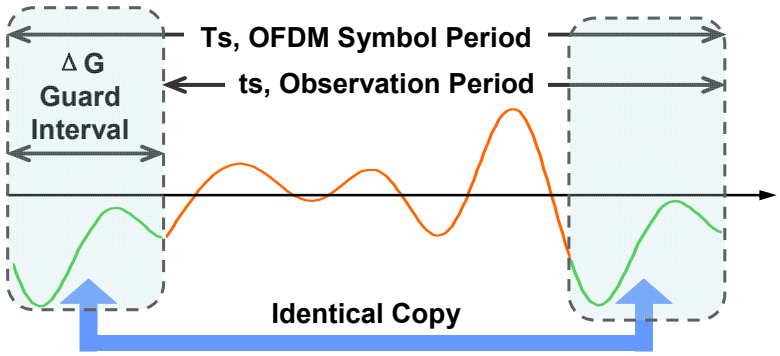

Figure 3.3 The time-domain OFDM signal for one complete OFDM symbol with cyclic prefix.

3.3 Coherent Optical OFDM Systems

3.3.1 CO-OFDM System Architecture

For CO-OFDM systems, the most critical assumption is a linear transformation in modulation, transmission, and demodulation. In general, electrical OFDM signals are complex valued data signals. There are two methods to linearly convert a complex valued data signal into the optical domain. First, upon applying a complex electrical I/Q mixer, the signal can be electrically up-converted with an electrical IF carrier. The resulting

up-converted electrical OFDM data signal can be E/O converted using an optical amplitude modulator. Alternatively, a complex E/O I/Q modulator can be driven directly by the complex electrical OFDM signal and thus converted into the optical domain. In optical receivers, optical coherent detection discussed in Section 2.2.3 are applied to realize a linear transformation from optical signal to RF (or electrical) signal via a direct detection or IF detection approach. By putting together such a composite system cross RF and optical domain, a linear channel can be constructed. Since the transmitter can be of either direct or IF up-conversion architecture, and the receiver can be of either direct or IF down-conversion architecture, there are four design choices for a CO-OFDM system.

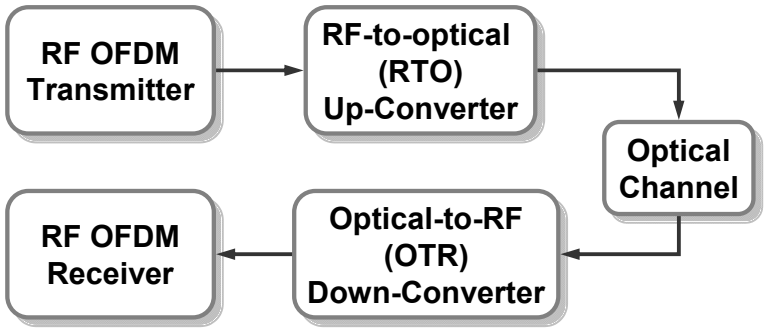

Figure 3.4 A generic CO-OFDM architecture

A generic CO-OFDM system can be divided into five functional blocks as shown in Figure 3.4. The RF OFDM transmitter is used to generate baseband OFDM signal. The main function of RTO up-converter is to convert OFDM signal from base-band to optical domain. The electrical signal can be obtained at the output of OTR down-converter. In the RF OFDM receiver, the down converted baseband OFDM signal is used to recover the data. A detailed discussion of CO-OFDM system architecture will be presented in Chapter 4.

3.3.2 Spectral Efficiency of OFDM Systems

In the CO-OFDM system, if N_{sc} subcarriers are transmitted in every OFDM symbol period, the total baud rate of a CO-OFDM signal can be calculated as

$$R = \frac{N_{sc}}{T_s} \tag{3.13}$$

where T_s is the symbol period including guard time and observation period as shown in Figure 3.3. Figure 3.5 shows the optical spectrum of a CO-OFDM signal. The bandwidth of one subcarrier is $2/T_s$. The frequency distance Δf between each subcarrier is $1/t_s$. The OFDM bandwidth, B_{OFDM} is thus given by

$$B_{OFDM} = \frac{2}{T_s} + \frac{N_{sc} - 1}{t_s} \tag{3.14}$$

where t_s and T_s is respectively the observation period and symbol period of one OFDM symbol. Assuming a large number of subcarriers used, the bandwidth efficiency of OFDM η is expressed [105]

$$\eta = 2\left(\frac{R}{B_{OFDM}}\right) = 2\alpha,\ \alpha = \frac{t_s}{T_s} \tag{3.15}$$

where R is the baud rate, the factor of 2 in Eq. (3.15) accounts for two polarizations in the fibre. Using a typical GI length of 1/8 [6,118] of the symbol period, we get an optical spectral efficiency factor of 1.8 Baud/s/Hz. The optical spectral efficiency is 3.6 bit/s/Hz if 4-QAM modulation is used for each subcarrier. The spectral efficiency can be further improved by using higher-order QAM modulation [119-120].

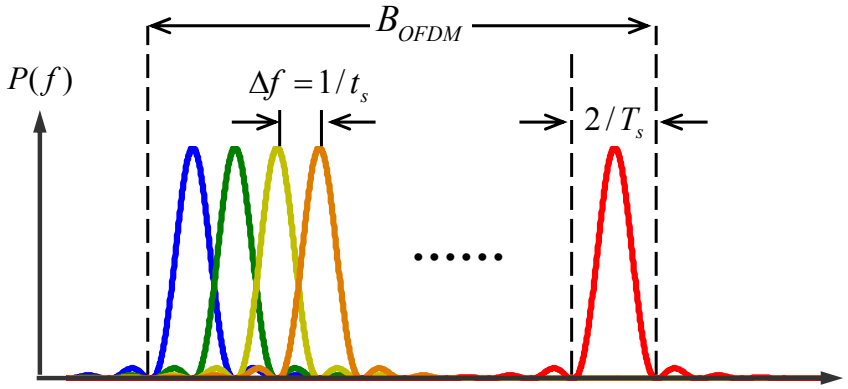

Figure 3.5 Optical spectrum of CO-OFDM signal with N_{sc} subcarriers.

3.3.3 Coherent Optical MIMO-OFDM Models

It is well known that the single-mode fiber supports two modes in the polarization domain. Each polarization mode travels with a slightly different speed due to PMD and undergoes

different loss due to polarization-dependent loss (PDL). Thus, instead of being represented by one element, the CO-OFDM signal model requires the mathematical description of the polarization effects as well as the fiber chromatic dispersion. Therefore, the optical channel model for a CO-OFDM signal can be represented by a multiple-input multiple-output (MIMO) model [34]. The transmitted baseband OFDM timed domain signal $s(t)$ of MIMO-OFDM model is described using Jones vector given by

$$\overrightarrow{s}(t) = \sum_{i=-\infty}^{\infty} \sum_{k=1}^{N_{sc}} \overrightarrow{c}_{ik} \prod (t - iT_s) e^{j2\pi f_k (t - iT_s)} \tag{3.16}$$

$$\overrightarrow{s}(t) = (s_x \quad s_y)^T, \ \overrightarrow{c}_{ik} = (c_{ik}^x \quad c_{ik}^y)^T \tag{3.17}$$

$$\prod(t) = \begin{cases} 1 & (0 < t < T_s) \\ 0 & (t \le 0, t > T_s) \end{cases} \tag{3.18}$$

We use *i* and *k* as the indices for OFDM symbol and OFDM subcarrier, respectively. N_{sc} is subcarrier number. s_x and s_y are the two polarization components for $\overrightarrow{s}(t)$, $\overrightarrow{c}_{ik}$ is the transmitted OFDM information symbol in the form of Jones vector for the *kth* subcarrier in the *ith* OFDM symbol.

The optical field launched into fiber is

$$E(t) = e^{(j\omega_{LD1} t + j\phi_{LD1})} \cdot \overrightarrow{s}(t) \tag{3.19}$$

where ω_{LD1} and ϕ_{LD1} are respectively the angular frequency and phase of the transmitter laser. The up-converted signal *E(t)* transmit through the optical medium with impulse response *h(t)*, and the received optical signal becomes

$$E_s(t) = e^{(j\omega_{LD1} + j\phi_{LD1})} \overrightarrow{s}(t) \otimes h(t) \tag{3.20}$$

where '$\otimes$' stands for convolution. The optical OFDM signal is then fed into the OTR down-converter where it is down converted to a frequency near-DC. By using optical I/Q detection and polarization diversity receiver, the electrical signal is a linear representation of the optical field. The resultant received base-band time domain signal is given by

$$r(t) = e^{(j\omega_{IF}t + j\Delta\phi)} \cdot \vec{s}(t) \otimes h(t)) \tag{3.21}$$

Where ω_{IF} and $\Delta\phi$ is the frequency and phase difference between transmitter laser and LO. The received information symbol after proper DFT window and frequency offset synchronization is given by

$$\vec{c_{ik}}' = e^{j\phi_i} \cdot H(f_k) \cdot \vec{c}_{ik} + \vec{n}_{ik} \tag{3.22}$$

$$H(f_k) = e^{j\Phi_D(f_k)} \cdot T_k \tag{3.23}$$

$$T_k = \prod_{l=1}^{N} \exp\left(-\frac{1}{2}j \cdot \vec{\beta}_l \cdot f_k - \frac{1}{2}\vec{\alpha}_l\right) \cdot \vec{\sigma} \tag{3.24}$$

$$\Phi_D(f_k) = \phi_0 + 2\pi\tau_0 \cdot f_k + \pi \cdot c \cdot D_t \cdot \frac{f_k^2}{f_{LD1}^2} \tag{3.25}$$

where $\vec{c}_{ik}{}' = (c_{ik}^{'x} \quad c_{ik}^{'y})^T$ is the received information symbol in the form of the Jones vector for the k_{th} subcarrier in the i_{th} OFDM symbol, $\vec{n}_{ik} = (n_{ik}^x \quad n_{ik}^y)^T$ is the noise including two polarization components. $H(f_k)$ is a 2×2 channel response matrix that includes CD and DGD. T_k is the Jones matrix for the fiber link, N is the number of PMD/PDL cascading elements represented by their birefringence vector $\vec{\beta}_l$ and PDL vector $\vec{\alpha}_l$ [121], $\vec{\sigma}$ is the Pauli matrix vector [121], f_k is the frequency of k_{th} subcarrier, $\Phi_D(f_k)$ is the phase dispersion owing to the fiber accumulated CD D_t is the fiber CD parameter, and ϕ_i is the OFDM symbol phase noise owing to the phase noises from the lasers and RF LO at both the transmitter and receiver. ϕ_i is usually dominated by the laser phase noise. Eq. (3.22) shows a MIMO model relating the two outputs $c_{ik}^{'x}$ and $c_{ik}^{'y}$ to the two inputs c_{ik}^x and c_{ik}^y.

Figure 3.6 shows a MIMO CO-OFDM system which consists of two CO-OFDM transmitters (one for each polarization), an optical link and two CO-OFDM receivers. As discussed in Section 3.3.1, the CO-OFDM transmitter comprises an RF OFDM transmitter and RTO up-converter whereas the CO-OFDM receiver comprises an OTR

down-converter and RF OFDM receiver. Each fibre span consists of chromatic dispersion and PMD/PDL. The optical noise is added from the optical amplifiers (OA) at the end of each span.

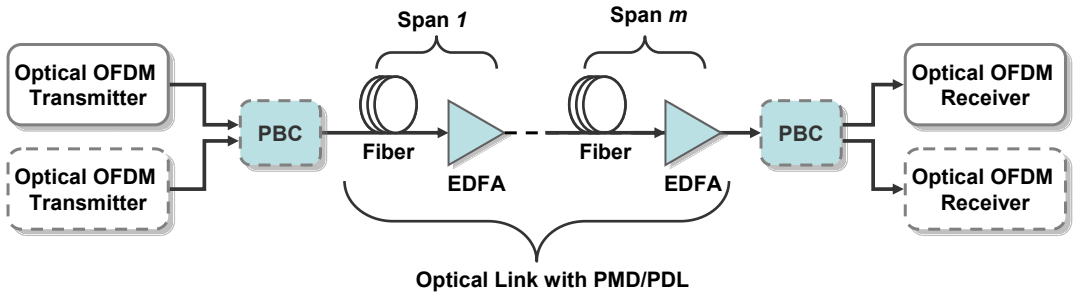

Figure 3.6 Conceptual diagram of a TITO coherent optical MIMO-OFDM model

According to the number of the transmitters and receivers used in the polarization dimension, for the MIMO system, the architecture of CO-OFDM system can be divided into four categories: single-input-single-output (SISO), single-input-two-output (SITO), two-input-single-output (TISO) and two-input two-output (TITO). The dashed line on the devices in Figure 3.6 indicates the variations of the architecture with the option to remove the device from the configuration.

- ***Single-input single-output***

One optical OFDM transmitter and one optical OFDM receiver are used for SISO CO-OFDM transmission. The SISO configuration is susceptible to the polarization mode coupling in the fiber, thus, a polarization controller is needed before the receiver to align the input signal polarization with the local oscillator polarization [35, 101]. More importantly, in the presence of large PMD, due to the polarization rotation between subcarriers, even the polarization controller will not function well. This is because there is no uniform subcarrier polarization that the local receiver laser can align its polarization with.

- ***Single-input two-output***

For SITO architecture, only one optical OFDM transmitter is used at the transmit end.

The polarization diversity receiver is employed at the receiver, meaning there are two optical OFDM receivers, one for each polarization. Therefore, there is no need for optical polarization control. Furthermore, the impact of PMD on CO-OFDM transmission can be easily treated through channel estimation and constellation reconstruction [106]. Coherent optical SITO-OFDM is resilient to PMD when the polarization-diversity receiver is used.

- ***Two-input single-output***

For TISO architecture, two optical OFDM transmitters are used at the transmit end, one for each polarization. Such transmitter configuration is called polarization-diversity transmitter. However, at the receive end, only one optical OFDM receiver is used. By configuring the transmitted OFDM information symbols properly, the CO-OFDM transmission can be performed without a polarization controller at the receiver. One possible transmission scheme is shown as follows:

At the transmitter, the same OFDM symbol is repeated in two consecutive OFDM symbols with orthogonal polarizations. For instance, this can be done by simply turning on and off the two transmitters alternately in each OFDM symbol. The transmitted OFDM information symbols for the two consecutive OFDM symbols are written as

$$\overrightarrow{c}_{(2i-1)k} = a_{ik}\begin{pmatrix}0\\1\end{pmatrix} \tag{3.26}$$

$$\overrightarrow{c}_{(2i)k} = a_{ik}\begin{pmatrix}1\\0\end{pmatrix} \tag{3.27}$$

By combining two consecutive OFDM symbols (number $2i-1$ and number $2i$), the received Jones vector is given by

$$\overrightarrow{c}'_{ik} = a_{ik}T_k\begin{pmatrix}1\\0\end{pmatrix} \tag{3.28}$$

It can be seen from Eq. (3.28) that TISO can also achieve PMD supported transmission. However, same information symbol is repeated in two consecutive OFDM symbols, and subsequently the electrical and optical efficiency is reduced by half, and the OSNR requirement is doubled, compared with the SITO scheme.

- ***Two-input two-output***

Both a polarization-diversity transmitter and a polarization-diversity receiver are employed in the TITO scheme. Firstly, the capacity is doubled compared with SITO scheme. As the impact of the PMD is to simply rotate the subcarrier polarization, and can be treated with channel estimation and constellation reconstruction, and therefore the doubling of the channel capacity will not be affected by PMD. Secondly, due to the polarization-diversity receiver employed at the receive end, TITO scheme does not need polarization tracking at the receiver.

3.3.4 Signal Processing of CO-OFDM Systems

Advanced DSP which relays on the increased performance, speed, and reliability with reduction in size and cost of integrated circuits is one of the enabling factors of the rebirth of coherent detection optical system. As a multi-carrier coherent detection optical system, DSP also plays an important part in CO-OFDM systems. Compared to the conventional single-carrier coherent system which relays on the blind equalization, for instance, Constant Modulus algorithm (CMA) algorithm, or decision feedback, all of which is prone to error propagation, CO-OFDM provides easiness of signal processing by using pilot symbols and pilot subcarrier. The signal processing for CO-OFDM system includes: FFT window synchronization, frequency synchronization and subcarrier Recovery.

- ***FFT Window Synchronization***

Synchronization is one of the most critical functionalities for a CO-OFDM receiver. It can be divided into three levels of synchronization: DFT window timing synchronization, carrier frequency offset synchronization, and subcarrier recovery. Figure 3.7 shows the time-domain structure of an OFDM signal consisting of many OFDM symbols. Each OFDM symbol is comprised of guard interval and observation period.

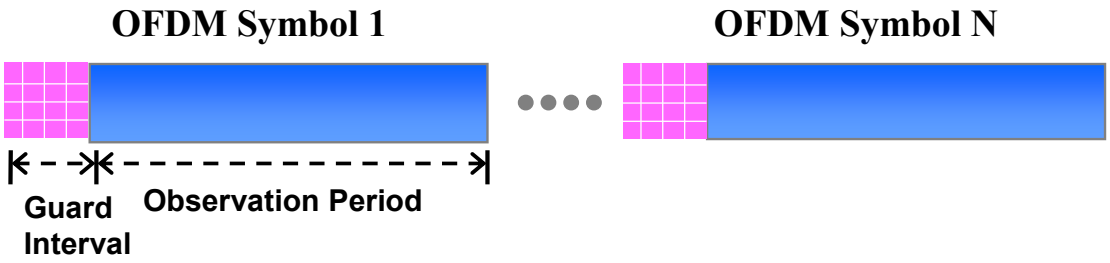

Figure 3.7 Time-domain structure of an OFDM signal

It is imperative that the start of the DFT window, i.e., the observation period, is determined properly, as an improper DFT window will result in ISI and ICI [117]. A popular method of window synchronization was proposed by Schmidl and Cox [122]. In this method, a pilot symbol or preamble is transmitted consisting of two identical segments as

$$s_m = s_{m-N_{sc}/2}, \quad m \in [N_{sc}/2+1, N_{sc}] \tag{3.29}$$

where s_m is the m_{th} digital signal with a random value. The received pilot symbol will have the form

$$r_m = r(mt_s/N_{sc}) = r_m^0 e^{j\omega_{off} m t_s/N_{sc}} + n_m \tag{3.30}$$

A correlation function of the sampled received signal r_m is then calculated:

$$R_d = \sum_{m=1}^{N_{sc}/2} r_{m+d}^* r_{m+d+Nsc/2} \tag{3.31}$$

Because the second half of r_m is identical to the first half except for a phase shift, assuming the frequency offset ω_{off} is small to start with, when $d = 0$, i.e. at the correct timing, the correlation function reaches its maximum value.

- ***Frequency Offset Synchronization***

The frequency offset in an OFDM system breaks the orthogonality between the subcarriers, incurring ICI penalty. The frequency synchronization process for CO-OFDM systems is divided into two phases, frequency acquisition and frequency tracking [123].

The purpose of the frequency acquisition is to coarse estimate the frequency offset to simplify the receiver signal processing and bring the receiver laser approximately within several times of the subcarrier frequency spacing, typically approximately 100–500 MHz from the transmit laser. Frequency acquisition can be achieved by sending a long-stream CW and measuring the frequency of the offset tone. The purpose of the frequency tracking is to identify the magnitude of the frequency offset and compensate for it. Although various approaches can be used for this purpose, we also use the Schmidl and Cox approach for the frequency tracking [122]. From eq. (3.31) we get

$$R_{\hat{d}} = \sum_{m=1}^{N_{sc}/2} \left| r^{0}_{m+\hat{d}} \right|^{2} e^{j(\pi f_{off}/\Delta f)} + o(n) \tag{3.32}$$

where $o(n)$ stands for the residual term with the magnitude of the order of the noise component. Then the offset frequency can be estimated as

$$\hat{f_{off}} = \frac{\Delta f}{\pi} \arg\left(R_{\hat{d}}\right) \tag{3.33}$$

Once the frequency offset is estimated, the received sampled signal will be compensated as

$$r_c(t) = \exp\left(-j2\pi \hat{f_{off}} t\right) r(t) \tag{3.34}$$

- ***Subcarrier Recovery: Phase Estimation and Channel Estimation***

There are three factors that leads to the rotations of the receiver information symbol constellation for $\overrightarrow{c}_{ik}{}'$ as shown in E.q (3.22), which are the channel dispersion, the DFT sampling timing offset, and the phase noises. In the receiver signal processing, the first two factors are dealt with through channel estimation. The third factor is treated through phase estimation and compensation. The signal processing is assumed to be performed in blocks, each containing a large number of OFDM symbols. Within each block, the optical channel is assumed to be invariant, whereas the laser phase noise varies on the OFDM

symbol basis. For the sake of simplicity, we only show the channel estimation and phase estimation for SISO system and the subcarrier recovery can be performed in the same way for other MIMO architectures.

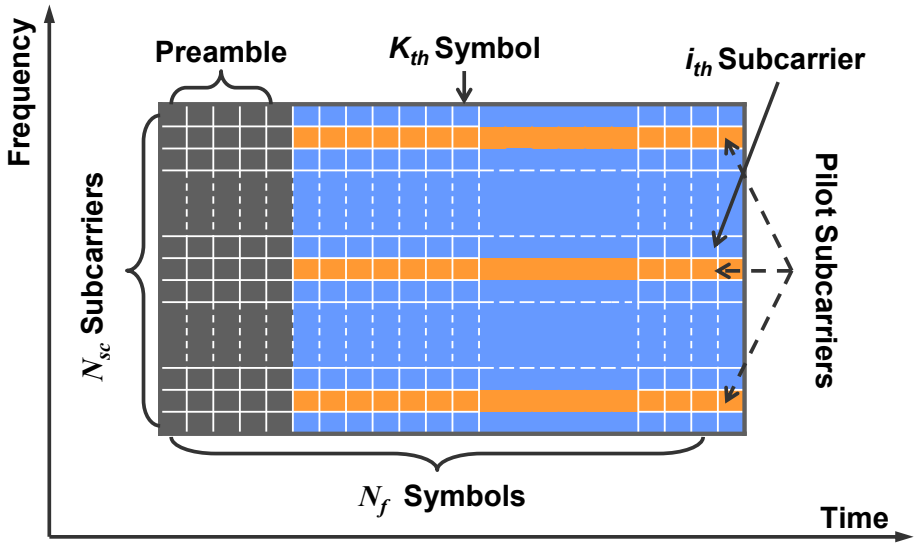

Figure 3.8 Time and frequency representation of a block of CO-OFDM signal

There are various methods of channel estimation such as time-domain pilot-assisted approach and frequency-domain assisted approach [124-125]. We will focus on the carrier recovery based upon frequency-domain pilot carriers or pilot symbols. Figure 3.8 shows the two dimensional time/frequency structure for one OFDM block, which includes N_{sc} subcarriers in frequency domain and N_f OFDM symbols in time domain. The preamble is added at the beginning to realize DFT window synchronization and channel estimation. The channel transfer function can be estimated as

$$\hat{h_k} = \sum_{i=1}^{p} e^{-j\angle r_{k_l i}} \frac{r_{ki}}{c_{ki}} \tag{3.35}$$

where c_{ki} and r_{ki} are respectively transmitted and received pilot subcarriers, $\angle r_{k_l i}$ is the angle for the k_l th carrier (an arbitrary reference carrier) in the ith OFDM symbol, p is the number of pilot symbols in preamble. The additional phase compensation of $-\angle r_{k_l i}$ is

needed to remove the influence of the common phase error (CPE). The estimated channel transfer function has uncertainty of a common phase, which can be included in the CPE ϕ_i.

The phase estimation is to estimate the ϕ_i due to the laser phase noise. We assume that N_p pilot subcarriers are used for phase estimation, the maximum likelihood CPE can be estimated as [126]

$$\phi_i = \arg\left(\sum_{k=1}^{N_p} \frac{c'_{ki} h_k^* c_{ki}^*}{\delta_k^2}\right) \tag{3.36}$$

where δ_k is the standard deviation of the constellation spread for the k_{th} subcarrier.

3.4 Advantages Offered by CO-OFDM Systems

CO-OFDM combines the advantages of 'coherent detection' and 'OFDM modulation' and offers many advantages:

1) With the insertion of CP, the CD and PMD of the transmission system can be effectively estimated and mitigated at receiver end through signal processing, thus no dispersion compensation fiber is needed. Such dispersion compensation-free design enables the dynamically reconfigurable networks where ROADMs are deployed to increase network transparency.

2) The spectra of OFDM subcarriers are partially overlapped, resulting in high optical spectral efficiency which is very suitable for the future high capacity optical transmission system.

3) By using direct up/down conversion, the electrical bandwidth requirement can be greatly reduced for the CO-OFDM transceiver, which is extremely attractive for the high-speed circuit design, where electrical signal bandwidth dictates the cost.

4) The signal processing in the OFDM transceiver can take advantage of the efficient algorithm of FFT/IFFT. Without any hardware change, each subcarrier can have different modulation formats which suggests that OFDM has superior scalability over the channel dispersion and data rate. One of the most simple and effective ways,

called bit and power loading, is done by optimally allocating different modulation schemes or power across all the subcarriers [127]. In such a scheme, different frequency tones are loaded with a different modulation format or power [128]. In so doing, the system performance, such as BER, can be improved [129].

5) The fiber nonlinear phase noise can be mitigated by digital signal processing. For example, the nonlinear phase noise can be mitigated through receiver digital signal processing based on a lump nonlinear compensation [36] or using digital phase conjugation (DPC) and distributed nonlinearity compensation [130]

3.5 Comparison of Single-carrier and Multi-Carrier Coherent Optical Systems

For the single-carrier and multi-carrier system, there are two conspicuous differences: i) the single carrier system usually employ a relatively 'conventional' and simpler architecture. In contrast, for the CO-OFDM architecture, the electronic DSP module and DAC are required for complex OFDM signal generation at the transmit end. The OFDM transmitter strictly enforces linearity in each components associated with the CO-OFDM transmitter. (ii) In the single-carrier systems, the information is coded in the time domain whereas the in CO-OFDM, the information is encoded in the frequency domain. Centred on these two basic differences, CO-OFDM provides the following advantages:

- ***Easiness of signal processing.***

In CO-OFDM based multi-carrier systems, by using pilot symbols and pilot subcarriers, the channel estimation and phase estimation can be relatively simple. However, in the single-carrier coherent systems, the channel estimation has to rely on the blind equalization, for instance, using CMA algorithm, or decision feedback, all of which is prone to error propagation. The phase estimation usually adopts Viterbi algorithm, which is mostly effective for the pure phase modulation and less effective to other constellation modulation. Furthermore, the differential-phase coding needs to be employed to resolve

the intrinsic phase ambiguity for Mth-power law algorithm, resulting in the approximately a factor of 2 of BER increase [46].

- ***Higher-order modulation***

With the increasing of spectral efficiency in transmission, optical transmission system should be designed to support high-order modulation format. For CO-OFDM system, the scale to higher-order modulation format can be simply achieved via the software to reconfigure the DSP and DAC. In contrast, the higher-order single-carrier optical system requires more complicated optical modulators configuration, which inevitably increases the system complexity and cost.

- ***Tight-bounding of spectral components.***

The OFDM spectral shape is tightly bounded and is more tolerant to the filter narrowing effect. Even if the edge subcarriers are attenuated by the narrowing filtering, some bit and power loading scheme along the spirit of water filling [131] can be employed to mitigate the effect. In contrast, the filtering narrowing effect not only causes the pulse distortion, but also makes it susceptible to the timing jitter for the single-carrier system.

3.6 Conclusion

OFDM is a special form of a broader class of MCM. It has an important property that the carrier spacing is minimized since each of its frequency is orthogonal with every other frequency. The introduction of IDFT/DFT for OFDM modulation/demodulation not only greatly reduces the transmitter/receiver complexity but also increase the computation efficiency. Another enabling technique for OFDM is the insertion of CP which is an identical copy of the last portion of the data symbol appended to the front during the guard interval. This CP preserves the orthogonality of the subcarriers and prevents the ISI between successive OFDM symbols.

Combined with coherent detection, OFDM is an effective way to eliminate the CD and PMD distortion. A generic CO-OFDM system can be divided into five functional blocks as RF OFDM transmitter, RTO up-converter, OTR down-converter, optical

channel and RF OFDM receiver. Based on the fact that single-mode fiber supports two modes in the polarization domain, MIMO OFDM can be realized for optical communication. Except for SISO-OFDM, all MIMO-OFDM variations can be PMD resilient and support coherent detection without optical polarization tracking. Before the signal can be correctly received, a series of signal processing need to be carried out to synchronize the FFT window and frequency offset and recover the subcarrier. Compared with single carrier optical system, multi-carrier system offers more benefits as easiness of signal processing, higher-order modulation, tight-bounding of spectral components and so on.

Chapter 4

Optimum Design for CO-OFDM Transmitter

4.1 Introduction

It is well known that OFDM is very sensitive to nonlinearity. Therefore, a linear transformation is the key goal for the OFDM implementation. A generic optical OFDM system can be divided into five functional blocks including (i) the RF OFDM transmitter, (ii) the RTO up-converter, (iii) the optical channel, (iv) the OTR down-converter, and (v) the RF OFDM receiver. If the fiber nonlinearity is not considered, the challenges for CO-OFDM implementation are to obtain a linear RTO up-converter and linear OTR down-converter. It has also been shown in Chapter 2 that by using coherent detection, a linear transformation from optical field signal to RF (or electrical) signal can be achieved. Thus, the investigation of the nonlinearity of RTO up-converter is of vital importance. For CO-OFDM system, RTO conversion is performed by two MZMs. It has been shown that the MZM has a *sine* shape transfer function and large signal will add nonlinearity impairment to the system. Therefore, MZM nonlinearity has significant impact on the CO-OFDM system performance. Subsequently, a thorough investigation of compensation of the MZM nonlinearity is of great interests.

In this chapter, we conduct analysis on the optimum design for a coherent optical OFDM up-converter using an optical I/Q modulator. We first present the architecture choices for a generic CO-OFDM system in Section 4.2. A brief introduction on the principle of MZM is given in Section 4.3. In Section 4.4, the optical I/Q modulator nonlinearity in coherent optical OFDM system based on direct up/down conversion is analyzed. Section 4.5 focuses on the CO-OFDM transmitter design employing digital pre-distortion. The optimum transmitter design is presented in terms of clipping ratio, I/Q modulator excess insertion loss, and DAC resolution.

4.2 Up/down Conversion Design Options for CO-OFDM Systems

As we have known that a generic CO-OFDM system consists of RF OFDM transmitter, RTO up-converter, Optical channel, OTR down-converter and RF OFDM receiver. Figure 4.1 (a) and Figure 4.1 (b) show respectively a CO-OFDM system uses direct up/down conversion architecture and IF architecture. The direct-conversion architecture eliminates a need for narrow OBPF in both transmitter and receiver.

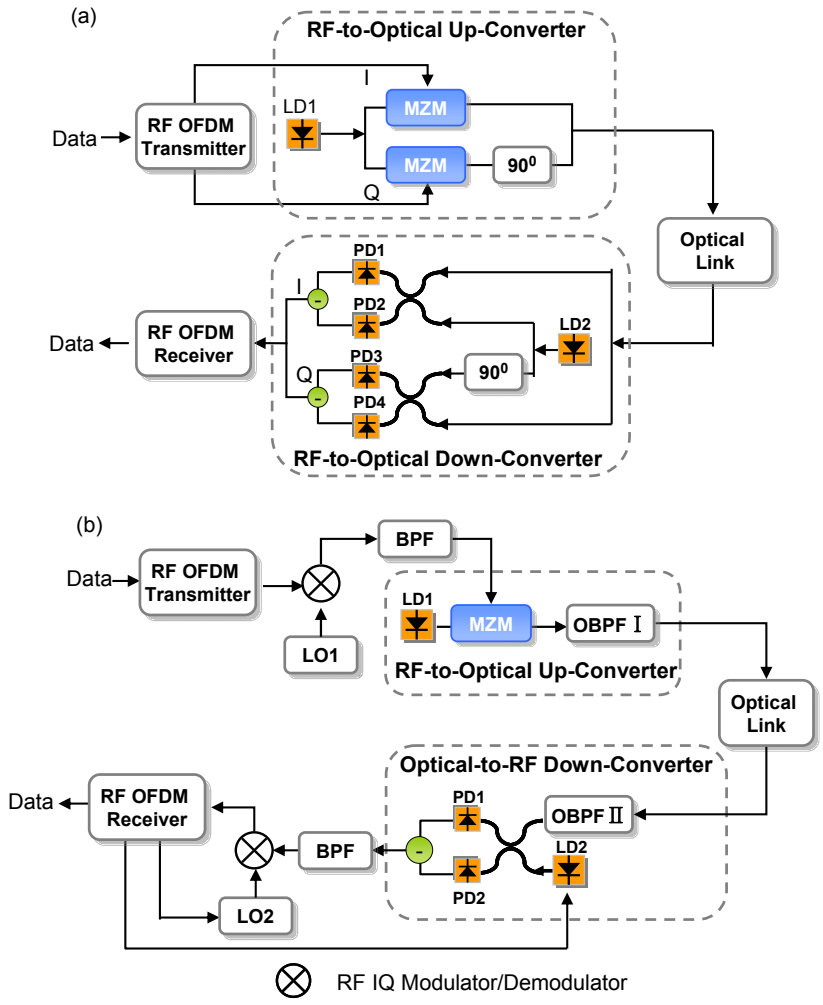

Figure 4.1 A CO-OFDM system with (a) direct up/down conversion architecture, (b) intermediate frequency architecture

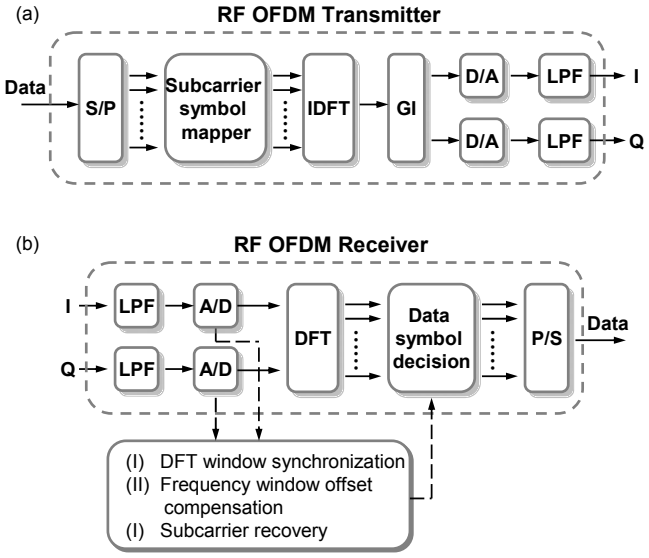

Figure 4.2 Conceptual diagram for the RF-OFDM transmitter and receiver

- ***RF OFDM Transmitter***

The RF OFDM transmitters in both architectures share the same functionality and are used to generate baseband OFDM signal. The detailed architecture for the RF OFDM transmitter is shown in Figure 4.2 (a). The function of RF OFDM transmitter including, i) convert the input stream of binary digits from serial into N_{sc} parallel sub-streams, and each sub-stream will be mapped to a complex symbol c_{ki} using some modulation scheme such as QAM or Phase Shift Keying (PSK). ii) the complex digital time domain OFDM signal is obtained by computing IDFT on each set of complex symbol and inserted with guard interval to prevent inter-symbol-interference induced from channel dispersion. The resultant base band time domain digital is

$$S_B(t) = \sum_{k=-N_{sc}/2+1}^{k=N_{sc}/2} C_k \exp(j2\pi k f_k t), \quad f_k = (k-1)/t_s \tag{4.1}$$

where N_{sc} is the number of subcarriers, t_s is the OFDM symbol period, c_k is the information symbol at the kth subcarrier, f_k is the frequency of the subcarrier. For the sake of simplicity, the OFDM signal in (4.1) only shows one OFDM frame. iii) The digital signal is then converted to analog through two DACs, and filtered with a low-pass filter (LPF) to remove the alias sideband signal.

- ***RF-to-optical up-converter***

The main function of RTO up-converter is to convert OFDM signal from banes-band to optical domain. For the direct conversion architecture, the RTO up-converter uses an optical I/Q modulator which comprises two MZMs to up convert the real/imaginary parts of the $S_B(t)$ from the RF domain to the optical domain, i.e., each MZM is respectively driven by the real or imaginary part of the $S_B(t)$. In the IF architecture, the OFDM base-band signal is first up-converted to an intermediate frequency f_{LD1}. The real part of the IF signal is further up-converted to optical domain with one MZM.

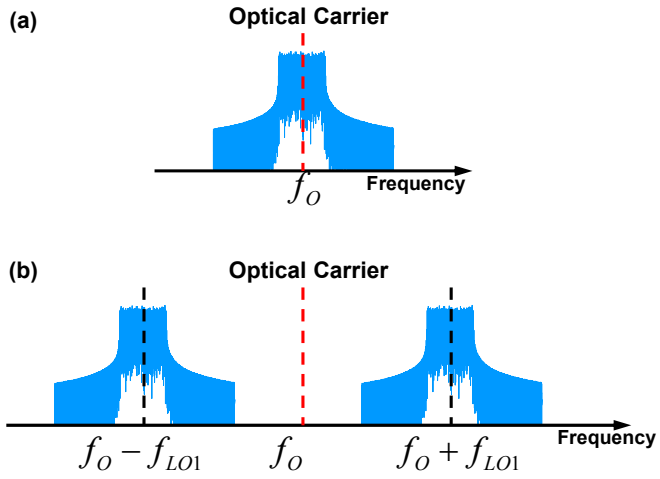

Figure 4.3 Optical OFDM spectrum for the (a) direct up/down conversion and (b) IF architectures

Figure 4.3 (a) and (b) respectively shows the optical OFDM spectrum for direct up/down conversion architecture and IF architecture. It can be seen that, for direct up/down conversion architecture, because of the I/Q modulation, only one side-band is transmitted and the optical carrier is at the middle of the signal spectrum. For IF architecture, at the output of RTO up-converter, two optical OFDM sidebands are generated which are $\pm f_{LD1}$ away from the optical carrier. Thus, one of the two optical sidebands should be selected with an optical band-pass filter and all other sidebands plus the optical carrier should be rejected.

- ***Optical-to-RF down-converter***

The electrical signal can be obtained at the output of OTR down-converter. For the direct up/down conversion architecture, the OTR down-converter uses two pairs of balanced receivers and one optical hybrid to perform I/Q detection optically. In the IF architecture, OTR down-converter consists of one pair of balanced photodetectors to down convert the optical OFDM signal to an intermediate frequency. An OBPF is used before photodetectors to eliminate interference and optical noise from the image frequency to the OFDM spectrum. The OFDM IF signal will be further down-converted to baseband and the I/Q detection is performed in electrical domain.

- ***RF OFDM receiver***

In RF OFDM receiver, the down converted base-band OFDM signal is first sampled with an ADC. The sampled data is then processed with a DFT block. Then the signal needs to go through a three-level synchronization as addressed in Section 3.3.4 before the symbol decision can be made.

4.3 Principle of MZM

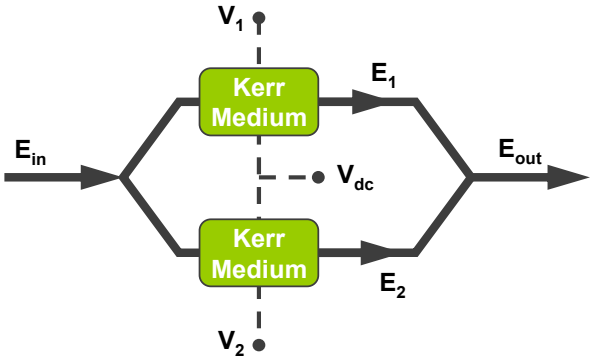

Figure 4.4 Structure of a MZM

MZM is a basic building block used to design optical communication links by the principle of interference based on the electro-optic crystal. The MZM can be fabricated using various materials [132-138]. The main stream is based on the LiNbO3 crystal. Nowadays, almost all commercial long-haul WDM systems use LiNbO MZMs.

A diagram of a MZM is shown in Figure 4.4. The incoming optical source E_{in} is split

into two fields E_1 and E_2. Each field then propagates through a Kerr medium. Due to the electro-optic effect, each field experiences a phase delay ϕ_1 and ϕ_2 which can be controlled by the applied voltages $V_1(t)$ and $V_2(t)$ as shown in Figure 4.4. Such phase delay can be expressed as

$$\phi_{1/2}(t) = K \cdot V_{1/2}(t) = \phi_0 - \pi \frac{V_{1/2}}{V_\pi} \tag{4.2}$$

Where K is electro-optic factor, ϕ_0 is the phase shift when the applied voltage is zero and V_π is the voltage required to induce a π phase shift. Then the fields are re-combined to give the output E_{out}, which has the form

$$\begin{aligned} E_{out} &= \frac{E_{in}}{2}\left(\exp\left(j\phi_1(t)\right) + \exp\left(j\phi_2(t)\right)\right) \\ &= E_{in}\cos\left(\frac{\phi_1(t) - \phi_2(t)}{2}\right)\exp\left(j\frac{\phi_1(t) + \phi_2(t)}{2}\right) \end{aligned} \tag{4.3}$$

The phase of E_{out} is given by the complex exponential term in Eq. (4.3) which can be expressed as

$$\phi_{out} = \frac{1}{2}\big(K \cdot V_1(t) + K \cdot V_2(t)\big) \tag{4.4}$$

Typically, MZMs are operated in the "push-pull" mode meaning $V_2(t) = -\zeta V_1(t), \zeta = 1$. This gives the output phase and amplitude of the modulator as,

$$\phi_{out} = \frac{KV_1(t)}{2}(\zeta - 1) \tag{4.5}$$

$$E_{out} = E_{in}\cos\left(\frac{K \cdot V_1(t)}{2}(1 + \zeta)\right) \tag{4.6}$$

When $\zeta = 1$, the output phase is zero and the output field is written as:

$$E_{out} = E_{in}\cos\big(K \cdot V_1(t)\big) \tag{4.7}$$

Converting the output field in Eq. (4.7) and to intensity and using E.q (4.2) we can get

$$I_{output} = \frac{1}{2} I_0 \cos(\phi_0 - \pi \frac{V(t)}{V_\pi}) \tag{4.8}$$

Because ϕ_0 is constant, for the purpose of studying chirp, without loss of generality, we can set it to zero, then E.q (4.8) can be written as

$$I_{output} = \frac{1}{2} I_0 \left(1 + \cos \left(\frac{\pi V(t) + V_{DC}}{V_\pi} \right) \right) \tag{4.9}$$

where, $I_0 = |E_{in}|^2$ is the input optical intensity, *V(t)* is the applied voltage, V_π is the voltage required to change the output light intensity from its maximum value to its minimum value, V_{DC} is the DC voltage used to control the modulator bias point. From Eq. (4.9) we can see that MZM has a sine shape transfer curve as shown in Figure 4.5. It is common practice to set bias point at 50% transmission point, known as the Quadrature bias point. The electrical digital signals are transformed into optical digital signal by switching voltage to both ends from quadrature point.

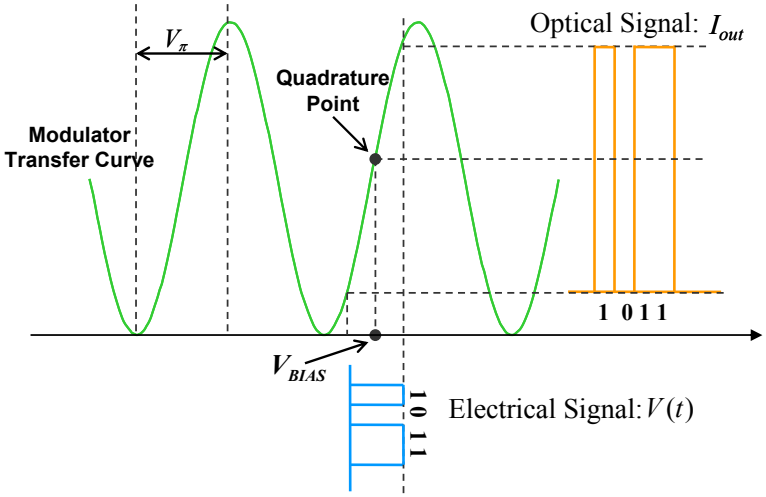

Figure 4.5 Power transmission function of a MZM

The integrated optical I/Q Modulator has a nested MZM structure which is capable of converting the full complex plane of the optical field. Each of the two primary arms contains sub MZM structures, as shown in Figure 4.6. Two independent electrical signals are applied to two RF ports (RFA and RFB) for modulation. Two sub-MZMs (MZMA and MZMB) are operated at chip-free (push-pull) mode. Three DC ports (DCA, DCB and

DCC) are for biasing two sub-MZMs and one primary MZM. The real and imaginary part of the electrical signal are applied to RFA and RFB respectively. The 90^0 phase shift between MZMA & MZMB can be achieved by applying DC voltage to port DCC.

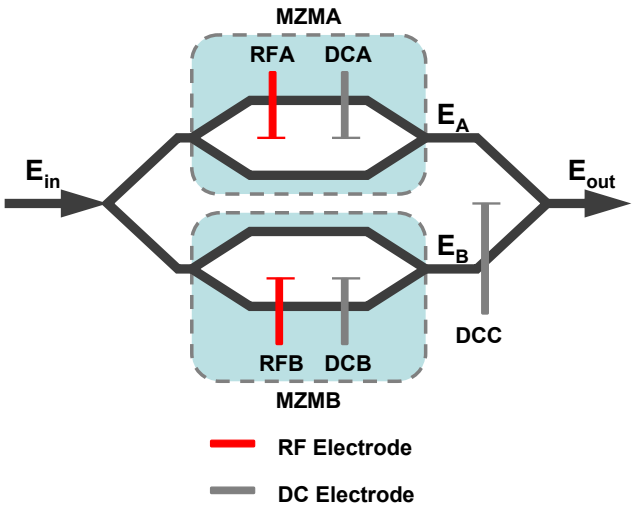

Figure 4.6 Structure of a nested MZM

4.4 Modulator Nonlinearity Impact on CO-OFDM Systems

4.4.1 Two-tone Inter-modulation Analysis

The CO-OFDM system which uses direct up/down conversion architecture (Figure 4.1 (a)) is used for the investigation of the modulator nonlinearity impact. A two-tone inter-modulation analysis is used to study the impact of I/Q modulator nonlinearity impact on the coherent optical OFDM system.

Two-tone inter modulation measurement is a common way to analyse the nonlinear RF devices, such as receivers, linear amplifiers and mixers. For MZM, the modulated light intensity is proportional to the product of the input intensity and the driving voltage, thus it can be viewed as a RF mixer. The optical I/Q modulator used by the direct up/down conversion architecture consists of two MZMs for respectively modulating the I and Q components of a complex driving signal. Thus, the optical I/Q modulator can be treated as a complex mixer. In this case, the input optical signal is equivalent to the LO, and the electrical signal driving the modulator is equivalent to the RF input. The

photocurrent obtained by detecting the modulated light becomes the IF output of this mixer. The two-tone inter modulation analysis is usually performed by applying two equal amplitude *sine* tones at frequency ω_1 and ω_2 to the RF port or the electrical signal driving port of a MZM. Due to the nonlinearity, the n_{th} order inter-modulation products appears at n times the frequency spacing of the input tones as shown in Figure 4.7. For example, the second order terms are located at $\pm(\omega_{1,2} - \omega_{2,1})$, the third order terms are located at $\pm(2\omega_{1,2} - \omega_{2,1})$. The amplitude of the inter-modulation tones is measured at the output of the photo detector. For small electrical driving signals, the n_{th}-order terms grow as the cube of the input voltage while the first order terms grow linearly.

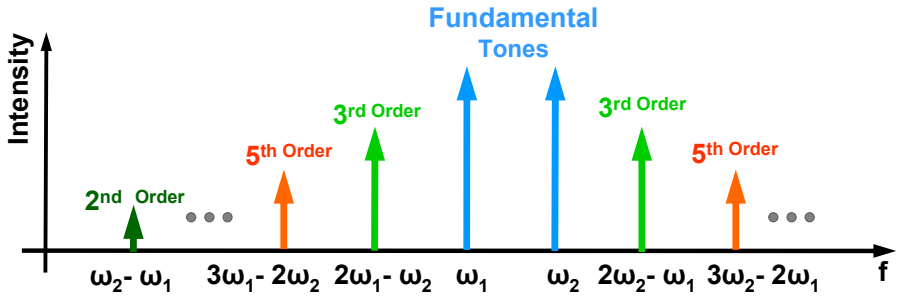

Figure 4.7 The n_{th} order inter-modulation products

The n_{th} order intercept point (IPN) is used to characterize the MZM nonlinearity which can be obtained graphically by plotting the output powers of the fundamental tone and the inter-modulation tone versus the input power/output power on logarithmic scales (e.g., decibels). Both curves are extended with straight lines. The point where the curves intersect is the intercept point. The third order intercept point is one of the key distortion parameters that is often used as a guideline for the upper limit on operating powers. The reason that the third-order term is particularly important is because it is only $\Delta\omega = \omega_1 - \omega_2$ away from the desired fundamental terms, and it may fall within the pass-band of the IF signall. In our study, since the I/Q modulator is equivalent to a complex mixer, two complex subcarrier tones will be applied. For the CO-OFDM direct down conversion architecture, the coherent detection is capable of linearly down convert an optical field directly to a baseband electrical signal. Therefore, we will measure the inter-modulation tone after the coherent detection instead of at the MZM output port.

By adopting the same procedures as described in the above paragraph, two complex subcarrier tones at $V_1 = ve^{j\omega_1 t}$ and $V_2 = ve^{j\omega_2 t}$ are applied to the input of the optical I/Q modulator. v is the root mean square (RMS) value of the complex subcarrier tone. By operating the MZM at 'push-pull' mode, the optical signal at the output of the RF-to-optical up-converter is

$$\begin{aligned} E(t) =& \alpha \cos\left(\frac{\pi}{2} \cdot \frac{V_I + V_{DC}}{V_\pi}\right) \exp\left(j\omega_{LD1} t\right) + \\ & \alpha \cos\left(\frac{\pi}{2} \cdot \frac{V_Q + V_{DC}}{V_\pi}\right) \exp\left(j\omega_{LD1} t + \pi/2\right) \end{aligned} \tag{4.10}$$

where α is a proportionality constant. All the proportionality constants will be omitted in the remainder of the paper. V_I and V_Q are real and imaginary part of the complex RF drive signal to each MZM, expressed as

$$\begin{aligned} V_I &= v(\cos\omega_1 t + \cos\omega_2 t) \\ V_Q &= v(\sin\omega_1 t + \sin\omega_2 t) \end{aligned} \tag{4.11}$$

V_{DC} is the DC bias voltage of the modulator, V_π is the half-wave switching voltage, ω_{LDI} is the modulator laser carrier frequency. Then the optical signal $E(t)$ is directly fed into the Optical-to RF down converter without going through the fiber link. The output of two balanced receivers can be written as

$$\begin{aligned} I_I(t) &= \cos\left(\frac{\pi}{2}\frac{V_I + V_{DC}}{V_\pi}\right) \\ I_Q(t) &= \cos\left(\frac{\pi}{2}\frac{V_Q + V_{DC}}{V_\pi}\right) \end{aligned} \tag{4.12}$$

It should be noted that the proportionality constants in Eq. (4.12) are omitted for simplicity. The signal feeding the RF OFDM receiver becomes

$$S(t) = \cos\left[\frac{M}{2}(\cos\omega_1 t + \cos\omega_2 t) + \frac{\phi}{2}\right] + j \cdot \cos\left[\frac{M}{2}(\sin\omega_1 t + \sin\omega_2 t) + \frac{\phi}{2}\right] \tag{4.13}$$

where *M* is defined as the modulation index, which can be expressed as

$$M = \frac{v\pi}{V_\pi} = \frac{v_{RMS}\pi}{V_\pi} \tag{4.14}$$

V_{RMS} is the RMS value of the complex driving signal, and $\phi = V_{DC}\pi/V_\pi$ is the static phase shift (bias point). The so-defined modulation index *M* equals the optical modulation index of the optical signal if the optical modulator is biased at quadrature in a direct-detected system. Expanding the *cosine* term in (4.13) using Bessel functions, we can get the expression for the fundamental output component with frequency ω_1 and ω_2 as

$$\begin{aligned} S_{\omega 1}(t) &= 2 \cdot \sin(\phi/2) \cdot J_0(M/2) \cdot J_1(M/2) \cdot e^{j\omega_1 t} \\ S_{\omega 2}(t) &= 2 \cdot \sin(\phi/2) \cdot J_0(M/2) \cdot J_1(M/2) \cdot e^{j\omega_2 t} \end{aligned} \tag{4.15}$$

The second-order intermodulation output with frequency $\omega_1 - \omega_2$ and $\omega_2 - \omega_1$ can be expressed as

$$\begin{aligned} S_{\omega 1-\omega 2}(t) &= 2 \cdot \cos(\phi/2) \cdot J_1^2(M/2) \cdot e^{j(\omega_1-\omega_2)t} \\ S_{\omega 2-\omega 1}(t) &= 2 \cdot \cos(\phi/2) \cdot J_1^2(M/2) \cdot e^{j(\omega_2-\omega_1)t} \end{aligned} \tag{4.16}$$

The third-order intermodulation output with frequency $2\omega_1 - \omega_2$ and $2\omega_2 - \omega_1$ will be

$$\begin{aligned} S_{2\omega 1-\omega 2}(t) &= 2 \cdot \sin(\phi/2) \cdot J_1(M/2) \cdot J_2(M/2) \cdot e^{j(2\omega_1-\omega_2)t} \\ S_{2\omega 2-\omega_1}(t) &= 2 \cdot \sin(\phi/2) \cdot J_1(M/2) \cdot J_2(M/2) \cdot e^{j(2\omega_2-\omega_1)t} \end{aligned} \tag{4.17}$$

The DC term or the amplitude of the optical carrier is given as

$$S_{DC} = \cos(\phi/2) \cdot J_0^2(M/2) \tag{4.18}$$

Notice that the bias point ϕ sets the values of the different mixing products. When

$\phi = \pm\pi, \pm 3\pi ...$, only odd-order terms remain and DC term is suppressed, and when $\phi = 0, \pm 2\pi, ...$, even-order and DC terms remain. Figure 4.8 (a) and (b) show the characteristics of the first-, second-, and third-order intermodulation as a function of the modulation index *M* for a bias point of π and quadrature respectively. It can be seen that at the bias point of π, the fundamental output is maximized while the second-order intermodulation product is eliminated in comparison with the quadrature bias point.

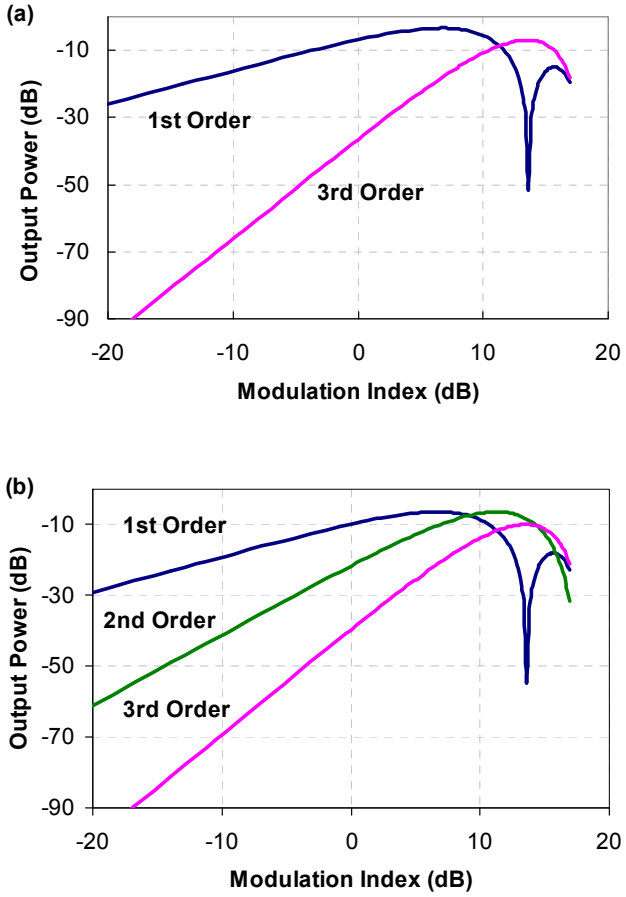

Figure 4.8 The first-, second-, and third-order output powers as a function of modulation index M(dB)=20logM at the bias points of (a) π, and (b) π/2

We then employ the standard IPN to characterize the modulator nonlinearity [139]. The intercept points are given in terms of fundamental output power. We can calculate the exact expression for the IP2 and IP3 by setting

$$|S_{\omega 1}(t)| = |S_{\omega 1-\omega 2}(t)|$$
$$|S_{\omega 1}(t)| = |S_{2\omega 1-\omega 2}(t)| \quad (4.19)$$

Then we get

$$\sin(\phi/2)J_0(M_{IP2}/2)J_1(M_{IP2}/2) = \cos(\phi/2)J_1(M_{IP2}/2)J_1(M_{IP2}/2) \quad (4.20)$$

$$J_0(M_{IP3}/2)J_1(M_{IP3}/2) = J_1(M_{IP3}/2)J_2(M_{IP3}/2) \quad (4.21)$$

Using the small argument asymptotic approximation for J_n, we get

$$M_{IP2} = 2\tan(\phi/2) \quad (4.22)$$

$$M_{IP3} = 4\sqrt{(2)} \quad (4.23)$$

IP2 and IP3 are calculated from Eqs. (4.20)- (4.23), and can be expressed as

$$\mathrm{IP2} = 2 \cdot \sin^2(\phi/2)/\cos^2(\phi/2) \quad (4.24)$$

$$\mathrm{IP3} = 4 \cdot \sin^2(\phi/2) \quad (4.25)$$

It can be shown that Eq. (4.24)-(4.25) are also valid for the IF architecture. Eq. (4.24)-(4.25) shows that when the modulator is biased at the zero output (ϕ=π), the IP2 is zero and the IP3 has the maximum value, or least non-linearity which means the optimum bias point should be π.

4.4.2 Discussion of the Null Bias Point of MZM

The quadrature bias point has been widely adopted for both analog and digital direct-detection systems. The null bias point for CO-OFDM up-conversion signifies a fundamental difference between the optical intensity modulation and optical field modulation. For instance, in coherent detection systems, the transformation between the electrical drive voltage and optical field is of the concern, whereas in the conventional direct detection systems, the transformation between the electrical drive voltage and the optical power is of the concern. Figure 4.9 shows the transfer functions for both the optical intensity and optical field (I/Q component) against the drive voltage. In Figure 4.9, we assume zero initial phase offset between the two arms of MZM at zero bias voltage. The transfer function for the direct detection is the optical intensity against the drive voltage, whereas the transfer function for the coherent detection is the *I/Q* component of

the optical field against the drive voltage. It is apparent from Figure 4.9 that the optimal MZM bias for optical intensity modulation is quadrature whereas the optimal bias for optical field modulation is the null point.

It is worth noting that the conclusion of the optimal modulator bias of π for the RTO up-conversion is fundamental in dependent of the detailed waveform of $V_{I/Q}$, i.e., $V_{I/Q}$ can be any arbitrary waveform, not necessarily limited to that of CO-OFDM. For instance, for direct detection optical OFDM, it is still optimal to bias the modulator at null point to minimize RTO up-conversion nonlinearity. However, the challenge there is how to reinsert the main optical carrier, which is lost due to the bias at null point. We anticipate a great deal of original research effort taking advantage of this linear transformation between the optical field and electrical drive voltage in coherent or incoherent, digital or analog systems.

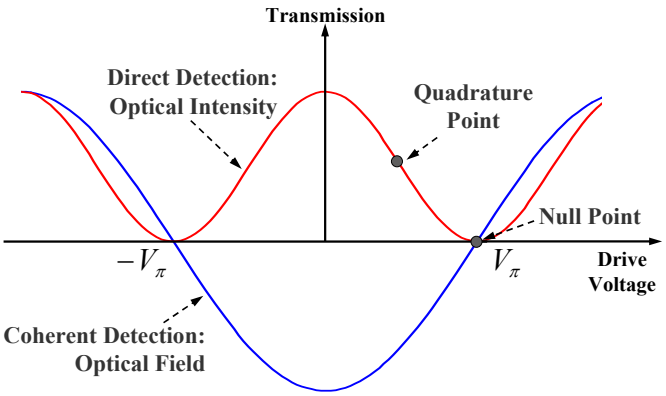

Figure 4.9 The transfer functions for the optical intensity and the optical field against the drive voltage.

4.4.3 Simulation Analysis for CO-OFDM RTO Up-converter

In order to identify the bias point impact on the CO-OFDM system, a Monte Carlo simulation is used to investigate the excess modulation insertion loss L_{EX}(dB) and the Q penalty of the OFDM RF-to-optical up-converter under different bias points. The modulator excess modulation insertion loss is defined as

$$L_{EX} = P_{in} - P_{out} - 3 \tag{4.26}$$

where P_{in} (dBm) is the input optical power and P_{out} (dBm) is the optical power in OFDM band at the output of the optical I/Q modulator. The modulator excess modulation insertion loss is defined in a way such that it equals zero for a conventional MZM biased at quadrature ignoring the physical loss of the modulator.

A CO-OFDM system with direct-conversion architecture shown in Figure 4.1 (a) is used in the simulation. The relevant OFDM system parameters used in the simulation are: OFDM symbol period t_s of 25.6ns, number of subcarriers N_{sc} of 256, and guard interval of 1/8 of the number of subcarriers, the Binary Phase-Shift Keying (BPSK) encoding is used resulting in a bit rate of 10 Gb/s. We use the data-assisted method instead of pilot symbols for phase estimation. Linewidth for the two laser sources is assumed to be 100 kHz each. The ASE noise is modeled as white Gaussian noise. The laser phase noise is assumed to be white frequency noise. Our simulation is conducted at an OSNR of 3.5 dB (0.1nm ASE noise resolution bandwidth), which gives a baseline Q value of 9.8 dB, or a BER of 10^{-3} without up-converter nonlinearity. Q penalty is defined as the Q reduction from this reference Q value of 9.8 dB due to up-converter nonlinearity.

Figure 4.10 (a) and (b) respectively show the Q penalty and excess modulation insertion loss as a function of modulation index, at a fixed OSNR of 3.5 dB while varying the bias point. For the bias points of $\pi/2$ or $\pi/4$, at the lower modulation index, the residual optical carrier takes a large portion of the signal power and does not contribute to the signal strength in the CO-OFDM systems, and subsequently severely increases the Q penalty. The Q penalty at the high modulation index is mainly caused by the nonlinear inter-modulation products. It can be seen that not only the bias point of π provides the least Q penalty (Figure 4.10 (a)), but also it incurs the least excess loss (Figure 4.10 (b)). In particular at a modulation index M of 0.6 (1.6), the Q penalty is about 0.2 dB (1 dB) and the insertion loss is about 8 dB (1dB), for the bias point at π. It should be noted that large modulation index helps to reduce the excess loss but inevitably introduces more nonlinearity. Thus, it is important to set a proper modulation index to keep a balance between the Q penalty and excess loss.

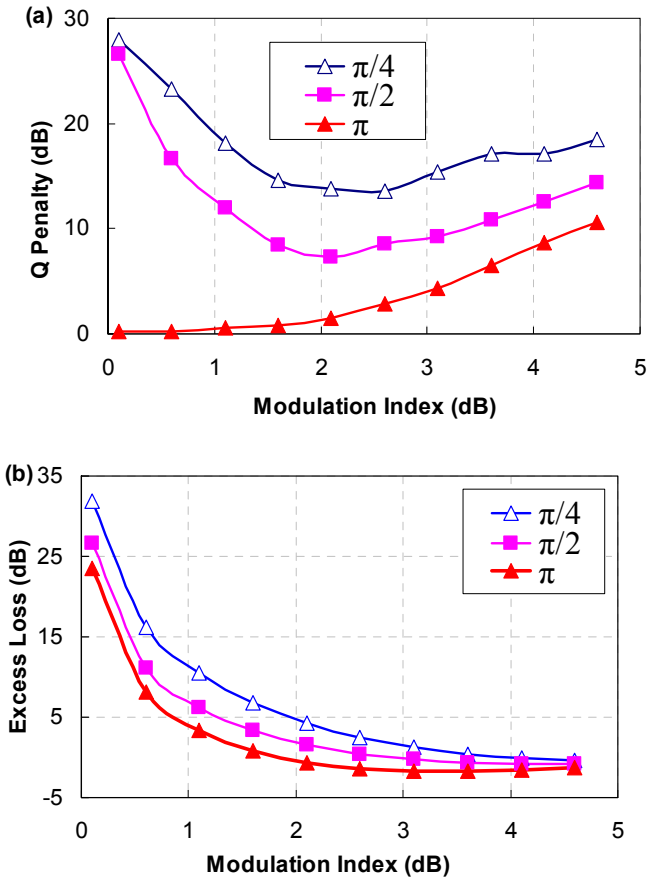

Figure 4.10 (a) Q penalty and (b) excess loss as a function of modulation index M with varying bias point. Q penalty is computed at an OSNR of 3.65 dB.

Figure 4.11 shows the OFDM spectra with a modulation index of 0.5 and 3 respectively at the bias point of π and π/2 which clearly displays the spectra distortion due to the nonlinearity and residual carrier. It can be seen that in Figure 4.11 (a), when the bias point at π and the modulation index is small, the signal spectrum is clean and signal power is confined in the OFDM band. However, a large modulation index introduces more intermodulation products as evidenced by the appearance of significant spectral components outside of the OFDM band (as shown in Figure 4.11 (a) and (b)). When the MZM is biased at π/2, a strong residual carrier exists in the middle of the OFDM band.

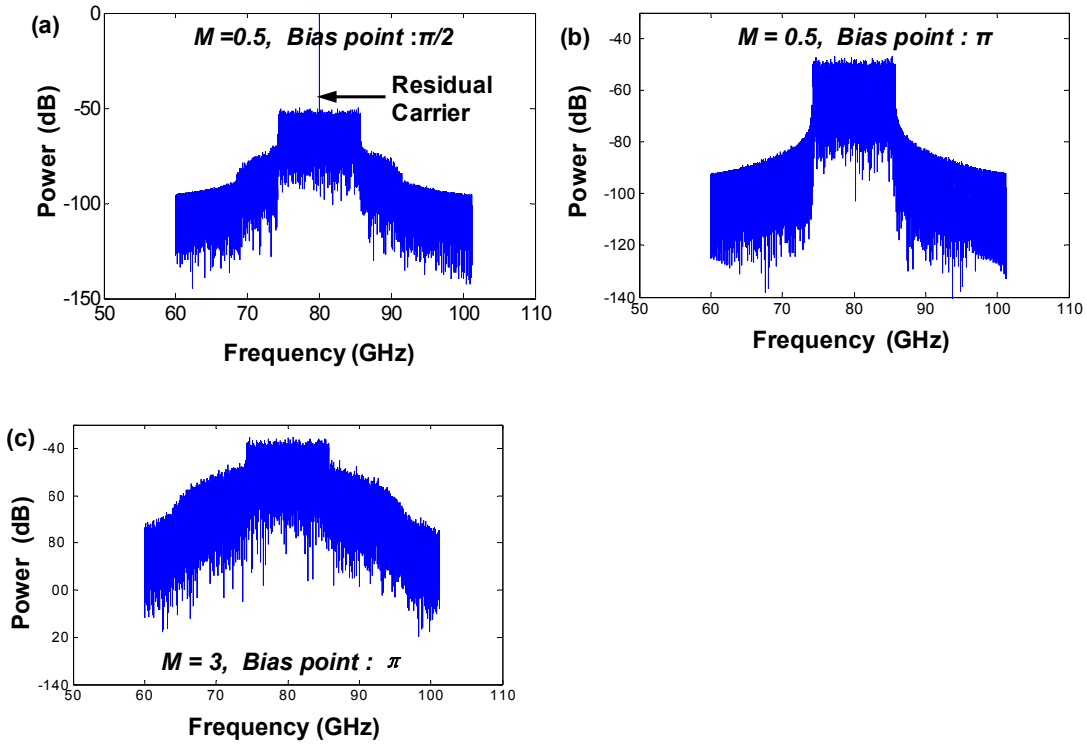

Figure 4.11 At bias point of π, the OFDM spectra with a modulation index of 0.5 and 3

4.5 CO-OFDM Transmitter Employing Pre-distortion

The goal of this section is to find an appropriate transmitter design to achieve an acceptable Q penalty while incur minimal excess modulation loss by using the least DAC resolution. In this section, we first analyze the amplitude statistic and PAPR of the OFDM signal. We then include the effects of the optical IQ modulator and provide extensive study of the predistortion techniques to mitigate the modulator nonlinearity. The optimal design is presented in terms of the clipping ratio, DAC resolution and optical IQ modulator excess modulation loss. The system performance with predistortion design to that without predistortion is also compared.

4.5.1 Peak-to-Average Power Ratio of OFDM Signals

The time domain OFDM signal is a sum of complex exponential functions, whose amplitudes and phases are determined by the random data symbols transmitted over the different carriers [117]. The complex envelope of the transmitted OFDM signal can be represented as

$$s(t) = \sum_{k=1}^{N_{sc}} c_k e^{j2\pi f_k t} \tag{4.27}$$

where c_k is the transmitted symbol (assume 4-QAM is used), N_{sc} is the subcarrier number. From central limit theorem, the resulting instantaneous time domain signal exhibits an amplitude probability density function (PDF) approaching the Gaussian distribution for a high number of subcarriers (subcarrier number >10) with zero mean and a variance σ^2 equal to the total signal power. That is, at any given time, the probability that *s(t)* takes the value *x* ($|x| \leq |s_{max}|$) is given by [140]

$$\text{Prob}\{s(t) = x\} = p(x) = \frac{1}{\sigma\sqrt{(2\pi)}} \cdot \exp\left[-\frac{x^2}{2\sigma^2}\right] \tag{4.28}$$

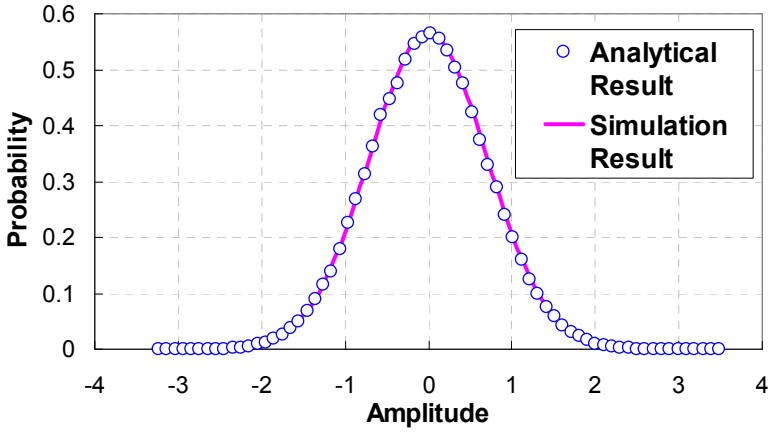

Figure 4.12 Statistics of amplitude histogram of the in phase component of a OFDM signal both simulation and analytical result are shown.

Figure 4.12 shows the measured histogram of the I component of an OFDM signal with 256 subcarriers. The power of the I component is 0.5. It can be seen that the OFDM amplitude obeys a Gaussian distribution (represented by the solid line) with a standard deviation of σ^2=1/2. From Figure 4.12 it can be shown that the OFDM signal may exhibit high instantaneous amplitude peak with respect to the average amplitude level which results in high PAPR. The PAPR is defined as

$$\text{PAPR} = \frac{\max |s(t)|^2}{\sigma^2} \tag{4.29}$$

Where σ^2 is the power or variance of $s(t)$. By setting $c_k = 1$ and $t = 1$ in Eq. (4.27). We can get the theoretical maximum PAPR as $10 * \log_{10}(N_{sc})$ (dB). For example, for an OFDM system with 256 subcarriers, the theoretical maximum PAPR can be as high as 24 dB. The statistic properties of PAPR can be described by cumulative density function (CDF), that is, the probability of the PAPR being above a given value. The CDF of PAPR can be expressed as

$$P_c = Pr\{\text{PAPR} > \zeta_p\} \tag{4.30}$$

Figure 4.13 shows the CDF with varying number of subcarriers. It can be noted that high PAPR is a rare event. Take $N_{sc} = 256$ for example, 24 dB PAPR only happens with probability less that 10^{-5}. For the most interested probability regime such as 10^{-3}, the PAPR is around 11 dB, which is much less than the maximum value of 24 dB. A PAPR of 11 dB implies that the peak value is about one order of magnitude stronger than the average power. It can be noted that PAPR increases slightly as a function of the subcarrier numbers, for instance, the PAPR increases about 1 dB when the subcarrier number increases from 32 to 256.

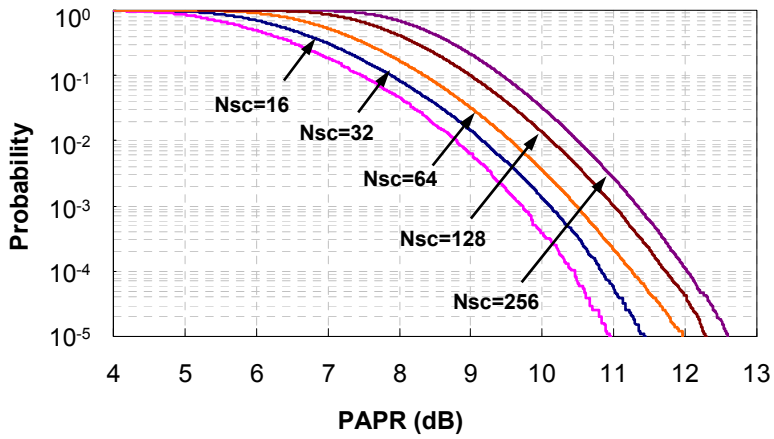

Figure 4.13 CDF of PAPR for different subcarrier number

It is obvious that the PAPR for OFDM is excessively high for either RF or optical communications. The PAPR has been cited as one of the drawbacks of the OFDM

modulation format and presents a challenge for optical fiber communications due to the influence of nonlinear devices and optical fiber nonlinearity. Large amplitude spikes also decrease the performance of a DAC in transmitter with limited number of quantization levels. In the RF communication system, a number of PAPR-reduction techniques and algorithms have been proposed:

i) PAPR reduction by limiting the time domain signal amplitude strength. A straight forward method is hard-clipping [141-143]. However it degrades the bit-error-ratio and induces strong out-of-band distortion.

ii) PAPR reduction by mapping the original waveform to the new set of waveforms that has lower PAPR without distorting the signal. These PAPR reduction algorithms include the selection mapping [144-145], optimization approaches such as partial transmit sequence [146-147], and modified signal constellation or active constellation extension [148-149].

Due to the simplicity of the clipping algorithm in terms of signal processing, we will use the hard-clipping in our CO-OFDM transmitter design scheme.

4.5.2 Optical IQ Modulation Impact on CO-OFDM Signals

It has been shown in Section 4.4.1 that by biasing the MZMs at null point ($\phi = \pi$), a linear transformation between the RF signal and optical field signal can be achieved at RF-to-optical up-converter. Under such a condition, the transfer function of MZM can be expressed as

$$E(t) = E_0 \sin\left(\frac{\pi V(t)}{2V_\pi}\right) \tag{4.31}$$

where $V(t)$ is the real/imaginary part of the OFDM signal, $E(t)$ is the real/imaginary part of the electric field, E_0 is the magnitude of the electric field, and V_π is the required voltage difference to switch on and off the modulator. The *sine* shaped nonlinear transfer function of MZM results in two issues: (i) With a high PAPR, the OFDM signal is severely distorted by MZM especially at high modulation index, which increases the Q penalty. (ii) To operate the MZM in linear region, a small modulation index of the input RF signal is

required, thus causing large excess modulation insertion loss. iii) In addition to the MZM nonlinearity, insufficient DAC quantization levels also increases the Q penalty.

4.5.3 OFDM Transmitter Architecture

Figure 4.14 shows the conceptual diagram for RF OFDM transmitter employing digital clipping and predistortion. Two digital signal processing blocks-digital clipping and digital predistortion are used before the DACs for both *I* and *Q* branches as shown in Figure 4.14 to mitigate the PAPR and modulator nonlinearity effect.

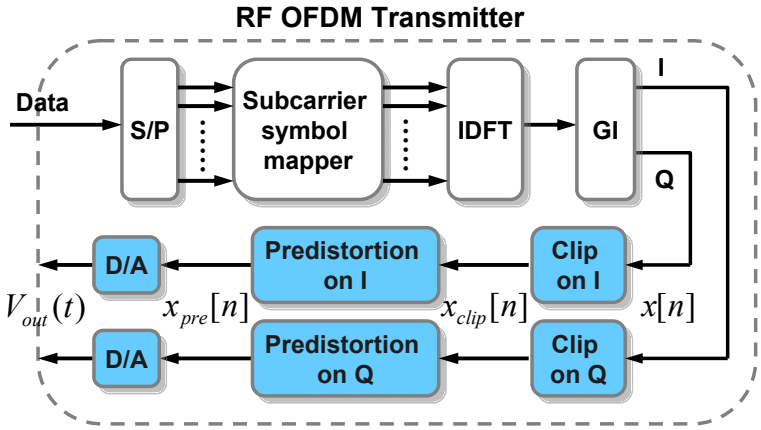

Figure 4.14 RF OFDM Transmitter with clipping and pre-distortion

A. Digital clipping

The nonlinear effects of MZM on the transmitted OFDM signal due to high PAPR are spectral spreading, intermodulation and harmonic generation [150-151]. Thus, the nonlinear distortion causes both in-band and out-of-hand interference to signals. The in-band interference decreases the BER performance of the received signal through warping of the signal constellation while the out-of-band interference causes adjacent channel interference through spectral spreading [151]. Large amplitude spikes also decrease the performance of a DAC with limited number of quantization levels. It has been shown that the instantaneous amplitude of the OFDM signal with N ($N > 10$) subcarriers can be modelled as Gaussian distribution. Large amplitude spikes occur infrequently because of statistic averaging [152], and subsequently it is feasible to reduce

the PAPR by clipping the OFDM signal. Let $x[n]$ and $x_{clip}[n]$ denote the baseband OFDM digital signal before and after digital clipping. Clipping through digital signal processing can be described as,

$$a_k = \begin{cases} x[n] & \text{if } x[n] \le A_{max} \\ A_{max} & \text{if } x[n] > A_{max} \end{cases} \tag{4.32}$$

$$A_{max} = \min\left(A_{clip,1}\right) \tag{4.33}$$

where A_{max} is the maximum permissible normalized amplitude, beyond which the signal will be clipped. Figure 4.15 shows an arbitrary OFDM waveform that is clipped to the bounded between $[-A_{max}, A_{max}]$. A_{max} can be obtained by taking the smaller value between A_{clip} and '*1*', as shown by Eq. (4.33). A_{clip} is determined by the clipping ratio which is defined as

$$\gamma \equiv \frac{A_{clip}}{x_{RMS}} \tag{4.34}$$

where x_{RMS} is the RMS value of $x[n]$. The reason of comparing A_{clip} with '1' in Eq. (4.33) is that the predistorter following the digital clipping has an *arcsine* transfer function with the input range of [-1, 1]. Eq. (4.33) indicates that OFDM signal could be further clipped by the predistorter at large modulation index.

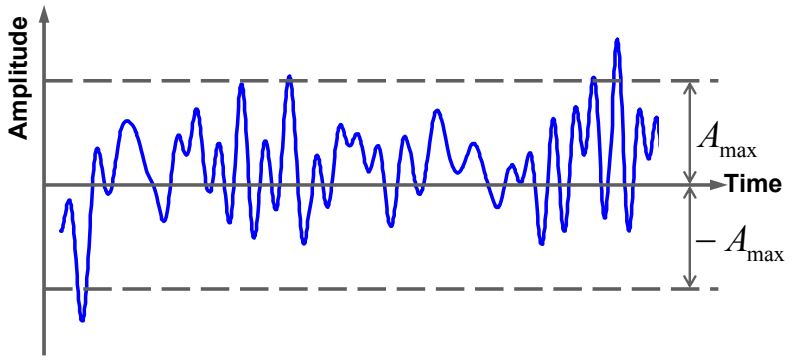

Figure 4.15 An arbitrary OFDM waveform that is clipped to the bounded between [-A_{max}, A_{max}]

B. Predistortion

A digital predistorter is used to compensate the nonlinear transfer characteristic of *sine* function for MZM modulator in Eq.(4.31). Predistortion function can be expressed as

$$x_{pre}[n] = \frac{2V_\pi \cdot \sin^{-1}(x_{clip}[n])}{\pi} \tag{4.35}$$

where $x_{cip}[n]$ and $x_{pre}[n]$ are the normalized input and output voltages of the predistortor, respectively. According to Figure 4.14, $x_{cip}[n]$ is the output of clipping block. Together with the MZM transfer function Eq. (4.31) we get the MZM output

$$E(t) = E_0 \cdot x_{clip}[n] \tag{4.36}$$

where, E_0 is the peak electrical field. The combined transfer characteristic provides a linear transformation from the digital waveform $x_{cip}[n]$ to the analogue optical field of $E(t)$.

C. DAC

Two DACs as shown in Figure 4.14 preceding the I/Q modulator are used to convert the digital I/Q waveforms into real time analog signal.

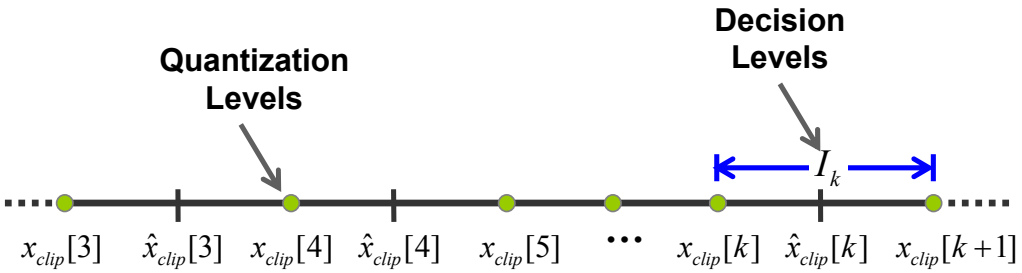

Figure 4.16 The quantization procedure

A quantizer is used in our study to emulate the quantization process of the DAC. Quantization is a nonlinear and noninvertible process that maps the rage of a discrete signal with a single number. Such procedure is illustrated in Figure 4.16. The input signal of the quantizer or the output signal of the clipping block $x_{cip}[n]$ is first divided into L intervals by $L+1$ decision levels. Each interval can be represented as:

$$I[k] = \{x_{clip}[k] < x_{clip}[n] \le x_{clip}[k+1]\} \quad k = 1, 2, ..., L \tag{4.37}$$

The quantization operation $Q(\cdot)$ can be represented as

$$\hat{x}_{clip}[n] = Q(x_{clip}[n]) \tag{4.38}$$

Where $\hat{x}_{clip}[n]$ is the quantized sample. A uniform quantizer is used in our system which can be defined as:

$$x_{clip}[k+1] - x_{clip}[k] = \Delta, \quad k = 1, 2, ..., L-1 \tag{4.39}$$

Where Δ is quantization step. In theory, DAC should be large enough to cover the total dynamic rage of the input signal. However, practical DAC only have finite range. In our simulation, the DAC input range corresponds to the signal $x_{cip}[n]$'s max and min values after clipping and predistortion. If we need to uniformly quantize the input signal in range *[-A, A]* into *L* levels, we should use *k* bits world length to present $2^k \geq L$ distinct levels. Thus, *k* should satisfy the following condition,

$$k \geq log_2 L \tag{4.40}$$

then the quantization step is

$$\Delta = \frac{2A}{2^k} \tag{4.41}$$

The k_{th} sub-interval can be expressed as

$$I_k = \left[-A + \frac{kA}{2^{k-1}}, -A + \frac{(k+1)A}{2^{k-1}} \right), \quad k = 0, 1, ...2^b - 1 \tag{4.42}$$

Then we can get the quantization function $Q(\cdot)$ as ,

$$\hat{x}_{clip}[n] = Q(x_{clip}[n]) = -A + \frac{(k+1/2)A}{2^{k-1}} \tag{4.43}$$

Where $x_{clip}[n] \in I_k$. Figure 4.17 shows the quantization characteristic function of a uniform quantizer with 3 bits word-length.

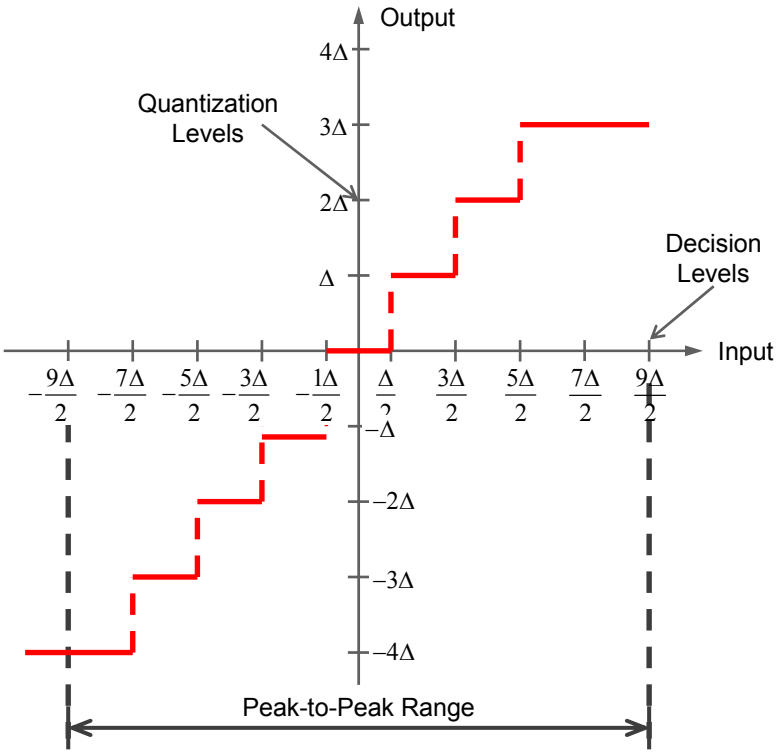

Figure 4.17 The quantization characteristic function of a uniform quantizer with 3 bits word-length.

4.5.4 Theoretical Analysis of the Clipping and Quantization Impact

In this section we use analytical approach developed in [153] to investigate the clipping and DAC quantization impact. It has been shown in Section 4.5.1 that the instantaneous amplitude of the OFDM signal can be modelled as Gaussian distribution with a zero mean and a variance σ^2 equal to the total signal power. Digital clipping introduces clipping noise thus decreases the signal to noise ratio. On the other hand, clipping also reduces the dynamic range of an OFDM signal and increases the signal to quantization noise ratio. Therefore there exists an optimum clipping ratio where the maximum SNR can be achieved.

The clipping noise power can be estimated as the total power lose of clipped signal which can be represented as

$$P_{clip} = 2 \cdot \int_{A_{max}}^{+\infty} (x - A_{max})^2 p(x) d(x) = \sqrt{\frac{8}{\pi}} \sigma^2 \gamma^{-3} e^{-\gamma^2/2} \tag{4.44}$$

where $p(x)$ is the probability density function of $x[n]$. γ is clipping ration defined in Eq. (4.34). The signal-to-clipping noise ratio (SCNR) is

$$SNR_{clip} = \frac{P_{tot}}{P_{clip}} = \sqrt{\frac{8}{\pi}}\gamma^3 e^{\gamma^2/2} \tag{4.45}$$

Assume a DAC with k-bit resolution is used. Then the quantization noise power P_{quan} is given by [154]

$$P_{quan} = \frac{(2A_{max})^2 \cdot 2^{-2k}}{12} = \frac{(\sigma\gamma)^2 \cdot 2^{-2k}}{3} \tag{4.46}$$

where A_{MAX} is the maximum value of the DAC input signal. The signal-to-quantization noise ratio (SQNR) is

$$SNR_{quan} = \frac{P_{tot}}{P_{quan}} = \frac{\gamma^2 \cdot 2^{-2k}}{3} \tag{4.47}$$

Then the signal to the total signal processing noise is

$$\begin{aligned} SNR_{sp} &= \frac{P_{tot}}{P_{clip} + P_{quan}} \\ &= \left(SNR_Q^{-1} + SNR_C^{-1}\right)^{-1} \\ &= \left(\sqrt{\frac{8}{\pi}}\gamma^{-3} e^{-\gamma^2/2} + \frac{\gamma^2 \cdot 2^{-2k}}{3}\right)^{-1} \end{aligned} \tag{4.48}$$

According to Eq. (4.48) we can plot the SNR as a function of clipping ratio with 3-, 4-, 5- and 6-bit resolution for 4-QAM OFDM signal as shown in Figure 4.18 . It can be seen that for a given number of bit resolution, there is an optimal clipping ratio γ due to the trade off between the SCNR and SQNR. The optimal clipping ratio is found to be respectively 2.2, 2.6, 3 and 3.4 for 3-,4-,5- and 6-bit resolution.

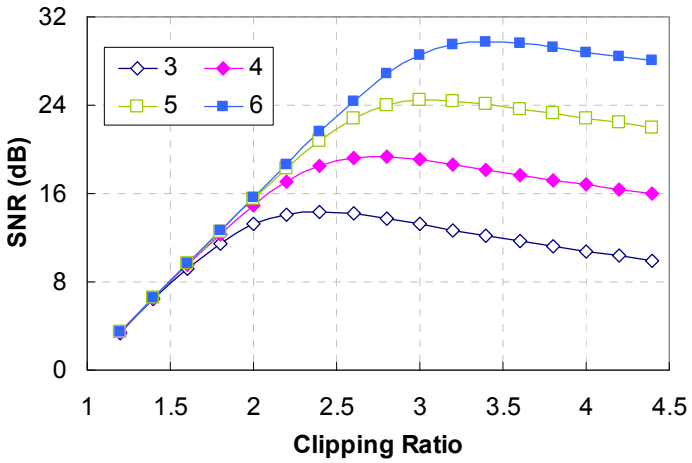

Figure 4.18 SNR as a function of clipping ratio with 3-, 4-, 5- and 6-bit DA/ADC resolution for 4-QAM signal

4.5.5 Simulation Analysis for CO-OFDM Transmitter

Monte Carlo simulation is employed to investigate the impact of transmitter design to the CO-OFDM systems. A CO-OFDM system with direct detection architecture is used as the simulation modal. The relevant OFDM system parameters used in the simulation are: OFDM symbol period of 25.6 ns, number of subcarriers of 128, and guard interval of 1/8 of an IDFT block, and 10,000 OFDM symbols are used for each simulation. Each subcarrier is 4-QAM encoded to provide a bit rate of 10 Gb/s. The signal PAPR before clipping is 11 dB. The baseline Q value is 9.8 dB calculated at an OSNR of 3.7 dB. The laser linewidth is assumed to be 100 kHz. The pilot-aided method [14] is used for phase estimation.

The first task of the design is to find the required clipping ratio for the transmitter. Figure 4.19 shows the Q reduction as a function of Q value at clipping ratios of 1.5, 2, 2.5, 3. When the clipping ratio is equal to 2.5, the BER curve is very close to the ideal performance with no clipping. The Q reduction is calculated by comparing the Q value obtained at clipping ratio of 1.5, 2, 2.5, 3 with the Q value obtained at infinite clipping ratio. The simulation is conducted with a DAC with infinite number of levels. Figure 4.19 shows that higher Q leads to larger Q reduction especially for small clipping ratio，implies that for small clipping ratio larger Q gives more Q reduction. The Q reduction introduced by 2.5 clipping ratio is only around 0.05dB which implies that a clipping ratio of 2.5

should provide satisfactory performance with sufficient margin. Using a larger clipping ratio will incur a bigger penalty from a finite DAC resolution. The High-order modulation format (e.g. 64-QAM) is more sensitive to distortion and requires higher SNR to achieve the same BER performance, compared with low-order modulation format. Therefore, for high-order modulation format a larger clipping ratio and higher DAC resolution are required.

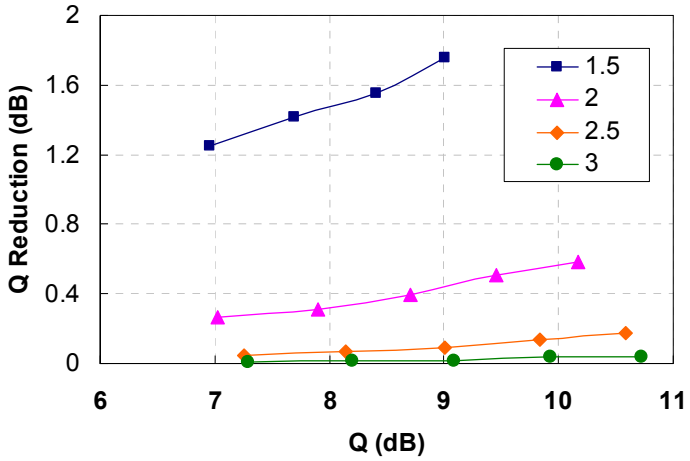

Figure 4.19 Q reduction as a function of Q with varying clipping ratio

Assuming a clipping ratio of 2.5, the impact of modulation index (or amplitude of the modulation voltage) and DAC resolutions is investigated. Figure 4.20 (a) shows the Q penalty as a function of modulation index while varying the DAC resolution with digital predistortion. Q penalty is defined as the Q reduction from this reference Q value of 9.8dB due to up-converter nonlinearity and impact of DAC resolution. DAC resolutions used for simulation are 3, 4, 5 and 7 bits. Due to the compensation by the predistorter, Q penalty does not increase with the modulation index before it exceeds 1.0. After the modulation index reaches 1.0, Q penalty rises dramatically since the predistorter has a strong clipping effect on signal. Thus, a modulation index of 1.0 should be used regardless of DAC resolution. From Figure 4.20 (a), the 4-bit DAC resolution only gives around 0.3-dB Q penalty. Figure 4.20 (b) shows the Q penalty performance without predistortion at 3 to 7-bit DAC resolutions. The application of predistortion significantly reduces the Q penalty for all resolutions, especially when the modulation index is beyond

1.0, indicating that predistortion effectively increases the dynamic range of the modulation index.

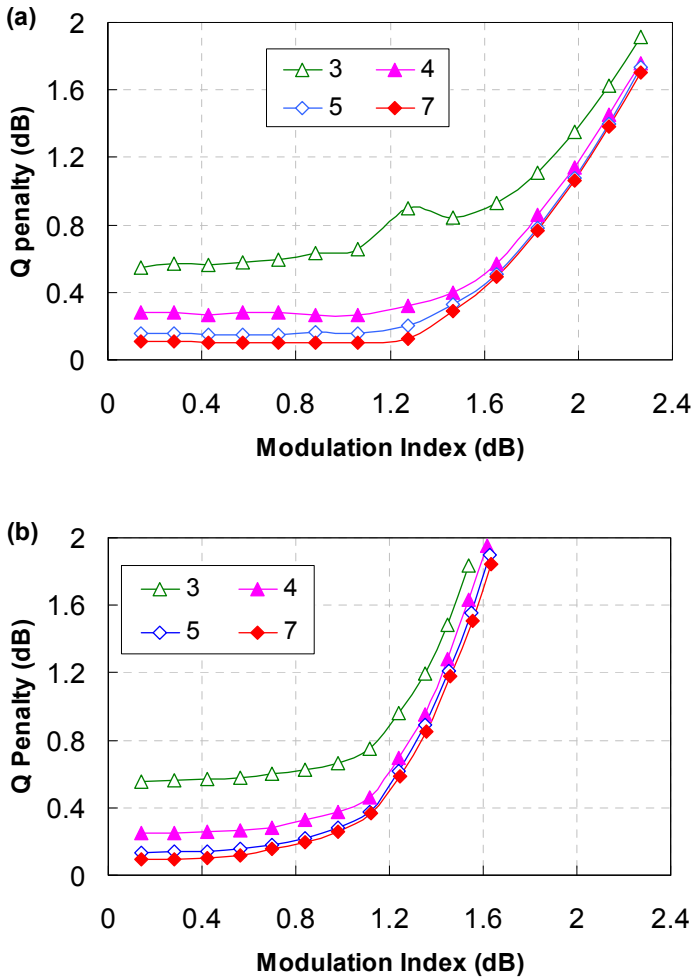

Figure 4.20 (a) Q penalty as a function of modulation index and DAC resolution with predistortion. (b) Q penalty as a function of modulation index and DAC resolution without pre-distortion.

The excess modulation loss is shown in Figure 4.21 as a function of modulation index with predistortion under the fixed clipping ratio of 2.5 and DAC resolution of 4-bit. The excess modulation insertion loss of the optical I/Q modulator is defined in such a way that the excess loss is equal to zero for a conventional MZM biased at quadrature point by ignoring the physical loss of the modulator. At the modulation index of 1.0, the excessive loss with predistortion is about 6.0 dB. It is noted that there exists a trade-off between DAC resolution, Q penalty and excess loss. For example, if the system uses DAC

resolution of 4-bit, and can tolerate 0.5 dB Q penalty, the modulation index can be as high as 1.6, resulting in 3.4 dB excess loss.

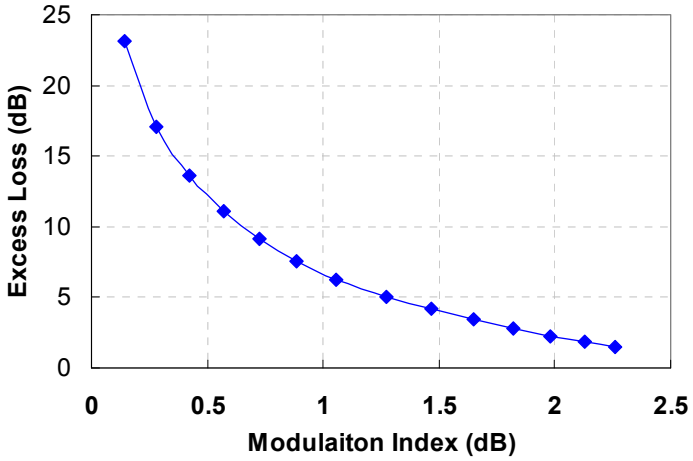

Figure 4.21 Excess loss as a function of modulation index

4.6 Conclusions

In this paper, we demonstrate the optimum design for coherent optical OFDM transmitter design.

We first presented the direct up/down conversion and intermediate frequency architecture for the coherent optical OFDM system design. Direct up/down conversion architecture provides the advantage of requiring less electrical bandwidth, less RF components and eliminating the need for narrow OBPF in both transmitter and receiver, but it has a more complex receiver structure. We then investigate the optical I/Q modulator nonlinearity in CO-OFDM system based on direct up/down conversion. We first derive closed-form expressions for the nonlinearity in the optical I/Q modulator, represented by two-tone intermodulation products as a function of the bias point and modulation index. Additionally, we perform a numerical simulation to identify the excess modulation insertion loss and Q penalty from I/Q modulator nonlinearity for the CO-OFDM system. The theoretical analysis and numerical simulation results obtained in our study show that, in contrast to the direct-detected system, the optimal modulator bias point for the coherent system is π where the nonlinearity and excess modulation loss are minimized. In particular at a modulation index M of 0.6 (1.6), the Q penalty is about 0.2

dB (1 dB) and the insertion loss is about 8 dB (1dB), for the bias point at π.

The Digital clipping and predistortion are then used to compensate the nonlinearity induced by the OFDM PAPR effect and MZM nonlinearity. The transmitter design is presented in terms of clipping ratio, optical IQ modulator excess modulation loss and DAC resolution . The DAC impact on the RF OFDM system has been discussed in [5] for wireless communications. The major contribution of our study is to include the effects of the optical IQ modulator and provide extensive study of the predistortion techniques to mitigate the modulator nonlinearity. Theoretical and numerical results show that for 4-QAM signal the optimal clipping ratio is 2.5 for 4 bit DAC resolution which introduces only 0.05dB Q reduction at 9.8dB Q value. It can be shown that 4-bit DAC resolution is sufficient for a CO-OFDM transmitter to incur only 0.3 dB Q penalty while maintaining the excess modulation insertion loss below 6.0 dB.

Chapter 5

Study of the Nonlinearity and Dynamic Range of CO-OFDM Receivers

5.1 Introduction

Coherent optical OFDM is a combination of OFDM technology and optical coherent detection. In a coherent receiver, the received optical signal is mixed coherently with a LO before feeding into the photodetector. With coherent receivers, the full information of an optical signal (including amplitude and phase) can be linearly down-converted to a baseband electrical signal with homodyne or heterodyne detection. Coherent optical detection system was extensively studied in 1980s [155-156] and viewed as a promising technique to improve the receiver sensitivity [157-159]. However, with the invention of EDFAs, direct detection system can achieve sensitivity within a few decibels of that of coherent receivers. Besides, the technical difficulties such as dynamic polarization control and implementation of optical phase locked loop (OPLL) also make it less attractive. Because of these reasons, further research of coherent optical communications has been abandoned for nearly 20 years. Coherent detection has restarted to attract a large interest over recent years highlighted by the remarkable theoretical and experimental demonstrations from various groups around the world [31-35]. The drive behind using the coherent communication techniques nowadays is two-fold. First, current coherent detection systems are heavily entrenched in DSP. By taking the advantages of the high-speed DSP, both polarization and phase management can be easily realized, thus, a free running laser can be used as a local oscillator. Optical coherent detection in conjunction with high-speed DSP has the potential to increase the spectral efficiency and the ability to compensate linear transmission impairments such as chromatic dispersion and polarization mode dispersion in the electrical domain [37, 39]. Second, in contrast to the optical system that was dominated by a low-speed, point-to-point, and single-channel

system a decade ago, modern optical communication systems have advanced to massive WDM and reconfigurable optical networks with a transmission speed approaching 100 Gbits/s. The primary aim of coherent communications has shifted toward supporting these high-speed dynamic networks by simplifying the network installation, monitoring, and maintenance. Besides, OFDM, which has emerged and thrived in the RF domain during the past decade, has gradually encroached into the optical domain. The combination of OFDM and coherent detection not only realizes a dispersion free transmission, but also brings the benefits of computation efficiency and ease of channel and phase estimation.

For a CO-OFDM system, coherent detection is used to realize a linear transformation from optical field signal to RF (or electrical) signal. Compared with the direct-detection optical OFDM [13], the CO-OFDM comprises with two pairs of balanced receivers and is more costly and complex. It is desirable to reduce the cost and complexity of the receiver using balanced receivers that are tolerant of imbalance, or using simpler single-ended receiver. Furthermore, a linear transformation in modulation, transmission, and demodulation is the most critical assumption for CO-OFDM system. The receiver imperfections such as the imbalance between the two ports of a balanced receiver will destroy the receiver linearity. Such imbalance not only results in DC offset but also introduces nonlinearity into the system by generating intermodulation products of the OFDM signal.

In this section, we analyze the impact of the imbalance of the balanced detector on the CO-OFDM system. We first show that coherent detection is capable of linearly down-converting the optical field to a base-band electrical signal in Section 5.2. In Section 5.3 we formulate the theory for the I/Q coherent detection including OFDM signal, nonlinearity, and noise. A numerical simulation is then conducted to identify the Q penalty and signal power dynamic range for the CO-OFDM system under the impact of imbalance.

5.2 Optical Coherent Receivers

5.2.1 Basic Concept

In a coherent receiver, the received optical signal is mixed coherently with a local oscillator before feeding into the photodetector. The optical field of the received optical signal E_S can be expressed as,

$$E_s = A_s(t)\exp\left(j\omega_s t + j\phi_s(t)\right) \tag{5.1}$$

Where $A_s(t)$ is the complex amplitude, ω_S is the carrier angular frequency. The optical field of the local oscillator E_{LO} can be expressed as

$$E_{LO} = A_{LO}(t)\exp\left(j\omega_{LO}t + j\phi_{LO}(t)\right) \tag{5.2}$$

where $A_{LO}(t)$ is the complex amplitude, ω_{LO} is the angular frequency of local oscillator. For coherent detection, balanced receiver is generally used to suppress the DC component and minimize the intensity noise. Figure 5.1 shows the block diagram of a balanced receiver. The optical signal and local oscillator are mixed with a 3-dB coupler that adds a 180^0 phase shift to either the signal or the LO field and split the signals into two equal parts which followed by two photodetectors. When the signal and LO share the same polarization, the electrical fields (Figure 5.1) at the output of optical coupler are given as

$$\begin{aligned} E_1(t) &= \frac{1}{\sqrt{2}}(E_s + E_{LO}) \\ E_2(t) &= \frac{1}{\sqrt{2}}(E_s - E_{LO}) \end{aligned} \tag{5.3}$$

The output photo current of the photodetector can be expressed as

$$\begin{aligned} I_+(t) &= R\left|E_1\right|^2 \\ &= \frac{R}{2}[P_s + P_{LO} + 2\sqrt{P_s P_{LO}}\cos\left(\omega_{IF} + \phi_s(t) - \phi_{LO}(t)\right)] \\ I_-(t) &= R\left|E_2\right|^2 \\ &= \frac{R}{2}[P_s + P_{LO} - 2\sqrt{P_s P_{LO}}\cos\left(\omega_{IF} + \phi_s(t) - \phi_{LO}(t)\right)] \end{aligned} \tag{5.4}$$

where $\omega_{IF} = \omega_S - \omega_{LO}$. $\phi_{LO}(t)$ is the phase of LO, P_s and P_{LO} is respectively the power of the received signal and LO, R is the responsivity of photodetector. The output of balanced receiver can be given as

$$\begin{aligned} I(t) &= I_+(t) - I_-(t) \\ &= 2R\sqrt{P_s P_{LO}} \cos\left(\omega_{IF} t + \phi_s(t) - \phi_{LO}(t)\right) \end{aligned} \tag{5.5}$$

When using the homodyne detection, the LO frequency ω_{LO} is set to the same with the signal frequency so that $\omega_{IF} = 0$ and the optical signal can be directly demodulated to base band.

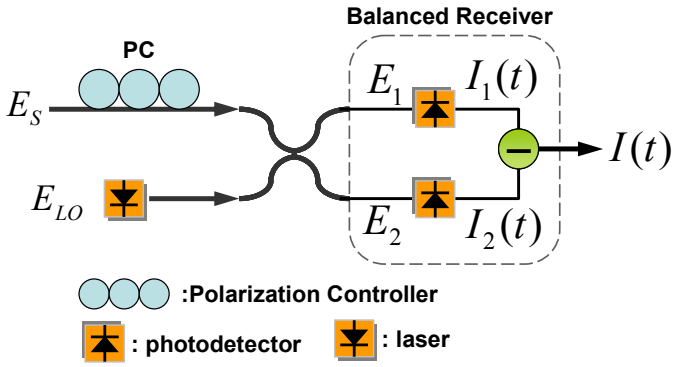

Figure 5.1 Configuration of a coherent receiver with a balanced detector

5.2.2 Receiver Noise for Coherent Detection

One of the inherent problems of the optical receiver is the receiver noise which usually responsible for fluctuation of electrical output current even when the incident optical signal has a constant power. After the coherent detection, the noise terms include shot noise, thermal noise and beat noise [160-161]. Shot noise is a manifestation of the fact that an electric current consists of a stream of electrons that are generated at random times. Thermal noise arises from random motions of mobile carriers in resistive electrical materials at non-zero temperature. Furthermore, the optical amplifier always adds ASE. Sig-ASE beat noise is generated by beating between the signal and ASE noise. Beating between ASE noise and ASE noise generates ASE-ASE beat noise. For coherent detection, beating between LO and ASE noise adds LO-ASE beat noise. Figure 5.2 (a)

and (b) shows the generating of Sig-ASE beat noise, LO-ASE beat noise and ASE-ASE beat noise [162]. Figure 5.2 (a) shows the optical spectrum of an optical signal, LO and ASE noise, the optical bandwidth isΔf. Sig/LO-ASE beat noise originates from the mixing or beating of the coherent signal/LO with the incoherent ASE in the same polarization [161]. Figure 5.2 (b) shows the optical spectrum of ASE noise in the optical bandwidth of Δf. Beating of co-polarized spectral components of ASE generates ASE-ASE beat noise [161].

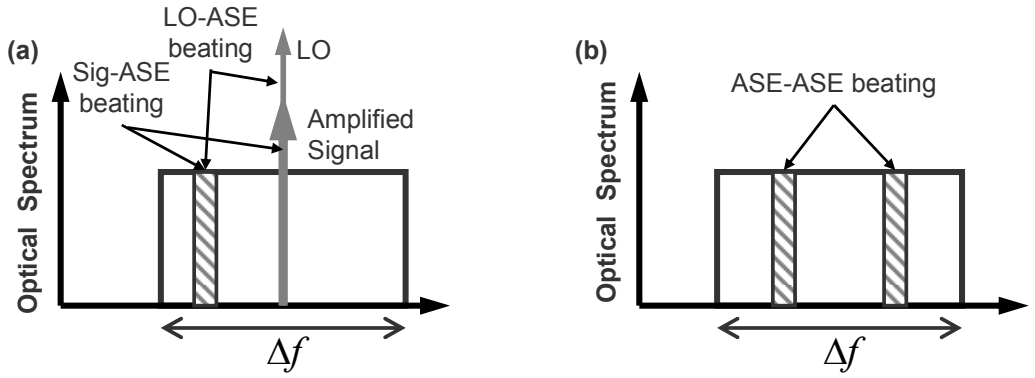

Figure 5.2 Generation of beat noise [162], (a) generation of Sig-ASE , LO-ASE beat noise and (b) generation of ASE-ASE beat noise.

Assume an optical amplifier with uniform gain G over an optical bandwidth Δf. The ASE spectral density (W/Hz) in a single polarization is expressed as [160]

$$D_{ASE} = \eta_{sp} h\nu (G-1) \tag{5.6}$$

where η_{sp} is the spontaneous emission noise factor and $h\nu$ is the photon energy. Then the ASE power is $D_{ASE}\Delta f$.

Now we are ready to find the mathematical expression for each noise terms. For a balanced detector as shown in Figure 5.1, the only difference between the up-branch and the lower branch is that an 180^0 relative phase difference exists between two LO fields at the output of the coupler, thus the analysis for both branches should be the same. Therefore, we will only analyse the noise terms of the up-branch. The optical power P at

the detector surface is the combination of signal power P_s, ASE power $D_{ASE}\Delta f$ and LO power P_{LO}, expressed as

$$P = P_s + D_{ASE}\Delta f + P_{LO} \tag{5.7}$$

The noise terms after the detection are expressed as

$$i_{shot} = 2qBR(P_s + D_{ASE}\Delta f + P_L O) \tag{5.8}$$

$$i_I = 2R^2 P_{LO}^2 (RIN)B \tag{5.9}$$

$$i_{th} = (4k_B T/R_L)\Delta f \tag{5.10}$$

$$i_{beat} = R^2 B(2P_s D_{ASE} + 2P_{LO} D_{ASE} + D_{ASE}^2 \Delta f) \tag{5.11}$$

where, B is the bandwidth of the receiver, R is the receiver responsivity and q is the electron charge. i_{shot} is the shot noise, i_I is the intensity noise, i_{th} is the thermal noise, i_{beat} is the beat noise, The first, second and third term in Eq. (5.11) are respectively Sig-ASE beat noise, LO-ASE beat noise and ASE-ASE beat noise. Due to 180^0 relative phase difference exists between two LO fields, the common-mode components of ASE-ASE beat noise and Sig-ASE beat noise are removed after detection and subtraction and only the signal and LO-ASE beat noise remains. Besides, since the same LO signal is provided to each branch, the intensity noise associates to the DC term in two branches can be perfectly cancelled out during the subtraction of I_+ and I_-.

5.3 Imbalance of Balanced Receiver

For the sake of illustration simplicity, instead of expressing OFDM as superposition of many subcarriers, we assume only two complex subcarrier tones $S_1(t)$ and $S_2(t)$ with equal amplitude at baseband frequency ω_1 and ω_2 are applied to the input of 90^0 hybrid, therefore

$$E_s(t) = S_1(t) + S_2(t) \tag{5.12}$$

$S_1(t)$ and $S_2(t)$ can be expressed as

$$S_1(t) = A\exp(j\omega_1 t + j\theta_1)\exp(j\omega_s t + j\theta_s)$$
$$S_2(t) = A\exp(j\omega_2 t + j\theta_2)\exp(j\omega_s t + j\theta_s) \tag{5.13}$$

where ω_s/θ_s is the signal laser frequency/phase, A is the amplitude of the baseband subcarrier tone, θ_1 and θ_2 is the subcarrier phase. The imbalance coefficient of the balanced receiver is defined by.

$$\alpha = \frac{G_1}{G_2} \tag{5.14}$$

where $G_{1/2}$ indicates the photo detector gain for PD1 and PD2 shown in Figure 5.3 (a). Similar definition is applied to the second balanced receiver pair consisting PD3 and PD4. The imbalance could be from the imbalance of optical hybrid and photodiode response mismatch. Figure 5.3 (b) shows an optical I/Q modulator using two single-ended photodetector. This can be considered as a special case of balanced receiver with infinite imbalance when G_2 is equal to zero. The LO signal is

$$E_{LO} = E_0 \cdot \exp(j\omega_{LO} t + j\phi_{LO}) \tag{5.15}$$

$E_S(t)$ and $E_{LO}(t)$ are split into two parts and feed into two detectors.

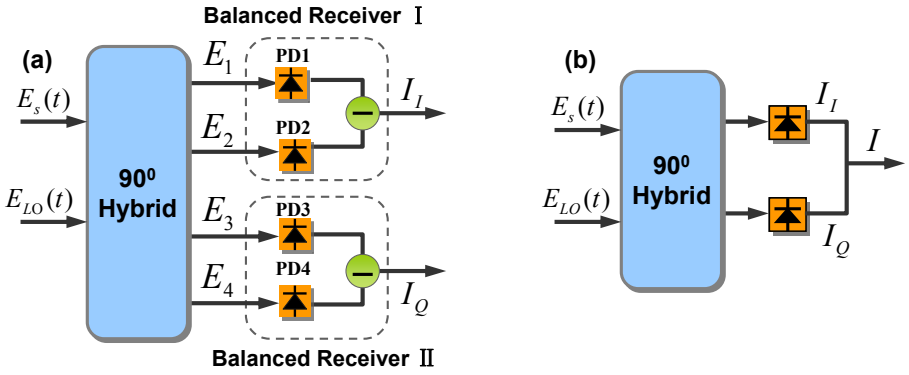

Figure 5.3 An optical I/Q receiver, (a) with balanced receiver, and (b) with single-ended receiver.

Using Eq.(5.4)-(5.5), the photo currents at the outputs of four photo detectors are,

$$I_{I+} = G_1 R \left| \frac{E_S(t)}{2} + \frac{E_{LO}(t)}{2} \right|^2 \tag{5.16}$$

$$I_{I-} = G_2 R \left| \frac{E_S(t)}{2} - \frac{E_{LO}(t)}{2} \right|^2 \tag{5.17}$$

$$I_{Q+} = G_1 R \left| \frac{E_S(t)}{2} + j\frac{E_{LO}(t)}{2} \right|^2 \tag{5.18}$$

$$I_{Q-} = G_2 R \left| \frac{E_S(t)}{2} - j\frac{E_{LO}(t)}{2} \right|^2 \tag{5.19}$$

Finally, the complex optical I/Q receiver output photo current *I* expresses as

$$I = I_I + I_Q = S_0(t) + S_1(t) + S_{NL}(t) + S_N(t) \tag{5.20}$$

where S_0 is the DC offset,

$$S_0 = R\left(\frac{A^2}{2} + \frac{E_0^2}{4}\right)(G_1 - G_2) \tag{5.21}$$

$S_1(t)$ is the signal fundamental term,

$$\begin{aligned} S_1(t) = & \frac{AE_0}{2} R(G_1 + G_2) \cdot [\exp j(\omega_1 t + \theta_1 + \omega_{off} + \theta_{off}) + \\ & \exp j(\omega_2 t + \theta_2 + \omega_{off} + \theta_{off})] \end{aligned} \tag{5.22}$$

$S_{NL}(t)$ is the nonlinear term or second order intermodulation term due to imbalance ,

$$\begin{aligned} S_{NL}(t) = & \frac{A^2}{2} R(G_1 - G_2) \\ & \cdot \left(\exp j(\omega_1 t - \omega_2 t + \theta_{off}) + \exp\left(-j(\omega_1 t - \omega_2 t + \theta_{off})\right)\right) \end{aligned} \tag{5.23}$$

$S_N(t)$ is the noise term,

$$S_N(t) = i_{th}(t) + i_{beat}(t) + i_{shot}(t) + i_I(t) \tag{5.24}$$

where, $\omega_{off} = \omega_S - \omega_{LO}$, $\theta_{off} = \theta_S - \theta_{LO}$. R is the photo detector responsivity. $i_{th}(t)$ is thermal noise with power, $i_{shot}(t)$ is the shot noise, $i_I(t)$ is normalized RIN of the

local laser, $i_{beat}(t)$ is the beat noise including Sig-ASE beat noise, ASE-ASE beat noise and LO-ASE beat noise. The noise power at the output of the balanced receiver is

$$\sigma_{shot}^2 = 2qB\left(\frac{A^2}{2} + \frac{D_{ASE\Delta f}}{4} + \frac{E_0^2}{4}\right)(G_1 + G_2) \tag{5.25}$$

$$\sigma_{th}^2 = 2(4\frac{k_B T}{R_L})\Delta f \tag{5.26}$$

$$\begin{aligned} i_{beat} = &\left(2 \cdot \frac{A^2}{2} \cdot \frac{D_{ASE}}{4} + \frac{D_{ASE}^2 \Delta f}{16}\right) \cdot (G_1 - G_2) + \\ &2 \cdot \frac{E_0^2}{4} \cdot \frac{D_{ASE}}{4}(G_1 + G_2) \end{aligned} \tag{5.27}$$

The second order intercept point (IP2) is used to characterize the second order nonlinearity. IP2 is the point where the linear extension of the second-order intermodulation output power intersects the linear extension of the fundamental output power. The intercept points are given in terms of fundamental output power. IP2 is calculated by setting

$$|S_1(t)|^2 = |S_{NL}|^2 \tag{5.28}$$

Solving Eq. (5.28), we get the amplitude of the input complex tone as

$$A = \frac{E_0(G_1 + G_2)}{G_1 - G_2} \tag{5.29}$$

Therefore, the second intercept point IP2 is

$$IP_2 = \frac{E_0^4 R^2 (G_1 + G_2)^4}{(G_1 - G_2)^2} = \frac{E_0^4 R^2 (1 + \alpha)^4}{(1 - \alpha)^2} \tag{5.30}$$

For the single-ended receiver,$\alpha = 0$

$$IP2 = E_0^4 R^2 \tag{5.31}$$

Due to the imbalance, the central subcarrier is corrupted by the DC offset as described in

Eq. (5.21), however, the DC offset induced Q reduction can always be excluded by disregarding the central subcarrier, which has been done in practice. In reality, OFDM signal contains large number of subcarriers, second-order intermodulation product will be generated by any pair of the subcarriers, resulting in both in-band and out-band intermodulation.

5.4 Simulation Analysis for the Optical I/Q Receiver

A Monte Carlo simulation is used to investigate the receiver performance of CO-OFDM system under the influence of receiver imbalance, RIN, and LO power. The simulation CO-OFDM architecture is the same with that used in Chapter 4. The relevant OFDM system parameters used in the simulation are: OFDM symbol period of 25.6ns, number of subcarriers of 128, 6 subcarriers are used for the pilot-aided phase estimation [125]. The guard interval is equal to 1/8 of the number of subcarriers. 4-QAM encoding is used resulting in a bit rate of 10 Gb/s. Linewidth of the two laser sources is assumed to be 100 kHz. The ASE noise is modeled as white Gaussian noise, and laser phase noise is assumed to be white frequency noise. 4,000 OFDM symbols are used for each simulation. The cumulative chromatic dispersion is assumed to be 34000 ps/nm. No PMD effect is considered in the simulation. In the simulation, the input optical signal power and LO power are measured at the input port of the optical 90° hybrid. The baseline Q value is 9.8 dB at an OSNR of 3.7 dB with $G_1 = G_2 = 1$ and without any receiver noise.

Figure 5.4 shows the Q penalty as a function of the receiver imbalance coefficient α and LO power for the balanced receiver. The signal power is -10 dBm, and RIN is -160 dBc/Hz. Q penalty is defined as the Q reduction of the reference value of 9.8 dB, all at an OSNR of 3.7 dB. As the DC offset impact is not included in the Q penalty calculation and according to Eq. (5.22)-(5.23) the Q penalty will mainly caused by the second order intermodulation term. From Eq. (5.30) we can see that both LO power and α will affect IP2. Large α decreases IP2 while large LO power increases IP2. As the IP2 decreases, the system nonlinearity increases, inducing increasing Q penalty as shown in Figure 5.4. When α equals to 0 (dB), IP2 approaches infinity, meaning the system has maximum linearity and zero Q penalty.

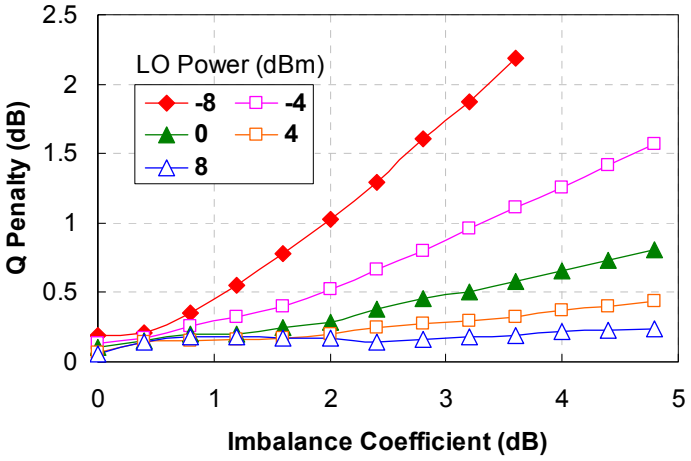

Figure 5.4 Q penalty as a function of α and LO power at fixed RIN of -160 dB and signal power of -10 dBm for the double-ended receiver

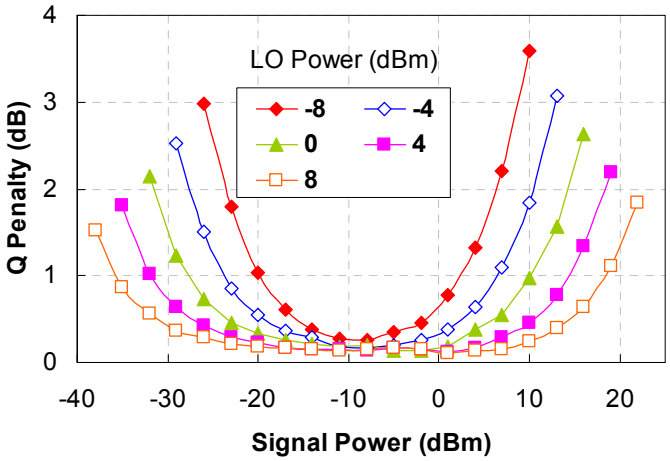

Figure 5.5 Q penalty as a function of signal power and LO power at RIN of -160 dBc/Hz and α of 0.5dB for the double-ended receiver

Figure 5.5 shows the Q penalty as a function of the signal power while varying the LO power. It can be seen that there is a signal dynamic range for each LO power. At the higher input power end, the Q penalty is dominated by the inter-modulation nonlinearity, whereas at the lower input power end, the Q penalty is dominated by the noise including shot noise, thermal noise and RIN noise. The increase of the LO not only improves the linearity, and extends the dynamic range at the higher bound, but also mitigates the impact of the shot noise and thermal noise, and extends the dynamic range at the lower bound. The analysis here help to understand the trade-off between the LO power and input signal dynamic range.

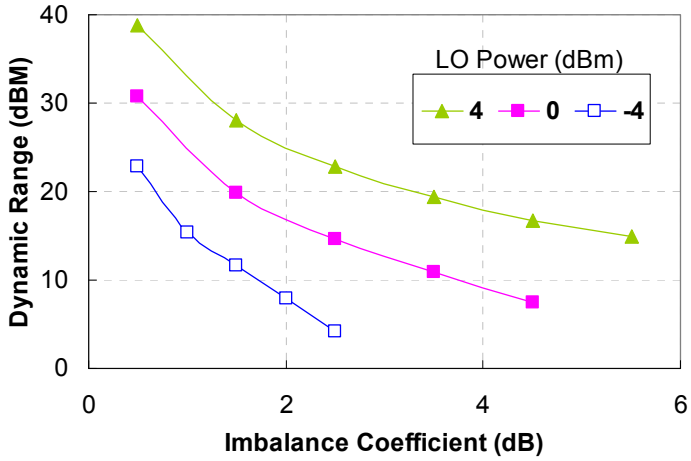

Figure 5.6 Signal dynamic range as a function of LO power and imbalance coefficient

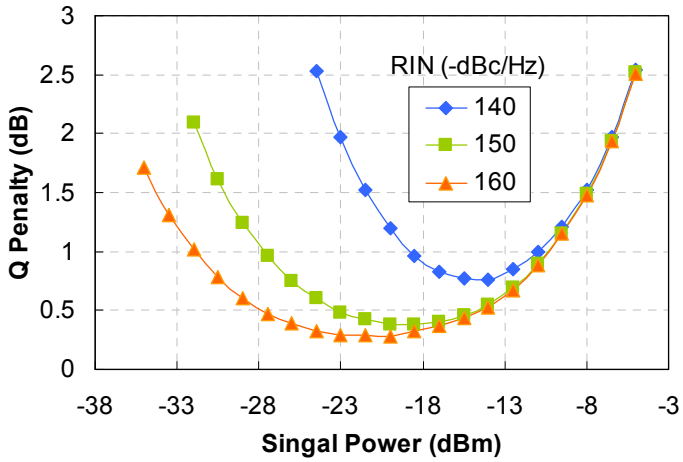

Figure 5.7 Q penalty as a function of signal power and RIN at LO power of 0dBm for single ended receiver.

Figure 5.6 shows the signal dynamic range as a function of LO power and imbalance coefficient. We can see that for 4 dBm LO power, the signal dynamic range is reduced from 39 dB to 28 dB when imbalance coefficient increases from 0.5 dB to 1.5 dB.

Figure 5.7 shows the Q penalty as a function of input signal power under RIN of -140, -150 and -160 dBc/Hz for single-ended coherent receiver. Small RIN value generates less noise thus has lower Q penalty. This figure shows that the laser RIN specification is important, and the RIN of -140 dBc/Hz will induce a minimum penalty of 0.7 dB.

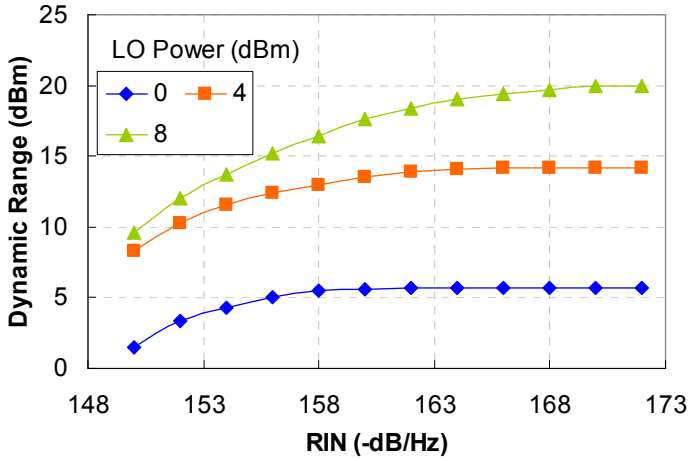

Figure 5.8 0.5dB dynamic range as a function of relative intensity noise and LO power at signal power of 0dBm for single ended receiver.

Figure 5.8 shows the 0.5 dB dynamic range as a function of RIN at different LO powers for single ended receiver. The dynamic rage increases with the decreasing of RIN values. The dynamic range rolls off at a RIN of -160 dBc/Hz as the shot noise will start to take over at this level of RIN and beyond.

5.5 Conclusion

For a CO-OFDM system, coherent detection is used to realize a linear transformation from optical field signal to the base-band electrical signal. However, such linearity can only be maintained with the perfect match between two pair of balanced photodetectors. It is well-known that OFDM signal is very sensitive to nonlinearity [5] which makes CO-OFDM vulnerable to receiver imperfections such as the imbalance between the two ports of a balanced receiver. This imbalance results in DC offset, second order intermodulation term and the increased noise.

In this section, the optical I/Q receiver nonlinearity induced by receiver imbalance in coherent optical OFDM system has been analyzed. The second order intercept point is used to characterize the second order nonlinearity. It can see that both LO power and imbalance coefficient will affect the Q penalty. Large imbalance coefficient decreases Q value while large LO power increases Q value. There is a signal dynamic range for each LO power, the increase of the LO not only improves the linearity, and extends the

dynamic range at the higher bound, but also mitigates the impact of the shot noise and thermal noise, and extends the dynamic range at the lower bound. It has been shown that for both balanced and single-ended receiver, 0.5-dB Q penalty dynamic range for double-ended receiver (single-ended receiver) is 39 dB (17.5 dB) with -160 dBc/Hz laser RIN and 4 dBm LO power.

Chapter 6

Coherent Optical OFDM Transmission up to 1Tb/s Per Channel

6.1 Introduction

Due to the rapid growth of internet traffic together with an increase in the number and range of new services, the optical network that was dominated by a low-speed point-to-point system a decade ago, needs to be replaced with the modern optical communication systems to support high transmission data rate. There is currently a major standardization effort of 100-Gb/s Ethernet (100 GbE) for both local area networks (LAN) and wide area networks (WAN). In fact, many feel that 100 GbE standardization is late and prefer to start with pre-standard 100 GbE gear. Furthermore, to cope with the ever increase of bandwidth-rich internet traffic, some industry experts believe that 1-Tb/s Ethernet standard should be available in the time frame of 2012-2013[163]. As discussed in Chapter 2, high-capacity WDM and OTDM are two promising techniques to realize such optical network. Recently, several pioneering Tb/s transmission experiments have been successfully demonstrated using WDM technique [164] and a combination of WDM and OTDM techniques [165-166]. However, there are several challenges related to the high-capacity WDM and OTDM systems. First, WDM systems need to use expensive broadband optical amplifier and highly stabilized wavelength light source to accommodate more usable channels and decrease the channel spacing. Second, OTDM system relies on precise timing alignment for multiplexing and de-multiplexing. Due to its extreme sensitivity to chromatic- and polarization mode dispersion, OTDM needs high-order optical compensation for either dispersion.

Accompanied with the rapid traffic growth, optical networks are becoming increasingly transparent and mesh-like with the help of ROADMs. Thus, it is necessary that any future high-speed transparent systems can accommodate narrowband optical

filtering introduced by cascaded ROADMs.

One promising alternative pathway toward ultra-high capacity transparent optical network is CO-OFDM due to its superior advantages such as easiness of CD/PMD estimation and mitigation, high spectral efficiency, adaptive data rate, etc. As well as its advantages, OFDM has a number of disadvantages. OFDM is generally susceptible to the nonlinearity owing to high peak-to-average power ratio. Therefore, it is critical to investigate CO-OFDM system transmission performance including fibre nonlinearity in order to ascertain its suitability for the high speed optical transmission.

For optical OFDM, the dispersion can be compensated for in the electrical domain by choosing an appropriate cyclic prefix [35, 101, 130, 167-168]. This could be beneficial for green field deployments, as the system configuration is simplified. However, a periodic inline DCF is widely used in the existing 10-Gb/s transmission systems and when a 40-Gb/s or 100-Gb/s OFDM channel would be used to upgrade such a link, a periodic dispersion map is inevitable for the OFDM signal.

In this chapter, we investigate the feasibility of transmitting up to 1-Tb/s high speed CO-OFDM signal as well as the DCF and ROADM impact on the high speed CO-OFDM system. The transmission performance for 100 Gb/s WDM systems with CO-OFDM through simulation is presented in Section 6.2. In Section 6.3 we conduct experimental demonstration and simulation analysis on the influence of dispersion map on 107-Gb/s CO-OFDM system. We identify that the DCF loss, the DCF nonlinearity impact and the dispersion map influence are three contributions to the Q reduction for the inline dispersion compensated WDM systems compared with the non-compensated counterpart. The performance of 100 Gb/s per channel CO-OFDM signal over transparent DWDM systems with 50-GHz channel spacing is presented in Section 6.4. The simulation transmission performance for 1-Tb/s CO-OFDM WDM systems including the fiber nonlinearity effect is presented in Section 6.5.

6.2 Transmission of the 100-Gb/s WDM System with CO-OFDM

The simplicity in channel estimation and distortion compensation makes CO-OFDM quite appealing for the forthcoming 100 Gb/s Ethernet transport systems. However, we have shown that OFDM signal has a large PAPR. The large spikes of the OFDM signal will easily make the fiber behave nonlinearly. In fact, fiber nonlinearity affects all types of long-haul optical system and it represent the fundamental limiting mechanisms to the amount of data that can be transmitted on a single optic fiber. Thus we expect that the CO-OFDM is sensitive to the fiber nonlinearity. Consequently, it is critical to investigate the CO-OFDM system transmission including fiber nonlinearity to ascertain its suitability for 100 Gb/s optical transmission. We note that 100 Gb/s incoherent optical DDO-OFDM has been proposed and analyzed for long haul transmission using a non-conventional dispersion map and requiring wide electrical bandwidth (>75 GHz) [170]. In this section, we present a scheme for the 100 Gbit/s system with CO-OFDM transmission for a conventional SSMF fibre link requiring an electrical bandwidth just over 30 GHz. In particular, we show the nonlinearity performance of a 100 Gb/s WDM systems with transmission through multiple spans of 100-km SSMF fibers using CO-OFDM, without dispersion compensation and with only EDFA. Through simulation, we find that the system Q of the received signal varies from 21 to 15 dB as the fibre length increases from 200 to 1000 km, and the optimal optical launch power into the fibre link is around 21 dBm. Based on our simulation, CO-OFDM may be an attractive choice of modulation format for 100 Gbit/s Ethernet metro or long-haul transport systems, without need for optical compensation.

6.2.1 WDM Transmission Systems with CO-OFDM

Figure 6.1 shows the basic single polarization WDM CO-OFDM transmission system. A generic CO-OFDM system consists of an OFDM transmitter, an RF-to-optical OFDM upconverter, an optical link, an optical-to-RF OFDM downconverter, and an OFDM receiver. Inside the OFDM transmitter, the input data bits are mapped onto corresponding

information symbols of the subcarriers within one OFDM symbol, and the digital time domain signal is obtained using inverse IDFT, which is subsequently converted into a real-time waveform through a DAC. A guard interval is inserted to prevent inter-symbol interference due to fibre dispersion. The OFDM RF-to-optical direct up-conversion is achieved by applying the OFDM signal to an optical IQ modulator biased at null point [34,169]. A detailed introduction on each CO-OFDM system function block can be found in Section 4.2. Multiple WDM channels with CO-OFDM modulation format are launched into the optical link. The optical link consists of multi-span SSMF and EDFAs to compensate for the fibre transmission loss. In contrast to the conventional design, the CO-OFDM systems do not use any dispersion compensation fibre. The WDM channels are de-multiplexed and detected using an optical coherent receiver including two pairs of balanced photo-detectors, an optical 90^0 hybrid, and a local oscillator laser, which serves as an optical-to-RF OFDM direct down converter. In the OFDM RF receiver, the signal is first sampled using an ADC, and demodulated by performing FFT to recover the data.

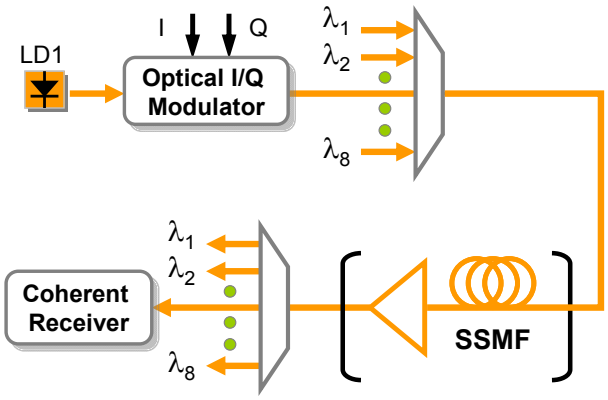

Figure 6.1 Conceptual diagram of WDM CO-OFDM system

6.2.2 Simulation Results and Discussions

A Monte Carlo simulation is conducted to identify the transmission performance of a CO-OFDM system. The optical link parameters used in the simulation are 8 WDM channels spaced at 100 GHz, 100 km span distance, fibre chromatic dispersion of 16 ps/nm/km, 0.2 dB/km loss, and a nonlinear coefficient of 2.6×10^{-20} m^2/W. The OFDM parameters are OFDM symbol period of 51.2 ns, 2560 subcarriers, a guard interval equal

to one quarter of the observation period, 4-QAM encoding for each subcarrier. The so-configured OFDM system will provide 100-Gbit/s net transmission rate. The fibre span loss is compensated for by an EDFA with gain of 20 dB and noise figure of 6 dB. The linewidths of the transmit and receive lasers are assumed to be 100 kHz, which is close to the value achieved with commercially available external-cavity semiconductor lasers. 20 OFDM symbols are simulated equivalent to 102400 (20 × 2560 × 2) bits. The simulation is carried out using the commercial simulation tool VPItransmissionMakerTMWDM V7.0. The receiver signal processing follows the procedure of Section 3.3.4. The relative phase shift between subcarriers or channel estimation is calculated using training sequences (five OFDM pilot symbols). The phase drift from the laser phase noise is also estimated and compensated for using pilot subcarriers described in [34, 170].

Figure 6.2 (a) shows the received constellations of 100Gb/s OFDM signal after transmitting 1000 km fiber. The sources of the noise spreading in each information symbol are mainly the laser phase noise, the nonlinearity of optical fibres and the ASE noise in the transmission system. It can be seen that the constellation is rotated with respect to each other owing to a phase shift from fiber chromatic dispersion and a phase noise from the transmitter and receiver laser. The phase shift ϕ due to chromatic dispersion can be written as

$$\phi = \frac{1}{2}\beta_2 \omega^2 L \tag{6.1}$$

$$\beta_2 = -\frac{\lambda^2}{2\pi c} D \tag{6.2}$$

where β_2 is the group velocity dispersion parameter, D is the fiber dispersion parameter, L is the fiber length, ω is the optical frequency at each subcarrier. The phase shift and phase noise can be estimated and compensated using training sequences as introduced in Section 3.3.4. Figure 6.2 (b) shows the signal constellation after removing the chromatic dispersion and doing the phase compensation. A clear constellation is recovered with four distinct clusters of data points corresponding four QAM information symbols. The

residual noises spreading for each OFDM constellation point are mainly from nonlinearity of optical fibers, ASE noise in transmission system, and intra-carrier interference due to the intra-symbol phase noise of lasers.

BER and Q-factor are used to identify the system performance. The Q is extracted from the constellation. Assuming the noises spreading of each information symbol is Gaussian noise and the Cartesian axes are the decision thresholds, we define Q of the received signal as

$$Q(dB) = 20\log_{10}(q) \tag{6.3}$$

The q factor is calculated as

$$q^2 = \frac{\mu_x^2}{\sigma_x^2} = \frac{\mu_y^2}{\sigma_y^2} \tag{6.4}$$

where $\mu_{x/y}$ is the mean value of a particular cluster from a decision threshold and $\sigma_{x/y}$ is the standard deviation, as illustrated in Figure 6.2 (b). The q factor can be further calculated as

$$q = \left(\frac{1}{NN_{sc}} \sqrt{\sum_{i=1}^{N} \sum_{k=1}^{N_{sc}} \frac{\left| C'_{ik} - C'_{i,AVG} \right|^2}{\left| C'_{i,AVG} \right|^2}} \right)^{-1}, \quad C'_{i,AVG} = \left\langle C'_{ik} \right\rangle_k \tag{6.5}$$

where C'_{ik} is the received information symbol for the *kth* subcarrier in the *ith* OFDM symbol, $C'_{i,AVG}$ is average of received information symbol, N and N_{SC} are the number of OFDM symbols and subcarriers respectively. The q-factor is related to the system's BER through the complementary error function *erfc()* given by

$$BER(q) = \frac{1}{2} \cdot \mathrm{erfc}\left(\frac{q}{\sqrt{2}}\right) \tag{6.6}$$

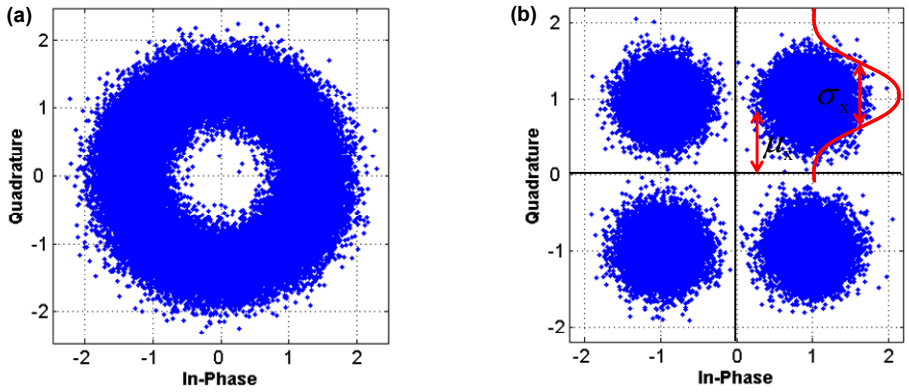

Figure 6.2 Optical constellations (a) before and (b) after equalization for a 1000-km system with a −6dBm fiber input power per channel.

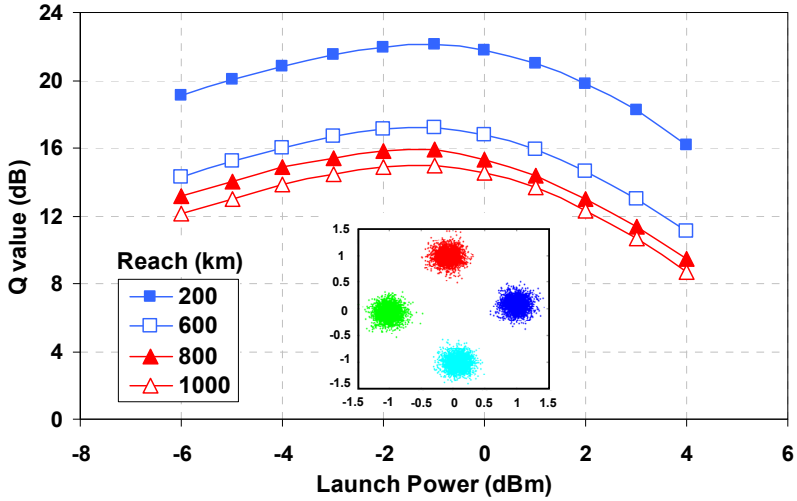

Figure 6.3 System Q against optical power of each WDM channel

Figure 6.3 shows the system Q of the received signal against the optical power of each WDM channel launched into the fibre link for different fibre lengths. The Q is obtained without noise loading at the receiver. It can be seen from Figure 6.3 that the optimal optical launch power of each WDM channel is about -1 dBm for the reaches from 200 to 1000 km. This optimal power insensitivity to the reach is due to the non-compensation dispersion map used in this work. If the power of each WDM channel is increased beyond these optimal values, the nonlinearity of optical fibre will degrade system performance, resulting in reduced Q. On the other hand, if the input power is reduced from these optimal values, the OSNR of the received signal becomes lower, also resulting in reduced Q. The inset in Figure 6.3 shows the constellation of 20 OFDM symbols after channel and

phase compensation at -1 dBm launch power for the reach of 1000 km. The clear constellation indicates successful transmission and reception of the 100 Gbit/s signal.

Figure 6.4 shows the Q sensitivity performance at different launch powers for the reach of 1000 km. Adjustment of the OSNR is done through noise loading at the receiver. The noise loading in Figure 6.4 is to identify the nonlinearity penalty at different launch powers. It is expected that at low launch powers (e.g. -6 dBm), the system is very linear and insignificant penalty is observed compared with the back-to-back transmission. At the optimal power of -1 dBm, the power penalty is about 0.5 dB at Q of 9.8 dB. At high launch powers, an error floor emerges owing to fibre nonlinearity, e.g. a Q ceiling of 8 dB at the launch power of 4 dBm as shown in Figure 6.4.

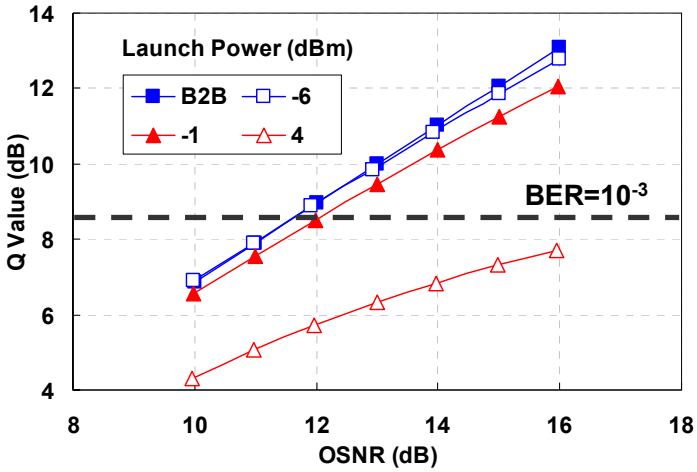

Figure 6.4 BER performance of WDM channels after 1000 km transmission with varying launch power

6.3 CO-OFDM Transmission with Inline Chromatic Dispersion Compensation

Due to the advantages provided by CO-OFDM, it is tempting to consider the CO-OFDM as the upgrade solution from today's 10-Gb/s to the future high speed optical systems. The chromatic dispersion of the transmission fiber is one of the key factors that reduce the performance of an optical fiber transmission system by limiting the maximum capacity and/or transmission distance of high-speed optical data channels. A DCF [171] is widely used in the existing IM/DD 10-Gb/s optical fiber transmission system. The DCF is a special fiber which is designed to have opposite dispersion parameters to that of

transmission fibers. DCF is capable of totally compensating the CD in transmission fibers and also allowed for broadband dispersion compensation. However, DCF obviously increases the ASE noise due to the adoption of double-stage amplifiers. Besides, DCF usually has a small core size; hence even optical signal of moderate power may cause DCF behave nonlinearly. Therefore, DCF will also introduce additional nonlinearity degradation because of its large nonlinear coefficient. What is more intriguing is the dispersion map impact on the nonlinearity performance [172] for CO-OFDM systems [173].

In this section, we conduct experimental demonstration and simulation analysis on the influence of dispersion map on the 107-Gb/s CO-OFDM system. Orthogonal-band-multiplexed OFDM (OBM-OFDM) Scheme [175] is proposed to overcome the electrical bandwidth bottleneck and obtain the 107 Gb/s signal. We first present the principle of OBM-OFDM and then study the dispersion map impact on the 10.7-, 42.8- and 107-Gb/s CO-OFDM system through the numerical simulation. Furthermore, we investigate the system performance at 107 Gb/s at varying dispersion compensation ratio (CR).

6.3.1 Orthogonal-Band-Multiplexed OFDM

As the IP traffic continues to grow at a rapid pace, the 100-Gb/s Ethernet is being considered as the next-generation transport standard for IP networks [174]. As the data rate approaches 100 Gb/s and beyond, the electrical bandwidth required for CO-OFDM would be at least 15 GHz [175] and is not cost-effective to implement even with the best commercial DACs and ADCs in silicon integrated circuit (IC) [176]. To overcome this electrical bandwidth bottleneck, we proposed the concept of OBM-OFDM [175]. The basic principle of OBM-OFDM is to divide the entire OFDM spectrum into multiple orthogonal bands. Due to the inter-band orthogonality, the multiple OFDM bands with zero or small guard bands can be multiplexed and de-multiplexed without inter-band interference.

A. Principle of OBM-OFDM

As shown in Figure 6.5, the entire OFDM spectrum comprise N OFDM bands, each with the subcarrier spacing of Δf, and band frequency guard spacing of Δf_G. The subcarrier spacing Δf is identical for each band due to using the same sampling clock within one circuit. The orthogonal condition between the different bands is given by

$$\Delta f_G = m\Delta f \tag{6.7}$$

Namely, the guard band is multiple (m) times of subcarrier spacing. In doing so, the orthogonality condition is satisfied for any two subcarriers inside the complete OFDM spectrum. Especially, when m equals to 1 in Eq. (6.7), the OFDM bands can be multiplexed/de-multiplexed even without guard band. We call this method of subdividing OFDM spectrum into multiple orthogonal bands OBM-OFDM. To detect OBM-OFDM, two approaches can be used as shown in Figure 6.5. First, the receiver laser is tuned to the centre of each band. Each band is detected separately by using an 'anti-alias filter *I*' that low-passes only one-band RF signal. Second, the local laser is tuned to the center of the guard band. Two bands are detected by using an 'anti-alias filter *II*' that low-passes two-band RF signal simultaneously. In either case, the inter-band interference can be avoided because of the orthogonality between the neighboring bands, despite the leakage of the subcarriers from neighboring bands.

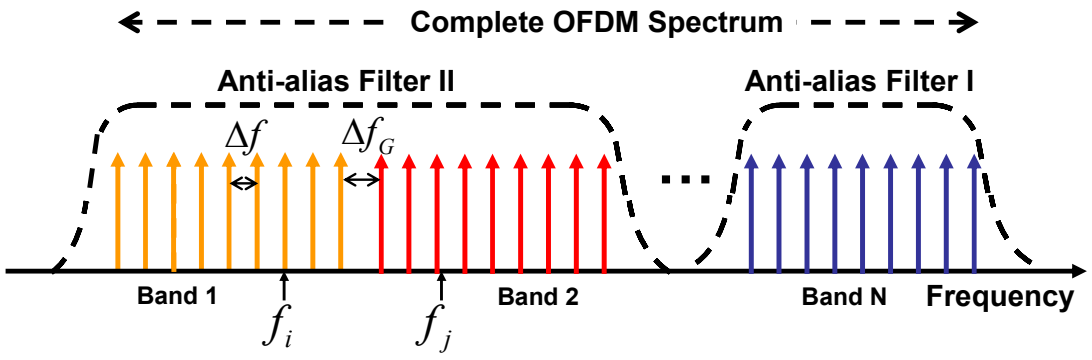

Figure 6.5 Conceptual diagram of OBM-OFDM. Anti-alias filters *I* and *II* correspond to two detection approaches illustrated in the text.

Using such a scheme, each OFDM sub-band can be de-multiplexed using an anti-alias

filter slightly wider than the signal band. By multiplexing and de-multiplexing multiple OFDM bands, OBM-OFDM has the following advantages: (i) high spectral efficiency can be achieved by allowing for zero or small guard band, (ii) OBM-OFDM offers the flexibility of demodulating two OFDM sub-bands simultaneously with just one FFT whereas three (I) FFTs would be otherwise needed for the same purpose, and (iii) OBM-OFDM can be readily partitioned with electrical anti-alias filters, and subsequently processed with lower-speed DAC/ADCs [177]. By using OBM-OFDM, CO-OFDM at 107 Gb/s is realized without forcing the DAC/ADC devices operated at the extremely high sampling rate.

B. Implementation of OBM-OFDM

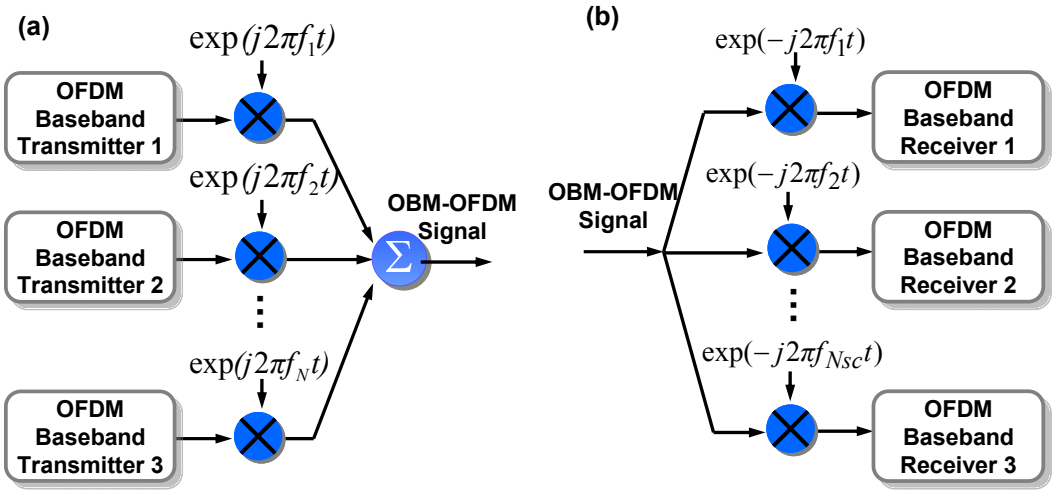

Figure 6.6 Schematic of OBM-OFDM implementation in mixed-signal circuits for (a) the transmitter, (b) the receiver

OBM-OFDM can be implemented in either electrical or optical domain. As mentioned earlier, OBM-OFDM is particularly suitable to be realized with mixed signal ICs to resolve ADC/DAC bandwidth bottleneck, while the optical realization of OBM-OFDM serves as an alternative to the other spectrally efficient multiplexing schemes including coherent WDM [178], all-optical OFDM [179] and electrooptically subcarrier-multiplexed OFDM [180].

Electrical implementation of OBM-OFDM can be realized by up-converting multiple OFDM basebands to appropriate RF bands with the centre frequency from f_1 to f_N using

one RF I/Q modulator or complex mixer for each OFDM baseband as shown in Figure 6.6 (a). Each OFDM baseband transmitter is implemented using digital IC design. The subsequent up-conversion, band-filtering, and RF amplification can be implemented in RF IC design. The range of f_1 to f_N is centered around zero, given by

$$f_l = l \cdot \Delta f_b \quad l \in [-L, L] \tag{6.8}$$

Where f_l is the center frequency of the *lth* OFDM band, Δf_b is the band spacing, and L is the maximum band number. Then the outputs of each electrical IQ modulator are further summed up at the output, namely, real and imaginary parts are added up in separate parallel paths. The combined complex OFDM signal is used to drive an optical IQ modulator to be up-converted to optical domain. At the receive end as shown in Figure 6.6 (b), the incoming signal is split into multiple sub bands and down-converted to base-band using electrical IQ de-modulators. Anti-alias filters should be used to remove unwanted high frequency components at the output of the demodulators. In such a way, the DAC/ADC only needs to operate at the bandwidth of each OFDM band, which is approximately scaled down by a factor equal to the number of subbands from the original complete OFDM spectrum. For instance, the bandwidth of 107 Gb/s data rate with 4-QAM modulation and polarization multiplexing is around 35 GHz. If the number of subbands is five, each OFDM band will only need to cover about 7 GHz optical bandwidth. The electrical bandwidth required is 3.5 GHz, or half of the OFDM band spectrum if direct conversion is used at transmit and receive ends. The DAC/ADC with bandwidth of 3.5 GHz can be implemented in today's technology [176], and using a wider bandwidth for each OFDM band will reduce the number of the OFDM bands further down to two or three.

The OBM-OFDM could be realized using either subcarrier multiplexing [181] or wavelength multiplexing to patch multiple orthogonal bands into a complete OFDM spectrum (Figure 6.5). The OBM-OFDM can be also optically implemented by transmitting OFDM data through many WDM channel and locking all the lasers to the common optical standard such as an optical comb [182]. In doing so, the orthogonality condition is satisfied for all subcarriers across the entire WDM channels. This form of

OFDM transmission is called cross-channel OFDM (XCOFDM). An optical filter or an electrical filter with bandwidth slightly larger than the channel bandwidth can be used to select the desired channel. Consequently, no frequency guard band is necessary between neighboring WDM channels.

6.3.2 Experiment Setup

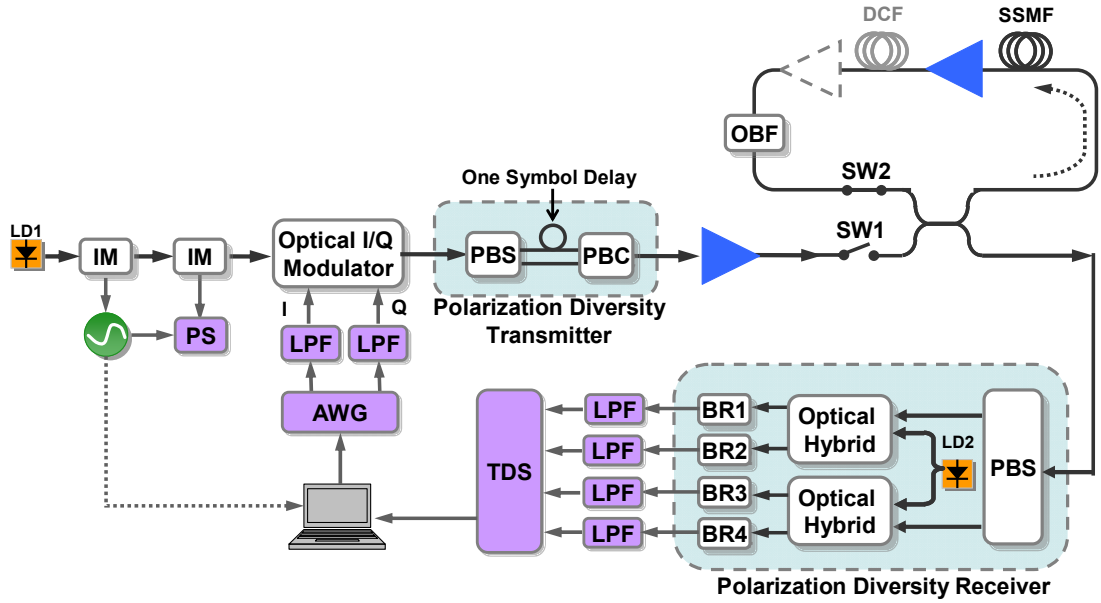

Figure 6.7 Experimental setup for 107-Gb/s OBM-OFDM transmission systems

In our experiment, OBM-OFDM scheme as described in Section 6.3.1 is used to obtain the 107-Gb/s data rate. Although the electronic OBM-OFDM is more cost-effective solution, the related research work will involve expensive high-speed mixed signal design, foundry run, and chip testing. Thus we choose optical multiplexing to obtain OBM-OFDM. Figure 6.7 shows the experimental setup for 107-Gb/s CO-OFDM transmission.

A. CO-OFDM Transmitter

The 107-Gb/s OBM-OFDM signal is generated by multiplexing 5 OFDM (sub) bands. In each band, 21.4-Gb/s OFDM signals are transmitted in both polarizations. The

multi-frequency optical source spaced at 6406.25 MHz is generated by cascading two intensity modulators (IMOD). The guard band equals to one subcarrier spacing (*m* equals to 1 in Eq. (6.7)). Figure 6.8 shows the multiple tones generated by two cascaded IMODs. Only the middle five tones with large and even power are used for performance evaluation. The baseband OFDM signal is generated off-line with a length of 2^{15}-1 Pseudo-Random Binary Sequence (PRBS) and mapped to 4-QAM. The total number of OFDM subcarriers is 128, and guard interval is 1/8 of the observation window. The middle 82 subcarriers are filled, from which 4 pilot subcarriers are used for phase estimation. The I and Q components of the time-domain digital signal are uploaded onto Tektronix Arbitrary Waveform Generator (AWG) provides 10 GS/s sampling rate for both I and Q parts. Figure 6.9 (a) shows the electrical spectrum of the I/Q channel at the output of AWG. It can be seen that the aliasing components of OFDM signal are present above 6 GHz. When combining multiple OFDM subbands, such aliasing frequency components will degrade the signals in the adjacent bands. A 3-GHz low-pass electrical filter is used to eliminate the aliasing OFDM components. Figure 6.9 (b) shows the electrical spectrum after low-pass filtering, where the aliasing spectrum components are removed.

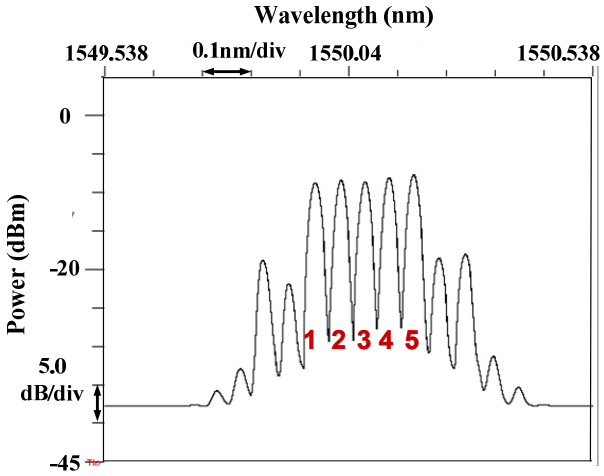

Figure 6.8 Multiple tones generated by two cascaded intensity modulators

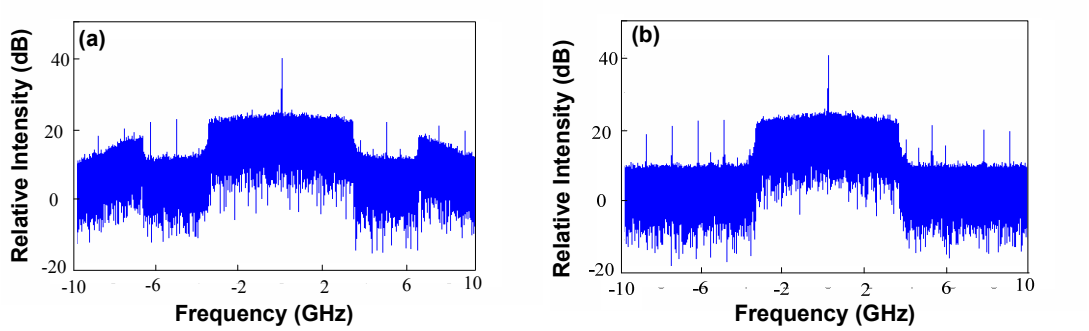

Figure 6.9 Electrical spectrum for (a) directly at the output of the AWG and (b)after 3-GHz anti-aliasing filters.

The AWG is phase locked to the synthesizer through 10-MHz reference. The optical I/Q modulator comprising two MZMs with 90^0 phase shift is used to directly impress the baseband OFDM signal onto five optical tones. The modulator is biased at null point to completely suppress the optical carrier and perform linear RF-to-optical up-conversion [169] as discussed in Chapter 4. The optical output of the I/Q modulator consists of five-band OBM-OFDM signals. Each band is filled with the same data at 10.7-Gb/s data rate and is called "uniform filling" in this thesis. 2×2 MIMO-OFDM as introduced in Section 3.3.3 is employed to improve the spectral efficiency. 2×2 MIMO-OFDM uses two OFDM transmitters to send two independent data into each polarization, which are then detected by two OFDM receivers (one for each polarization).

A cost-effective method to emulate the two transmitters is: the single-polarization optical OFDM signal at the output of the I/Q modulator is first evenly split into two polarization branches with a PBS. One of the PBS output branch is delayed by one OFDM symbol period (i.e., 14.4 ns in this experiment) which makes the two polarization components completely independent with each other. Then the two polarization branches are subsequently combined with polarization beam combiner (PBC), resulting in a composite data rate of 21.4 Gb/s. The two polarization components are completely independent due to the delay of 14.4 ns for each OFDM symbol.

B. Fiber Link

A recirculation loop consisting of shorter transmission link is used to emulate long-haul optical links. Figure 6.7 shows the structure of the recirculation loop. The loop consists of

two optical switches (OSWs), an optical amplifier, an optical band pass filter, an optical coupler and a fiber link. The OSW is used to allow data to flow into the fiber link (the load state) and then to allow data to circulate (the loop state). After the data circulating for a specified time, the state of the experiment toggles, and the load/loop cycle is repeated.

Two different dispersion maps as shown in Figure 6.10 are used in the recirculation loop: (I) Without inline compensation, namely, CD is compensated in electrical domain. The CD gradually accumulates with the increasing of fiber length. In this case, the recirculation loop only comprises 100 km of SSMF and an EDFA to compensate the fiber loss. (II) Inline compensation, namely, after 100 km SSMF, a DCF with length of 13.5km is used to compensate the CD. Two EDFAs are used to compensate the fiber loss as well as to control the input power into SSMF and DCF. Through simulation we found that 6 dB is the optimal input power difference between the SSMF and DCF. The total cumulated dispersion of SSMF and DCF is respectively 1600 ps/nm and -1536 ps/nm resulting in a residual dispersion per span of 64 ps/nm or 96% CR which is close to that used in most of the deployed systems [183]. No Raman amplification is used for the transmission.

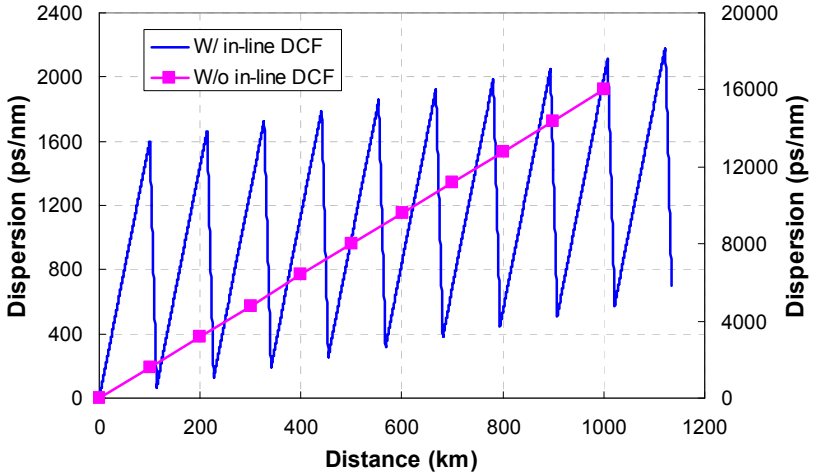

Figure 6.10 Two dispersion maps used in the recirculation loop

C. CO-OFDM Receiver

The signal is coupled out of the loop and received with a polarization diversity coherent receiver [184,185] comprising a PBS, a local laser, two hybrids, and four balanced

receivers. The complete OFDM spectrum comprised of five subbands and the entire bandwidth for 107-Gb/s OFDM signal is 32 GHz. The local laser is tuned to the center of each band, and the RF signals from the four balanced detectors is firstly passed through the anti-aliasing low-pass filters with a bandwidth of 3.8 GHz, such that only a small portion of the frequency components from other bands is passed through, which can be easily removed during OFDM signal processing. The performance of each band is measured independently. The detected RF signals are then sampled with a Tektronix time domain-sampling scope (TDS) at 20 GS/s. The sampled data is processed with a MATLAB program to perform 2×2 MIMO-OFDM processing [184]. The receiver signal processing involves: 1) FFT window synchronization using Schmidl format to identify the start of the OFDM symbol; 2) software estimation and compensation of the frequency offset; 3) channel estimation in terms of Jones Matrix *H*; 4) phase estimation for each OFDM symbol; and 5) constellation construction for each carrier and BER computation. The channel matrix is estimated by sending 30 OFDM symbols using alternative polarization launch. The total number of OFDM symbol evaluated is 500 symbols. Mathematically, the transmitter information symbol of the two polarizations in the forms of Jones vector are given by

$$c = \begin{pmatrix} c_1 \\ c_2 \end{pmatrix} \tag{6.9}$$

where c_1 and c_2 are transmitted OFDM information symbols for two polarizations, Assume the fiber transmission Jones Matrix *H* is

$$H = \begin{pmatrix} h_{11} & h_{12} \\ h_{21} & h_{22} \end{pmatrix} \tag{6.10}$$

Ignoring the additive noise, the two received OFDM symbol is thus given by

$$c^{'} = \begin{pmatrix} c_1^{'} \\ c^{'2} \end{pmatrix} = H \cdot c \tag{6.11}$$

or equivalently

$$\begin{cases} c_1^{'} = h_{11}c_1 + h_{12}c_2 \\ c_2^{'} = h_{21}c_1 + h_{22}c_2 \end{cases} \tag{6.12}$$

From Eq. (6.12), the transmitted information symbols can be recovered from the received signals by inverting H

$$c = H' \begin{pmatrix} c_1' \\ c_2' \end{pmatrix}, \; H' = \begin{pmatrix} h_{11} & h_{12} \\ h_{21} & h_{22} \end{pmatrix}^{-1} \tag{6.13}$$

The training symbols are generated by filling the odd symbols with known random data, while nulling the even symbols. After the polarization multiplexing emulator, the training symbols form a pattern of alternative polarization launch for two consecutive OFDM symbols. Using odd training symbols, the associated channel estimation can be expressed as

$$\begin{pmatrix} c_1' \\ c_2' \end{pmatrix} = \begin{pmatrix} h_{11} & h_{12} \\ h_{12} & h_{22} \end{pmatrix} \begin{pmatrix} c_1 \\ 0 \end{pmatrix} \Longrightarrow \begin{cases} h_{11} = c_1'/c_1 \\ h_{21} = c_2'/c_1 \end{cases} \tag{6.14}$$

and using even training symbols are

$$\begin{cases} h_{11} = c_1'/c_2 \\ h_{21} = c_2'/c_2 \end{cases} \tag{6.15}$$

It can be seen from Eq. (6.14)and Eq. (6.15) that, by using alternative polarization training symbol, the full channel estimation can be obtained. Then, using the inverse of this matrix in Eq. (6.13) and the received information symbols, the transmitted symbols in the two polarizations can be estimated. The estimated transmitted symbols will be de mapped to the closest constellation points to recover the transmitted digital bits.

6.3.3 Measurement Result and Discussion

Figure 6.11 (a) shows the RF spectrum after 1000-km transmission measured with the polarization diversity coherent receiver. No frequency guard band is used in our transmission measurement. It can be seen that five OFDM bands each with 6.4 GHz bandwidth are closely patched together and the entire OFDM spectrum occupied is about 32 GHz. The out-band components are due to the multi-frequency source generation not tightly bounded at five tones. This artifact will not exist in the real application using either subcarrier multiplexing or optical multiplexing OBM-OFDM. Figure 6.11 (b)

shows the detected electrical spectrum after using a 3.8 GHz electrical anti-alias filter for one-band detection. The anti-alias filter is critical for OBM-OFDM implementation. As is shown in Figure 6.11 (a), without electrical anti-alias filter, the electrical spectrum will be as broad as 16 GHz, indicating that at least 32 GS/s ADC has to be used. However, the filtered spectrum in Figure 6.11 (b) can be easily sampled with 20 GS/s or even at a lower speed of 10 GS/s. Additionally, despite the fact that there are some spurious components from the neighboring band that is leaked at the edge of the 3.8-GHz filter, since they are orthogonal subcarriers to the interested OFDM subcarriers at the center, they do not contribute to the interference degradation.

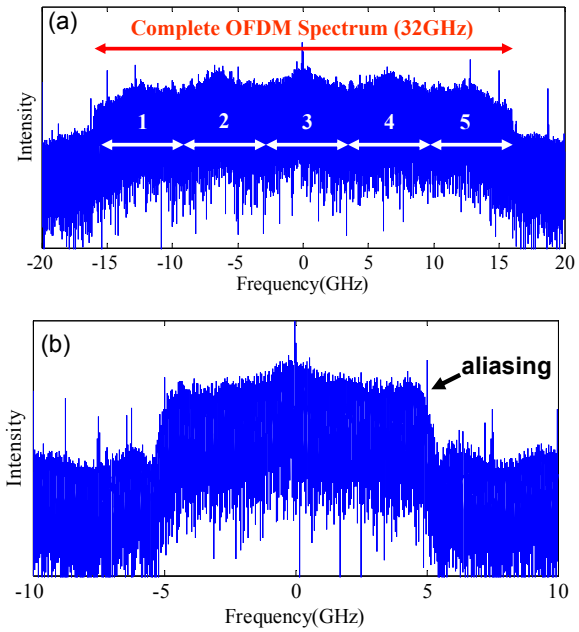

Figure 6.11(a) Optical Spectra for the 107-Gb/s signal using a polarization diversity coherent receiver, the band numbers are depicted next to the corresponding bands. (b) The electrical spectrum at the receiver after the 3.8 GHz anti-alias filter

Figure 6.12 shows the system Q as a function of launch power with and without inline DCF after 1000 km SSMF single channel transmission. Q calculation is the same with that introduced in Section 6.2. The optimum launch power is -4 and -1 dBm respectively while the maximum Q value difference is about 3.5 dB.

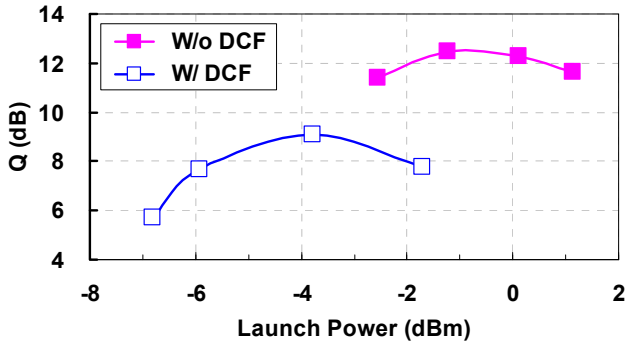

Figure 6.12 Q as a function of the launch power at the reach of 1000 km

Figure 6.13 shows the BER sensitivity comparison of two dispersion maps (with and without DCFs) at the back-to-back, 400-km and 1000-km transmission. For the inline compensated system, a BER of 10^{-2} emerges at the 1000-km transmission. The required OSNR for a BER of 10^{-3} for 400 km transmission is respectively 18.5 dB and 16.5 dB for inline compensation and no line compensation. The back-to-back OSNR sensitivity for a BER of 10^{-3} is 15.5 dB, which is a record for either single-carrier or multicarrier systems at 107 Gb/s.

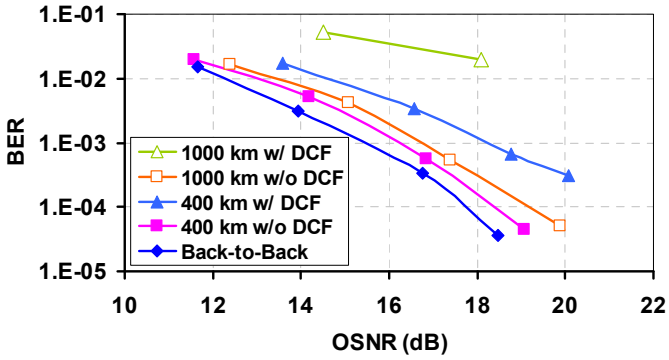

Figure 6.13 BER sensitivity of 107-Gb/s CO-OFDM signal

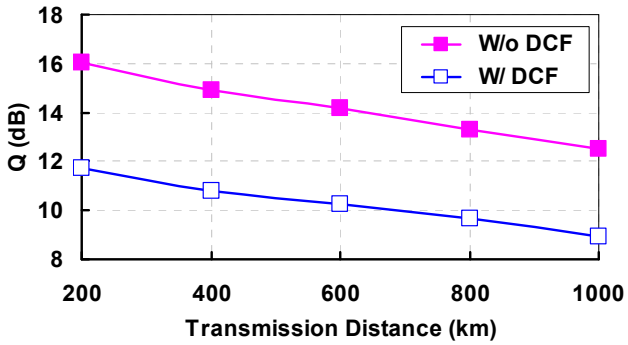

Figure 6.14 Q factor of 107-Gb/s CO-OFDM signal as a function of reach at launch power of -4 dBm (-1dBm) for the transmission with (without) DCF

Figure 6.14 shows the system Q performance as a function of reach up to 1000 km at optimum launch power. For the system without DCF, the Q difference between 200km and 400 km transmission distance is about 2dB. For system with DCF, signal has around 8dB Q value after 1000km transmission. It can be seen that the Q difference between two dispersion maps is around 4dB.

6.3.4 Simulation Model

We use CO-OFDM system with polarization multiplexing for simulation. The simulation schematic diagram is shown in Figure 6.15. Two optical OFDM signals are generated independently and combined with a polarization beam combiner. Multiple WDM channels with CO-OFDM modulation format are launched into the optical link. The optical link consists of 10 spans of cascaded inline-compensation sections. Each section consists of SSMF and DCF. Two EDFAs with 6 dB noise figure are used in each span. A ROADM node is connected after each span and the detailed discussion of ROADM will be introduced in section 6.4. The function of ROADM is disabled when only the DCF induced impairment is investigated. The output signal after fiber transmission is detected using a polarization diversity coherent receiver comprising a receiver local laser, a polarization beam splitter, two hybrids and four balanced receivers. The relative phase shift between subcarriers or channel estimation is calculated by using training sequences. The phase drift from the laser phase noise is also estimated and compensated using pilot subcarriers.

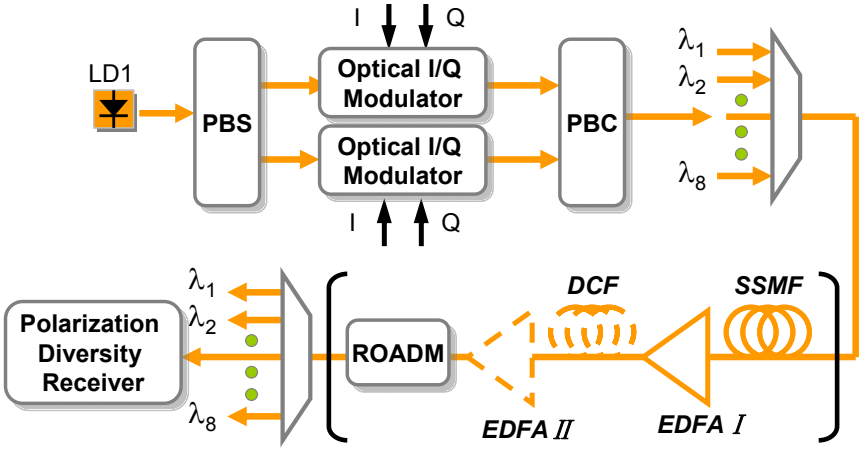

LD: Laser Diode PBS/C: Polarization Splitter/Combiner
ROADM: Reconfigurable optical add-drop multiplexer

Figure 6.15 Simulation schematic diagram

The simulation is carried out using the commercial simulation tool VPItransmissionMaker^{TM}WDM V7.6. The simulation parameters of SSMF and DCF are listed in TABLE-6.1. The dispersion compensation ratio for each span is 96%. The PMD effect is omitted in the simulation, and it is expected that CO-OFDM has high PMD tolerance [106,118]. The linewidths of the transmit and receive lasers are assumed to be 100 kHz. Three different CO-OFDM data rates, 10.7 G-, 42.8 G-, 107 Gb/s are simulated. All the data rates discussed in this chapter are the net data rate excluding the overhead of cyclic prefix and pilot subcarriers.

TABLE-6.1 Simulation Parameters of SSMF and DCF

	Length per Span (km)	Fiber Loss (dB/span)	Nonlinearity ($W^{-1}km^{-1}$)	Dispersion (ps/nm/span)
SSMF	100	20	1.3	1600
DCF	13.5	8.47	5.4	-1536

A detailed description of OFDM simulation parameter is shown in TABLE6.2. The basic data rate provided by one OFDM sub-band with 82 subcarriers is 21.4 Gb/s, which can be calculated as

$$\frac{82}{12.8\times10^{-9}\times(1+1/8)}=21.4\mathrm{Gb/s} \tag{6.16}$$

Scaling to the higher data rate is achieved by increasing the number of OFDM sub-bands.

For example, 2 OFDM sub-bands are used to generate 42.8 Gb/s signal. Due to band multiplexing, the OFDM symbol period for 42.8 G-, 107 Gb/s signal is maintained at 12.8 ns, independent of the net data rate. The subcarrier number for each data rate is *N* times of 82, where *N* is the number of multiplexed bands. The bandwidth of one OFDM sub-band is 6.4 GHz. Therefore, the bandwidth for each data rate is *N* times of 6.4 GHz. The 107 Tb/s signal occupies $6.4\ GHz \times 5 = 32.5$ GHz bandwidth. The special case of 10.7 Gb/s signal is generated by filling 42 subcarriers of one OFDM sub-band. At the receiver, each OFDM band is detected independently with 4 pilot subcarriers used for phase estimation. 4-QAM encoding is used for each subcarrier. The guard interval is set to 1/8 of the observation period for both simulations with and without DCF. 8 WDM channels spaced at 50 GHz are simulated.

TABLE6.2 OFDM Parameters

Data Rate (Gb/s)	10.7	42.8	107	1070
Subcarrier No.	42	164	410	4100
No. of bands	1	2	5	50
Symbol period (ns)	12.8	12.8	12.8	12.8
Symbol No.	200	150	120	20
CP	1/8	1/8	1/8	1/8

6.3.5 Simulation of Dispersion Map Impact

In the experiment shown in the last section, five OFDM bands with the same data are multiplexed (uniform filling) to generate an OBM-OFDM signal. There is a concern whether this uniform filling will underestimate the nonlinearity such that our experiment may overestimate the CO-OFDM transmission performance. Therefore, it is important to compare the performance difference between the uniform filling used in the experiment and the scenario for which each band is filled with independent data (random filling). Furthermore, while the experiment is more convincing and will be the ultimate method of validation, the numerical simulation is more flexible and can carry out many more measurement scenarios with relatively low cost. In this section, we first conduct the simulation to compare the nonlinearity performance difference between the uniformly

filled OBM-OFDM and randomly filled OBM-OFDM, in both single-channel and WDM environments. All the simulation results are based on random filling if no specific filling is indicated. We then proceed to conduct simulation to compare the nonlinearity performance difference of 10.7-, 42.8- and 107-Gb/s CO-OFDM transmission with and without the DCF in WDM environment. The simulation diagram and parameters are based on the simulation modal on section 6.3.4.

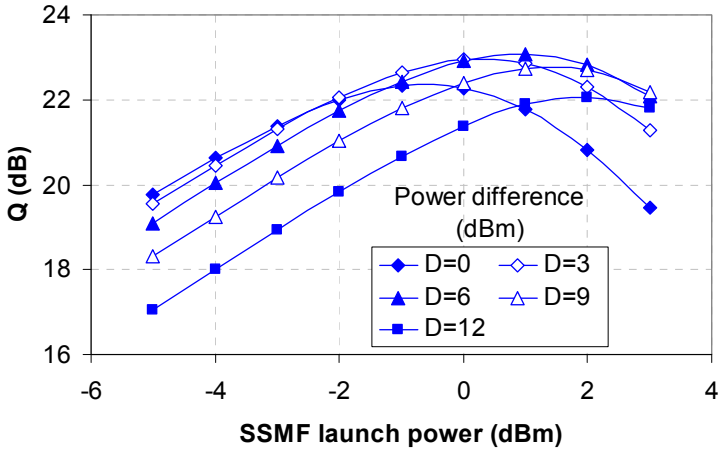

Figure 6.16 Q factor as a function of SSMF launch power under different *D* for a 200km CO-OFDM single channel system

We have known that the two of the major impairments introduced by DCF are the extra ASE noise and the DCF nonlinearity. To minimize the additional ASE noise, a large DCF launch power is preferred. However, the DCF linear performance gets worse for a large input power. Hence, a trade off must be made between the additional ASE noise and DCF linearity. The first task of the simulation is to find the optimum input power difference between SSMF and DCF *D* defined as

$$D(dB) = P_{SSMF} - D_{DCF} \tag{6.17}$$

where P_{SSMF} and P_{DCF} is respectively the SSMF launch power and DCF launch power. Figure 6.16 shows the Q factor as a function of SSMF launch power under different *D* for a 200km single channel system. The DCF input power can be made variable by adjusting the gain of the EDFA I (Figure 6.15), while the signal power into

each span can be kept the same as long as EDFA II (Figure 6.15) has enough gain. Thus, the larger the *D* the smaller the power launch into DCF. It can be seen from Figure 6.16 that the optimum power difference is 6 dB

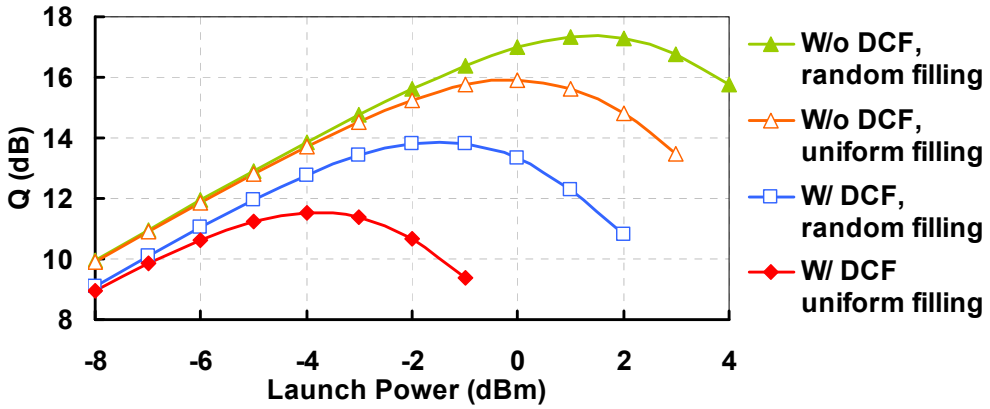

Figure 6.17 The simulated system performance as a function of the launch power for 1000 km single channel transmission with 96% compensation ratio.

Figure 6.17 shows the Q factor as a function of launch power after 1000 km single channel SSMF transmission for both random filling and uniform filling with 96% CR. For random filling, the single channel optimal launch power is respectively -1 and 1 dBm for the system with and without DCF, the maximum Q difference is 3.5 dB, whereas for uniform filling, the optimal launch power is -4 and 0 dBm with 4 dB maximum Q difference which agrees well with the experiment that shows the Q difference of 3.5 dB. As shown in Figure 6.17, uniform filling shows worse nonlinearity performance. The reason is that the uniform filling increases the PAPR due to the correlation between the bands.

Figure 6.18 shows the simulated Q factor as a function of CR for both 107-Gb/s single channel and WDM transmission after 1000 km SSMF. For each CR, the maximum Q is simulated when fiber launch power is set to optimum condition. When the CD is 100 % compensated, signal waveform repeats itself in each span, incurring the enhanced nonlinearity. Thus, the Q factor decreases from 17 dB/15.3 dB at 0% CR to 13.8dB/11.3 dB for single channel/WDM transmission. After the CR exceeds 100%, the overcompensated CD helps to reduce the signal nonlinearity and thus enhances the Q

factor. However, the Q factor starts to decrease when the CR is larger than 140% due to the increase of the loss and the nonlinearity in DCF.

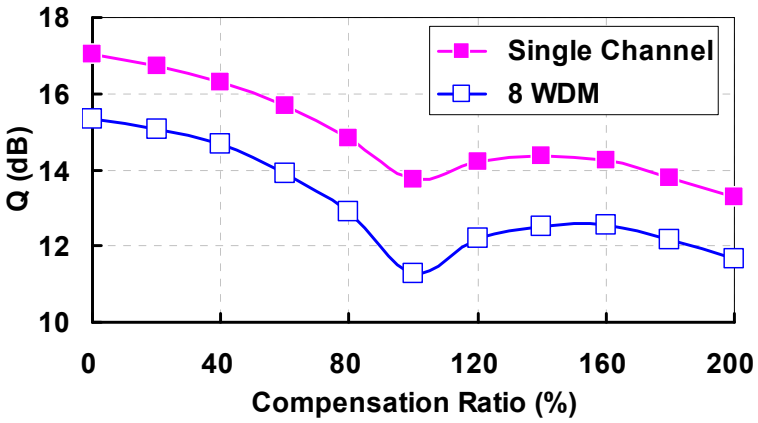

Figure 6.18 The simulated Q factor as a function of compensation ratio for 107-Gb/s signal after 1000 km transmission.

Figure 6.19 shows the Q factor as a function of launch power with and without DCF after 1000 km SSMF 8 WDM transmission at the data rate of 10.7, 42.8 and 107 Gb/s. CR is set to be 96% for the transmission with DCF. At low launch power, the system degradation is mainly due to the ASE noise. Therefore, at certain launch power, the Q increases linearly with the decreasing data rate. However, with the increasing of launch power, nonlinearity effect starts to degrade the system performance and the Q starts to decrease when the launch power exceeds the optimum point. As shown in Figure 6.19, without DCF, the optimal launch power is respectively -6, -4 and -1dBm for the data rate of 10.7, 42.8 and 107 Gb/s. This is in sharp contrast to the single carrier direct-detection systems where the dispersion compensated system has better performance at low bit rate of 10.7 Gb/s [172], where soliton-like nonlinearity effect helps the single-carrier pulse from spreading. But in the CO-OFDM system where the signal looks random in the time domain with occasional high-intensity peaks even at the beginning of the link, such soliton-like pulse narrowing effect does not hold. We anticipate that the pre- and post-optical dispersion compensation does not influence the performance of CO-OFDM as the OFDM signal itself has already exhibited a high PAPR at the beginning of the transmission. Possible method to improve the nonlinear performance of CO-OFDM

system with inline dispersion map is to reduce the signal PAPR at transmitter, or to perform pre- and post- electronic nonlinearity compensation [186].

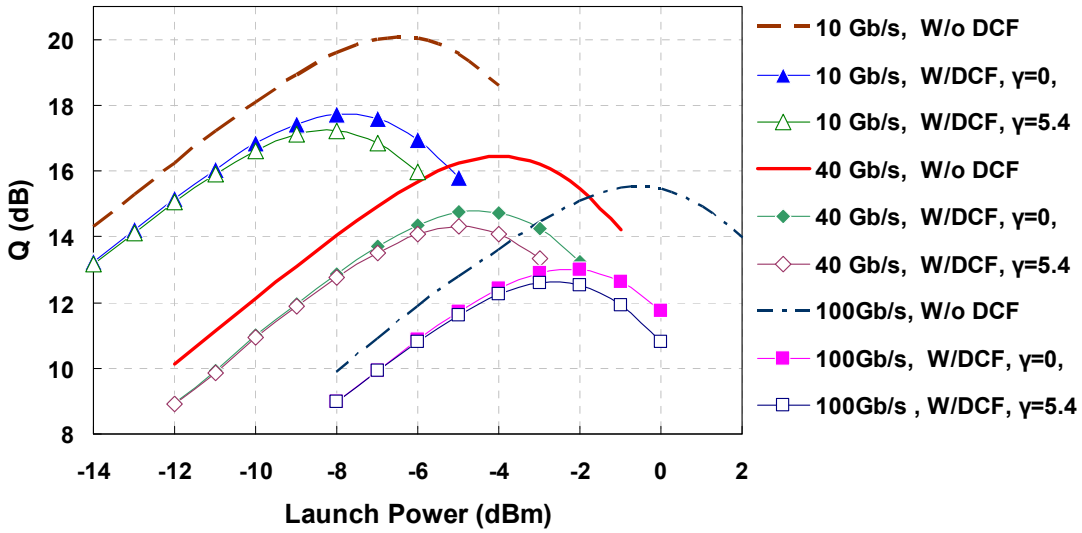

Figure 6.19 Q as a function of fiber launch power for 10.7-Gb/s, 42.8-Gb/s and 107 -Gb/s WDM signals with and without DCF.

In order to separate the contributing factors to the Q degradation from the dispersion compensation, we set the nonlinearity coefficient of DCF to zero and keep the input power difference between SSMF and DCF 6dB. The Q performance with zero DCF nonlinear coefficient is shown in Figure 6.19. The first contribution factor is the degradation due to the DCF nonlinearity. The Second factor is linear noise figure hit due to double stage amplifier, which can be measured by the performance difference for the two dispersion maps at the lower launch powers. The third contributing factor is the dispersion map influence: in CD compensated system, the OFDM signal almost resets itself at each span whereas in non-compensated system, the OFDM signal continues to evolve along the transmission. The dispersion compensation enables the coherent addition of the nonlinearity-induced distortion in each span, and therefore enhances the nonlinearity degradation [187]. Take the 107-Gb/s signal as an example, the degradation from DCF nonlinearity is 0.4 dB and the ASE noise hit is 0.8 dB. By subtracting these from the overall Q degradation 2.8 dB, we can deduce that the dispersion map influence contributes 1.6 dB degradation. As shown in Figure 6.19, at the optimum launch power,

the Q degradation from DCF impact is respectively 2.7dB, 2.2 dB and 2.8dB for 10.7-, 42.8- and 107-Gb/s WDM systems.

6.4 Filter Concatenation Impact for 107-Gb/s CO-OFDM

With the exponential growth of internet traffic, modern optical communication network needs to support high transmission data rate and provide dynamic link reconfiguration. For CO-OFDM system, CD and PMD can be compensated in electrical domain at receiver end through signal processing, thus no dispersion compensation fiber is needed. Such dispersion compensation-free design brings benefit to dynamically reconfigurable networks where ROADMs are deployed to increase network transparency.

One significant source of penalty for transparent DWDM networks is the signal degradation due to transmission through multiple ROADMs, namely filter concatenation effect. The bandwidth of all filters in an optical network is designed to be wide enough to pass the signal spectrum without any distortion. However, the filter concatenation effects must take into consideration if the signal passes through a large number of filters during its transmission. Assume a filter with transfer function $H(\omega)$, then the transfer function of N cascaded filters will be $H^N(\omega)$. The effective filter bandwidth becomes much narrower than the original value. The penalty introduced by filtering effect is mainly from 1) the spectral clipping due to the narrowing of the overall filter pass-band. 2) The group delay introduced by the impact of filter phase response. This dispersion leads to pulse distortion and ultimately resulting in transmission error, and limits the bit rate. Further more, as 100-Gb/s technology has become increasingly a commercial reality, it is desirable to design current 10-Gb/s based DWDM systems ready for future 100-Gb/s upgrade.

In this section, a numerical simulation is performed to study the feasibility of transmitting 100-Gb/s CO-OFDM signals over DWDM systems with 50-GHz channel spacing under the impact of the cascaded ROADMs. We show that 10 ROADM nodes only introduce 0dB/0.9dB Q penalty for the filter with aligned/misaligned center frequency.

6.4.1 ROADM Architecture

A ROADM is a form of optical add-drop multiplexer which enables fully automated optical transport on a per lambda basis. It enables the acceleration of service delivery and decrease of network costs [188]. Figure 6.20 shows a generic block diagram of a complete ROADM node which supports traffic in both east-to-west and west-to-east directions. This architecture is capable of dropping wavelengths from either path using block labeled 'D', while adding new wavelengths in the same direction using block labeled 'A'. Depending on the technology used, a 'B' block may be needed in the express path to block the dropped wavelengths and prevent interference with the same wavelength on the add side [189]. Despite several variations, there are two major architectures for implementing ROADM subsystems: the Wavelength Blocker architecture, or 1st generation ROADM [190] which are the most widely deployed, and the Wavelength Selective Switch (WSS) architecture or 2nd generation ROADM [190].

Figure 6.22 (a) shows one common implementation of ROADM based on wavelength blocker (WB) where all wavelengths are sent "broadcasted" to the site. An incoming multi wavelengths signal is split over a drop and a pass-through path. Pass-through signal traverses a wavelength blocker module that is used to block the dropped wavelengths and power balance the rest of them before the added lambdas are inserted. The WB-based architecture provides many advantages such as cost-effectiveness, remote configurability, 100% add/drop capacity and good optical performance. Currently, there are several versions of WB technology available for commercial use. Usually, they consist of diffraction-grating-based free-space dispersive optics coupled to either liquid crystal or Microelectromechanical systems (MEMS)-based attenuator arrays.

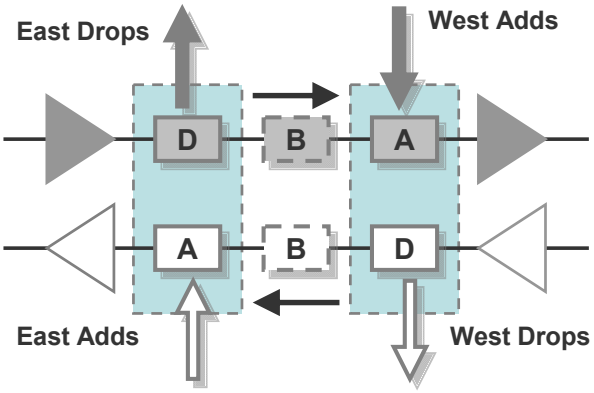

Figure 6.20 A Generic ROADM Subsystem

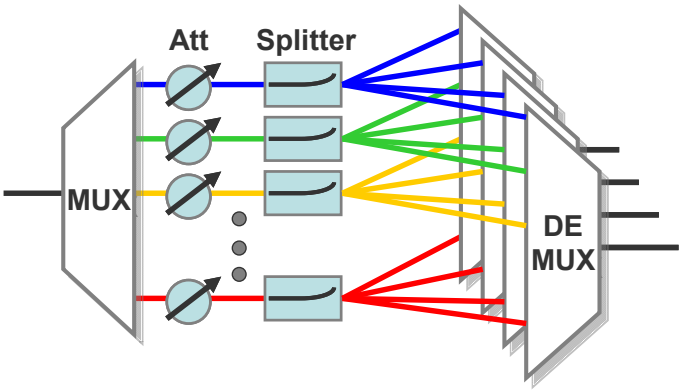

Figure 6.21 NxN Wavelength Cross-connect using WSS modules

Wavelength Selective Switch based ROADM architecture is emerged recently and it allows for full reconfigurable ROADM functionality. Figure 6.21 shows the functional representation of a 1×4 WSS. With WSS, any wavelength, group, or band of wavelengths can be directed to any output fiber. The output patterns may be changed or reassigned to different output fibers through an electrical interface. An attenuation function may also be employed to expand the dynamic capability. The WSS architecture includes fewer optical components than the WB architecture resulting in smaller insertion loss.

Wavelength blocker based ROADM is adopted for this study because of its popularity. Generally speaking, the ROADM based on wavelength technology consists of a few filters, such as interleaver and blocker. The interleaver usually has an ITU standard channel grid (e.g., 50-GHz spacing for 10-Gb/s DWDM system) and uniform passband bandwidth. Figure 6.22 (a) shows a transparent DWDM system with interleaver and wavelength blocker based ROADMs [188,191]. The DWDM channel is separated into the

"odd-channel" group and the "even-channel" group by the first interleaver and thus relaxing the pass-band requirement on the wavelength blockers. The second interleaver combines the two groups of channels. The add/drop module consists of a passive coupler and a multiplexer/demultiplexer.

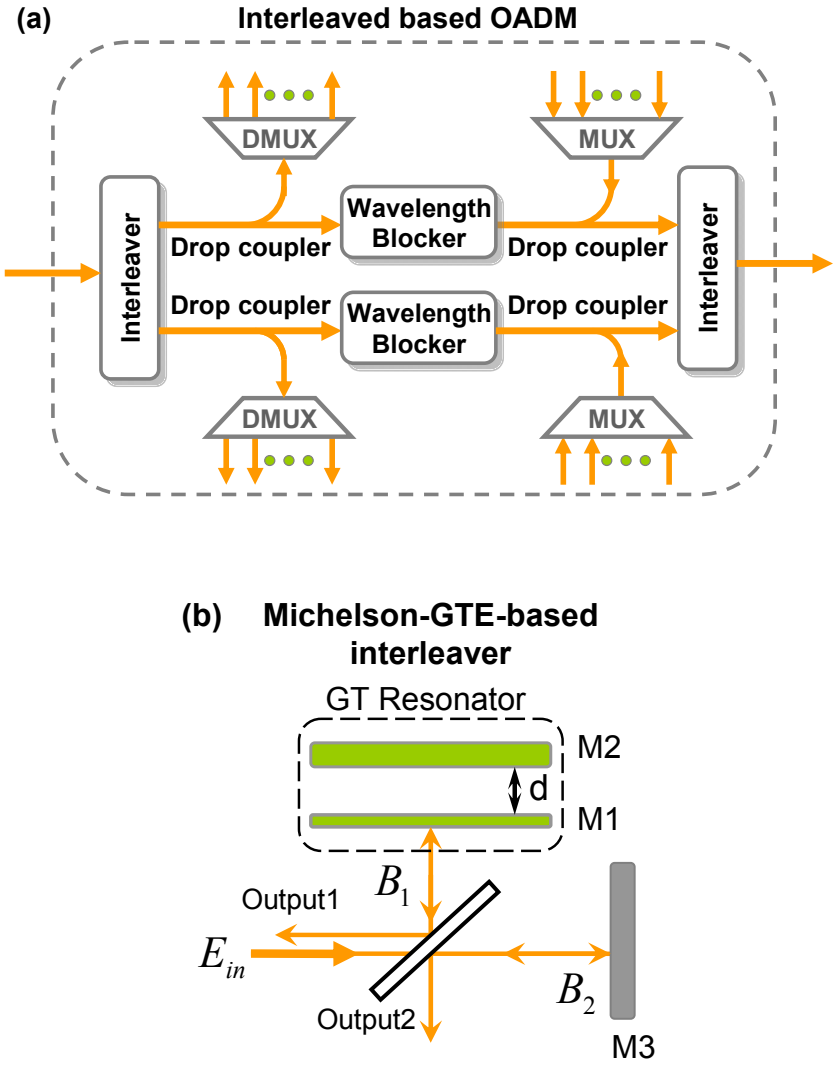

Figure 6.22 (a) Schematic of a transparent DWDM system with multiple interleaver-based ROADM. (b) Michelson-GTE-based interleaver.

The interleaver shown in Figure 6.22 (b) used in this study is based on the OBPF proposed by B. D. Benjamin [192]. Such OBPF is a modified Michelson interferometer in which one of its reflecting mirrors is replaced by a Gires–Tournois resonator (GTR) [192] with a cavity spacing d. The light wave E_{in} incident onto the filter is split into two

beams B_1 and B_2 with same intensity by a 50:50 beam splitter (BS). B_1 and B_2 propagate through two arms before they are reflected back by mirror M3 and the GTR mirror. The GTR, acting as phase dispersive mirrors, consists of a front mirror M1 of finite reflectivity and a rear mirror M2 of near 100% reflectivity. The reflected beams travel back toward BS form the output fields output1 and output2. The normalized output intensity (transmittance of the interleaver) I_1 and I_2 can be expressed as

$$I_1 = 1/2\left(1+\cos\left[\Omega+\delta\Omega-\tan^{-1}\left(\frac{1-\sqrt{R}}{1+\sqrt{R}}\tan(2\{\Omega+\delta\Omega\})\right)\right]\right) \quad (6.18)$$

$$I_2 = 1/2\left(1-\cos\left[\Omega+\delta\Omega-\tan^{-1}\left(\frac{1-\sqrt{R}}{1+\sqrt{R}}\tan(2\{\Omega+\delta\Omega\})\right)\right]\right) \quad (6.19)$$

The phase response of the interleaver is

$$\theta(R,d) = -2\cdot \mathrm{Tan}^{-1}\left(\left\{\frac{1-\sqrt{R}}{1+\sqrt{R}}\right\}\mathrm{Tan}\left(\frac{2\pi d}{\lambda}\right)\right) \quad (6.20)$$

where $\Omega = \pi d_0/\lambda$ is the normalized frequency with an initial GTR spacing d_0, and $\delta\Omega = \pi(d-d_0)/\lambda$ is the frequency difference produced by making the GTR cavity spacing variable, d is the GTR spacing, λ is vacuum wavelength. Michelson-GTR-based interleaver provides wide flat-top, square-like frequency response with zero ripple factor.

Figure 6.23 shows the transmittance profile (a) of 1, 4 and 20 cascaded interleavers and the group delay (b) of a single interleaver when the power reflectance of front mirror is 16%. It can be seen that the 1 dB/3dB bandwidth for a single interleaver filter is 44 GHz/50 GHz and narrowed down to 33 GHz/36.5 GHz after 20 stages. The peak-to-peak group delay response (GDR) within the 20-dB passband is 18 ps.

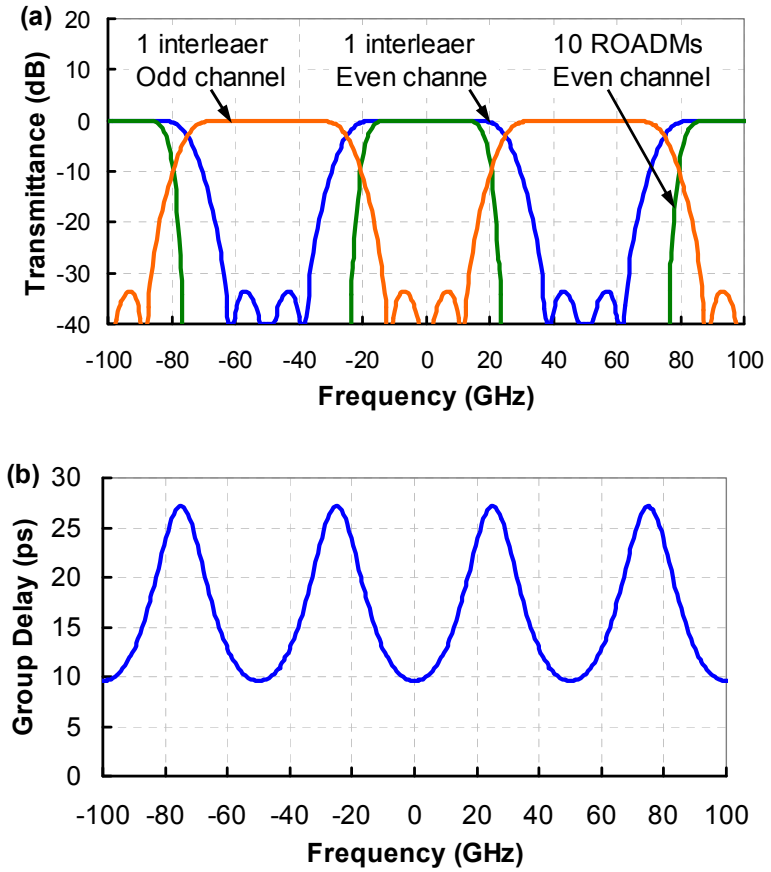

Figure 6.23 Transmittance and (b) group-delay responses of a Michelson-GTE-based interleaver.

6.4.2 Simulation Result

A Monte Carlo simulation is conducted to identify the filter concatenation impact on the performance of 8×107-Gb/s WDM CO-OFDM signal after 1000 km SSMF transmission. The simulation configuration is shown in Figure 6.15. The DCF function is disabled when only ROADM cascading effect is considered. The OFDM simulation parameters are shown in TABLE-6.2. The bandwidth of 107-Gb/s CO-OFDM signal is 32 GHz. The curve with open square in Figure 6.24 represents the Q penalty as a function of the number of ROADM nodes when filters and laser are perfectly aligned. It can be seen that the Q penalty is almost zero even for 10 cascaded ROADMs. This is because, 1) The 107 Gb/s CO-OFDM signal only occupies 32 GHz bandwidth. The 1 dB/3dB bandwidth of 10 cascaded ROADMs is 33 GHz/36.5 GHz, therefore, most of the signal spectral will be confined in the filter pass-band. 2) The guard interval ($12.8\ ns \times 1/8 = 1.6\ ns$) is larger

than the 0.36ns delay induced by the phase response of 20 interleaver filters, the filter induced dispersion impairment can be effectively eliminated.

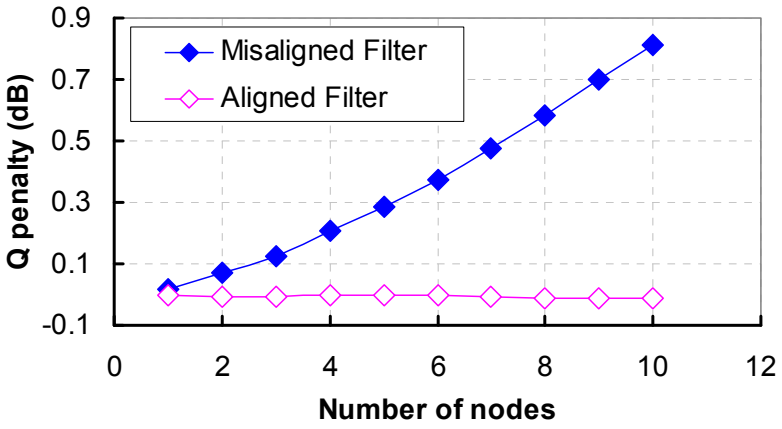

Figure 6.24 Q penalty (dB) as a function of number of nodes with and without filter misalignment.

To further investigate the filter concatenation performance, the tolerance to the filter misalignment was studied. The worst case of the filter misalignment was assumed, meaning the first interleaver of each ROADM was centered at +10% (+5 GHz) of the channel spacing while the second at -10% (-5 GHz). The Q penalty is indicated with the curve with solid square in Figure 6.24. The effect of detuning between the laser frequency and the filter center wavelength of 10 ROADMs was also examined (Figure 6.25). All of the filter center frequencies are assumed to be aligned. It can be seen that a 1.3 dB Q penalty is observed for 10 GHz (20% of the channel spacing) detuning. The Q degradation from the filter misalignment is mainly from the subcarriers which are on the edge of the OFDM spectrum, whereas the subcarriers at the center of the spectrum remain intact. One of the advantages of CO-OFDM is that the SNR of each subcarrier can be monitored through receiver signal processing, and the subcarriers with lower SNR value will be loaded with lower-order of modulation, and or even unfilled. Through judicious bit and power loading, the system Q degradation can be significantly minimized [129].

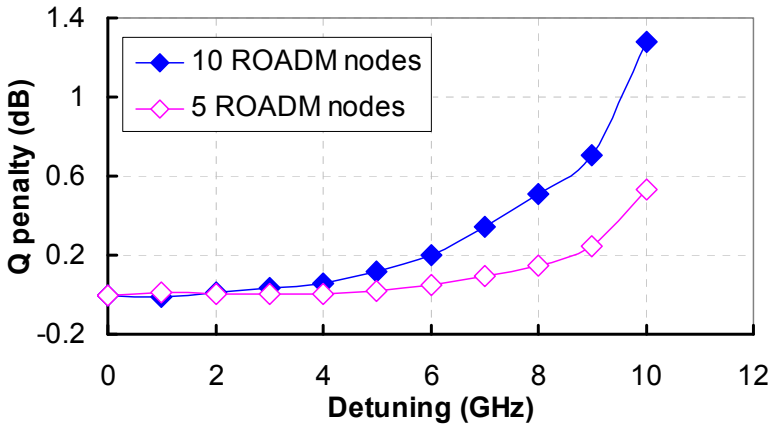

Figure 6.25 Q penalty as a function of the laser detuning for 8×107-Gb/s WDM systems.

6.5 1-Tb/s CO-OFDM Transmission

In this section, we first present the architecture of Tb/s CO-OFDM transceiver. We then demonstrate the transmission performance for WDM system with 1Tb/s per channel CO-OFDM signal.

6.5.1 Three-layer Mixed-signal Optoelectronic Architecture for the Tb/s CO-OFDM Transceiver

The optical bandwidth required for conveying Tb/s information is about 340 GHz, dependent on the detailed OFDM design, translated to about 170 GHz electrical bandwidth if polarization multiplexing and 4-QAM modulation for CO-OFDM systems are used. Such broad electronic bandwidth is unlikely to be supported in the next decade. Some kind of bandwidth down scaling is mandatory. Orthogonal-band-multiplexing (OBM) scheme as we discussed in Section 6.3 is a promising way to realize the 1-Tb/s CO-OFDM single channel transmission. However, to solely rely on the optical OBM-OFDM entails many coherent transmitter and receiver pairs, which is cost-prohibitive. It is thus imperative to introduce an immediate integration process in the RF layer. Figure 6.26 illustrates the concept of such three-layer IC architecture for Tb/s CO-OFDM system. For exhibitory clarity, the CO-OFDM is assumed at the rate of 1.2 Tb/s partitioned into 12 bands. The entire mixed-circuit IC design involves three-layer of

integration as follows:

(i) In the baseband layer, baseband OFDM is generated at the rate of 100 Gb/s,

(ii) In the RF layer, each of the four basebands is multiplexed up to an RF carrier and combined electrically to 400 Gb/s RF signal. The highest RF carrier is around 70 GHz which can be potentially realized using the state-of-the-art CMOS technology [193].

(iii) In the photonics layer, the output signal from the RF layer will modulate three frequency-locked wavelengths and combined optically into a 1.2 Tb/s optical signal.

The baseband layer and RF layers are ideally implemented in mixed-circuit CMOS ASICs, leveraging the recent progress made at millimeter-wave CMOS technology [193]. The photonic integration circuits (PIC) within the photonics layer or the integration of photonics and CMOS is of great importance for the 1-Tb/s transport. Compared with OTDM, the CO-OFDM-based Tb/s systems employs the multiplexing and de-multiplexing of each OFDM band with RF and wavelength combiners, eliminating the need for extremely tight timing alignment. Furthermore, the CO-OFDM has shown dispersion resilience over 1000 km SSMF [184,194], entirely doing away with the sophisticated higher-order optical dispersion compensation.

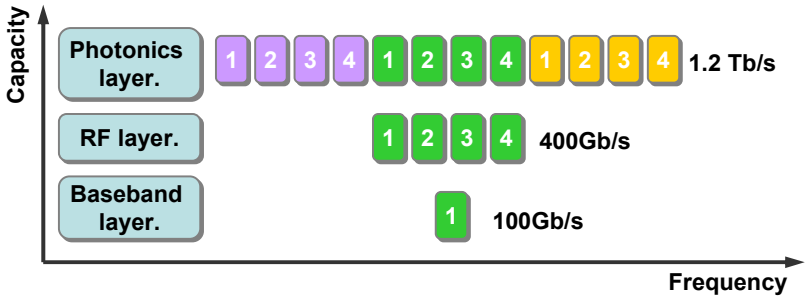

Figure 6.26 Conceptual diagram of the three-layer opto-electronic IC hierarchy for Tb/s CO-OFDM transceiver. Each box represents an OFDM band at 100 Gb/s. The color represents different wavelength.

6.5.2 1-Tb/s CO-OFDM System Performance

In this section we show the transmission performance of 1.07 Tb/s per channel

CO-OFDM signal with and without the DCF. Both single-channel and 3-channel WDM transmission are simulated. The channel spacing is 350 GHz. We also compared the system performance of 1-Tb/s with the data rate of 10.7 Gb/s, 42.8 Gb/s and 107 Gb/s. The system model used for the simulation is shown in Figure 6.15. The OFDM simulation parameters are listed in TABLE-6.1and TABLE6.2. After transmission, the time domain overlap of the Tb/s tributaries can be completely removed through the receiver signal processing. The bandwidth of 3 × 1 Tb/s WDM signal is over 900 GHz which is wider than that of 8 × 10 Gb/s WDM systems with 100 GHz channel spacing which is commonly used for lower bit rate simulation. Therefore, 3 WDM channels should be sufficient for simulating interchannel effect considering the large walk-off between these ultra-broad bandwidth channels.

Figure 6.27 shows the Q factor as a function of launch power for 1.07 Tb/s data rate after 1000 km SSMF under single-channel and WDM transmission. Without DCF, an optimum Q of 13.8/13.2 dB can be achieved at the fiber launch power of 7.6/7 dBm, for single channel/WDM transmission. It can be seen that without DCF, only small performance difference is observed between single-channel and 3WDM. The optimum Q difference is only 0.6 dB. The small difference is attributed to the large walk-off among the majority of the subcarriers within the relatively broad OFDM spectrum.

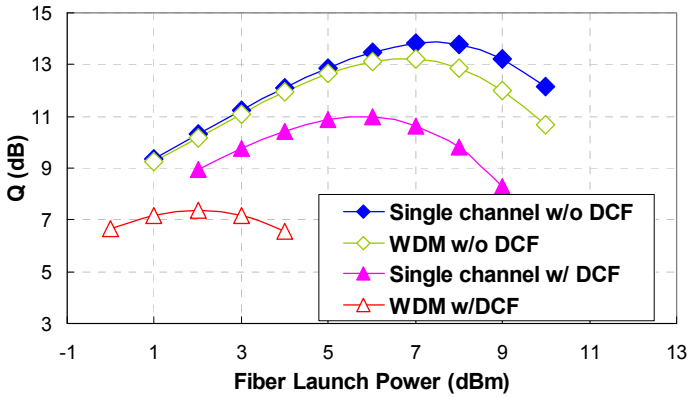

Figure 6.27 System performance as a function of the launch power for 1.07 Tb/s data rate at the reach of 1000 km

Figure 6.28 (a) and (b) respectively show the maximum system Q and optimum fiber launch power at the data of 10.7Gb/s, 42.8 Gb/s, 107 Gb/s and 1.07 Tb/s with and without DCF after 1000 km SSMF. It can be seen that, as the data rate increases, the maximum Q

decreases due to the increase of fiber nonlinearity. For example, the maximum Q of WDM transmission without DCF decreases from 20 dB to 13 dB as the data rate increases from 10.7 Gb/s to 1.07 Tb/s. For all of the data rates, the system Q is severely degraded due to the impact of DCF especially under WDM transmission. We find that the optimum fiber launch power increases almost linearly with the increase of data rate. As shown in Figure 6.28 (b) the optimum launch power of single channel without DCF 1.07 Tb/s data rate (8 dBm) is around 7 dB higher than that of single channel 107 Gb/s data rate (1 dBm).

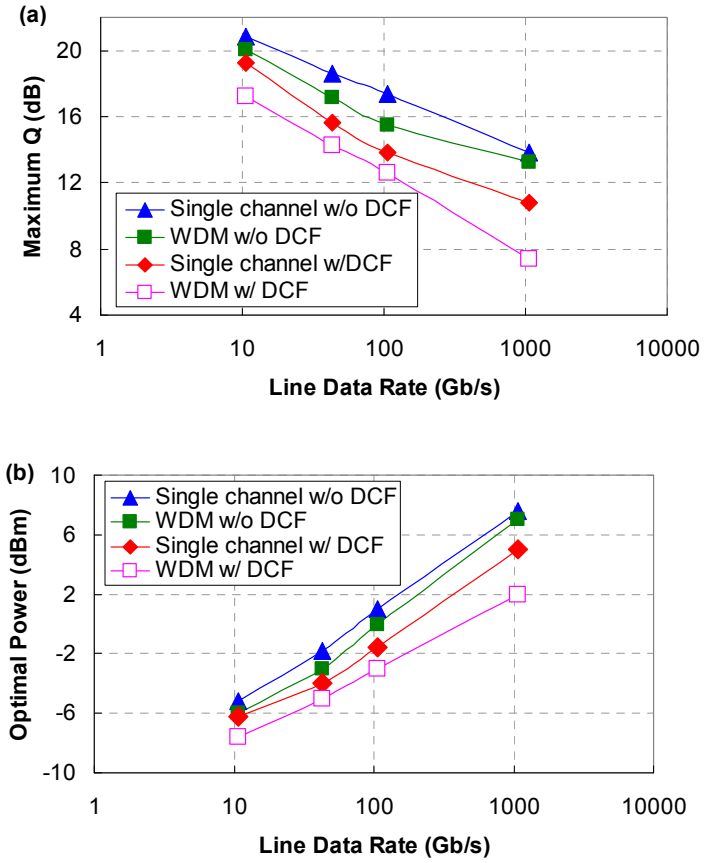

Figure 6.28 (a) Maximum Q and (b) optimum fiber launch power as a function of data rate.

Figure 6.29 shows the BER sensitivity comparison under different data rate after 1000-km transmission at optimum launch power. It can be seen that as the increasing of the data rate, signal suffers from more penalty due to the increasing of nonlinearity. For the 1 Tb/s transmission, the OSNR penalty for a BER of 10^{-3} is respectively 0.7 dB and 1.7 dB for inline compensation and no inline compensation.

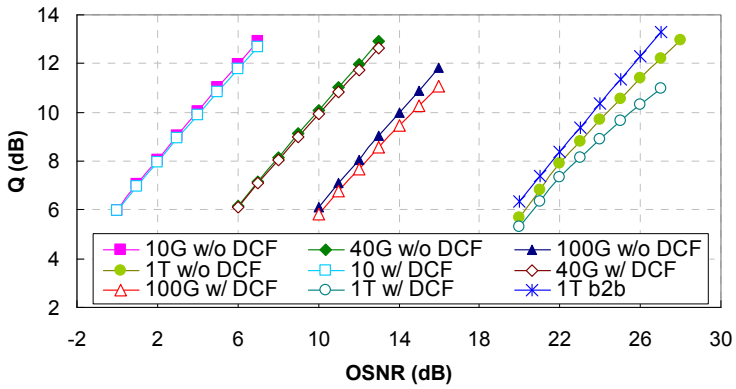

Figure 6.29 BER sensitivity comparison for 10.7Gb/s, 42.8 Gb/s, 107 Gb/s and 1.07 Tb/s signal with and without DCF.

6.6 Conclusion

In this chapter, we first conduct a Mote Carlo simulation on the transmission performance for 100-Gb/s WDM systems with CO-OFDM transmission. The simulation shows that the system Q of the WDM channels at 100 Gb/s is over 15.0 dB for a transmission up to 1000 km of SSMF without dispersion compensation.

We then investigate the system performance of CO-OFDM system up to 107 Gb/s data rate with inline dispersion-compensation through both experiment demonstration and simulation analysis. We find that for the WDM system, the total DCF induced Q reduction are about 0.8 dB penalty due to the DCF loss, 0.4 dB from DCF nonlinearity, and 1.6 dB from the dispersion map. We find that at the optimum launch power, the Q-factor degradation from DCF impact is respectively 2.7 dB, 2.2 dB and 2.8 dB for the data rate of 10.7 Gb/s, 42.8 Gb/s and 107 Gb/s WDM systems.

The CO-OFDM performance on the upgrade of 10-Gb/s based DWDM systems with 50-GHz channel spacing to 100 Gb/s per channel is also analyzed. The main limitations of the upgrade have been assessed by evaluating the impact of the filter concatenation on the system performance. It has been shown that due to the high spectral efficiency, 100 Gb/s CO-OFDM signals have very high tolerance to the filter narrowing effect, and are resilient to the group ripples from the filter cascade. 0dB /0.9 dB Q penalty for the filter with aligned/misaligned center frequency is found.

Finally, we discussed the three-layer integration circuit architecture for 1-Tb/s

OBM-OFDM implementation, and the system performance for Tb/s CO-OFDM system is also evaluated. Through the numerical simulation, we find that little performance difference is observed for single channel and WDM transmission at 1-Tb/s line rate. The results show that the system Q of the WDM signal at 1 Tb/s data rate is around 13.2 dB after 1000-km SSMF transmission. This may be tight in terms of margin with 7 % Reed-Solomon Forward Error Correction (FEC) code, but by using Raman amplification or more powerful error-correction codes such as LDPC, the CO-OFDM can be a promising candidate for future 1 TbE transport.

Chapter 7

Conclusions

7.1 Summary of the Work

In this thesis, we have conducted analysis on high-speed optical transmission system using coherent optical orthogonal frequency-division multiplexing. Two key problems have been addressed. The first one is the transceiver nonlinearity impact on coherent optical OFDM systems and the second one is the feasibility of transmitting up to 1-Tb/s per channel data rate over CO-OFDM WDM systems.

7.1.1 Optimum Design for CO-OFDM Transmitter

It is well known that OFDM is very sensitive to nonlinearity. Therefore, a linear transformation in modulation, transmission, and demodulation is the key goal for the OFDM implementation. Through our simulation study, we have identified that the nonlinearity of RTO up-converter comes from the Mach–Zehnder modulator since it has a *sine* shape transfer curve. A two-tone inter-modulation analysis was used to characterize the optical I/Q modulator nonlinearity which is expressed as two-tone intermodulation products as a function of the bias point and modulation index. The second order and third order intercept point of the optical I/Q modulator was derived which showed that when modulator is biased at the null point, the third order intercept point had the maximum value, or least non-linearity, which means that the optimum bias point should be null-point. Furthermore, to investigate the I/Q modulator nonlinearity impact we performed a numerical simulation for a 10-Gb/s CO-OFDM system under various modulation index and bias points. The simulation results showed that not only the null bias point provides the least Q penalty, but also it incurs the least excess loss.

The digital clipping and digital pre-distortion were then introduced to the RF OFDM transmitter to reduce the signal PAPR and compensate the MZM nonlinearity. The

functionality of digital clipping is to clip the signal amplitude to a level which is equal to the maximum permissible amplitude so that the signal range is within the MZM linear transfer range and DAC conversion range. Digital pre-distortion function has an *arcsine* transfer characteristic. Together with MZM transfer function, the combined transfer function provides a linear transformation from the digital waveform to the analogue optical field. We conducted a numerical simulation to evaluate the proposed digital signal processing schemes on the effect of the system performance improvement. We found that the Q reduction introduced by 2.5 clipping ratio at the Q value of 9.8 dB is only around 0.05dB, implying that a clipping ratio of 2.5 should provide satisfactory performance with sufficient margin. With the help of digital pre-distortion, system is more tolerant to the MZM nonlinearity. For example, the system Q value has increased 1.3 dB at 1.6 modulation index. Besides, assuming a clipping ratio of 2.5, we found that 4-bit DAC resolution is sufficient for a CO-OFDM transmitter to incur only 0.3 dB Q penalty while maintaining the excess modulation insertion loss below 6.0 dB.

7.1.2 Study of Nonlinearity and Dynamic Range of Coherent Optical OFDM Receivers

For a CO-OFDM system with direct-conversion receiver architecture, two balanced receivers are used to down convert the optical OFDM signal to baseband. Compared with the direct-detection optical OFDM, the CO-OFDM comprises with two pairs of balanced receivers is more costly and complex. It is desirable to reduce the cost and complexity of the receiver using balanced receivers that are tolerant of imbalance, or using simpler single-ended receiver. In this chapter we conducted analysis on the study of nonlinearity and dynamic range for a coherent optical OFDM receiver induced by the imbalance between the two ports of a balanced receiver. We first formulated the theory for the I/Q coherent detection with two-tone intermediation analysis on the balanced receiver and single-ended receiver. The second-order intercept point was used to characterize the receiver nonlinearity.

We then conducted a numerical simulation to investigate the receiver performance of

CO-OFDM system under the influence of receiver imbalance, RIN, and LO power. We find that both LO power and receiver imbalance will affect IP2. Large receiver imbalance decreases IP2 while large LO power increases IP2. As the IP2 decreases, the system nonlinearity increases, inducing increasing Q penalty. 0.5-dB Q penalty dynamic range for double-ended receiver (single-ended receiver) is 39 dB (17.5dB) with -160 dBc/Hz laser RIN and 4 dBm LO power.

7.1.3 Coherent Optical OFDM Transmission up to 1 Tb/s Per Channel

Recently, coherent optical OFDM has been considered as a promising pathway toward high capacity transparent optical network and upgrade solution from today's 10-Gb/s to the future 100-Gb/s systems due to its superior advantages such as easiness of CD/PMD estimation and mitigation, high spectral efficiency, adaptive data rate, etc. In this chapter, we investigated the feasibility of transmitting 100 Gb/s and beyond data rate over CO-OFDM systems.

We first conduced a Monte Carlo simulation on the WDM transmission performance for 100-Gb/s CO-OFDM systems. The simulation showed that the system Q of the WDM channels at 100 Gb/s is over 15.0 dB for a transmission up to 1000 km of SSMF without dispersion compensation.

We also discussed the three-layer IC architecture for 1-Tb/s OBM-OFDM implementation, and the system performance for Tb/s CO-OFDM system is evaluated. Through the numerical simulation, we find that little performance difference is observed for single channel and WDM transmission at 1 Tb/s line rate. The maximum Q is 13.8 dB and 13.2 dB respectively for single channel and WDM transmission. We also compared the CO-OFDM system performance under the data rate of 10.7 Gb/s, 42.8 Gb/s, 107Gb/s and 1.07 Tb/s with and without the impact of dispersion compensation fiber.

The main limitations of the upgrade 10-Gb/s system to 100-Gb/s system were assessed by evaluating the DCF and filter concatenation impact on the system performance. We showed through experiment demonstration that DCF greatly decrease the 107-Gb/s CO-OFDM nonlinearity performance. With DCF, the maximum Q value for 1000-km SSMF fiber transmission is 3.5 dB less than that without DCF. The required

OSNR for a BER of 10^{-3} for 400-km transmission is respectively 18.5 dB and 16.5 dB for inline compensation and non in-line compensation. We identify three contributions to the Q degradation for the inline dispersion compensated WDM systems, specifically for the 107 Gb/s WDM system, about 0.8 dB penalty due to the DCF loss, 0.4 dB from DCF nonlinearity, and 1.6 dB from the dispersion map. The filter concatenation impact is investigated in an 8×100 Gb/s DWDM system with 50-GHz channel spacing through simulation. It has been shown that due to the high spectral efficiency, 100-Gb/s CO-OFDM signals have very high tolerance to the filter narrowing effect, and are resilient to the group ripples from the filter cascade.

Bibliography

[1] G. P. Agrawal, Fiber-Optic Communication Systems, 3rd ed. New York: John Wiley & Sons, 2002.

[2] B. Zhu et al., "3.08 Tb/s (77 × 42.7 Gbit/s) transmission over 1200 km of non-zero dispersion-shifted fiber with 100-km spans using C-L-band distributed Raman amplification," in Optical Fiber Communication Conference and Exhibit, 2001 (OFC 2001), Mar. 2001, pp. PD23/1–3.

[3] Mao Qian, "Development Progress of 40 Gb/s (STM-256) SDH Optical System in China," China Communications, available from www.china-cic.org.cn/english/digital%20library/200512/9.pdf, pp. 54–58, 2005.

[4] Cisco Inc., "Approaching the Zettabyte Era." Information available at http://www.cisco.com/en/US/solutions/collateral/ns341/ns525/ns537/ns705/ns827/white_paper_c11-481374_ns827_Networking_Solutions_White_Paper.html.

[5] S. Hara and R. Prasad, Multicarrier Techniques for 4G Mobile Communications (Artech House, Boston, 2003).

[6] Shieh, W.; Athaudage, C., "Coherent optical orthogonal frequency division multiplexing," Electronics Letters , vol.42, no.10, pp. 587-589, 11 May 2006

[7] R. V. Nee and R. Prasad, OFDM for Wireless Multimedia Communications. Norwood, MA: Artech House, 2000.

[8] W. Liu, J. Lau, and R. S. Cheng, "Considerations on applying OFDM in a highly efficient power amplifier," IEEE Trans. Circuits Syst. II, vol. 46, pp. 1329–1336, Nov. 1999.

[9] D. J. G. Mestdagh, P. Spruyt, and B. Biran, "Analysis of clipping effect in DMT-based ADSL systems," in Proc. IEEE Int. Conf. Commun, vol. 1, 1994, pp. 293–300.

[10] Govind P. Agrawal, Nonlinear Fiber Optics (Academic Press, San Diego, 2001).

[11] M. T. Abuelma'atti, 'Large Signal Analysis of the Mach-Zehnder Modulator with Various bias', Proc. Natl. Sci. Counc. ROC(A), Vol. 25, pp. 254-258, 2001.

[12] M. Mayrock and H. Haunstein, 'Impact of Implementation Impairments on the Performance of an Optical OFDM Transmission System,' Tech. Dig. ECOC'2006, Cannes, France, Paper Th3.2.1.

[13] A. J. Lowery, et al., "Orthogonal frequency division multiplexing for adaptive dispersion compensation in long haul WDM systems," in Conf. Optical Fiber Communication (OFC), Mar. 2006, PDP39.

[14] I. B. Djordjevic and B. Vasic, "Orthogonal Frequency Division Multiplexing for High- Speed Optical Transmission," Optics Express, 14:9 (2006), 3767–3775.

[15] J. M. Tang and K. A. Shore, "30 Gb/s signal transmission over 40-km directly modulated DFB-laser-based single-mode-fibre links without optical amplification and dispersion compensation," J. Lightwave Technol. 24, 2318–2327 (2006).

[16] R.J. Essiambre, P.J. Winzer, and X. Wang, "Electronic predistortion and fiber nonlinearity," Photon. Technol. Lett. vol.17, pp. 1804 – 1806, 2006.

[17] K. Forozesh, S. L. Jansen, S. Randel, "The influence of the dispersion map in coherent optical OFDM transmission systems," LEOS Summer Topical Meeting'2008, paper WC2.4.

[18] Cisco Inc., “Approaching the Zettabyte Era.” Information available at http://www.cisco.com/en/US/solutions/collateral/ns341/ns525/ns537/ns705/ns827/white_paper_c11-481374_ns827_Networking_Solutions_White_Paper.html.

[19] S. Kawanishi, “Ultrahigh-speed optical time-division-multiplexed transmission technology based on optical signal processing,” IEEE J. Quant. Electron., 34, 2064–2079, 1998.

[20] S. Weisser, S. Ferber, L. Raddatz et al., “Single- and alternating polarization 170 Gbit/s transmission up to 4000 km using dispersion-managed fiber and all-Raman amplification,” Photon. Technol. Lett., 18(6), 1320–1322, 2006.

[21] H. G. Weber, S. Ferber, M. Kroh et al., “Single channel 1.28 Tbit/s and 2.56 Tbit/s DQPSK transmission,” Electron. Lett., 42, 178–179, 2006.

[22] Guifang Li, "Recent advances in coherent optical communication," Adv. Opt. Photon. 1, 279-307 (2009)

[23] X. Zhou, J. Yu, D. Qian, T. Wang, G. Zhang, and P. Magill, “8 114 Gb/ s, 25-GHz-spaced, PolMux-RZ-8PSK transmission over 640 km of SSMF employing digital coherent detection and EDFA-only amplification,” in Optical Fiber Communication Conference and Exposition and The National Fiber Optic Engineers Conference, OSA Technical Digest (CD) (Optical Society of America, 2008), paper PDP1.

[24] M. Seimetz, L. Molle, D.-D. Gross, B. Auth, and R. Freund, “Coherent RZ-8PSK transmission at 30 Gbits/ s over 1200 km employing homodyne detection with digital carrier phase estimation,” in Proceedings of the 33rd European Conference on Optical Communication (ECOC) (2007), paper WE 08.03.04.

[25] M. Yoshida, H. Goto, K. Kasai, and M. Nakazawa, “64 and 128 coherent QAM optical transmission over 150 km using frequency-stabilized laser and heterodyne

PLL detection," Opt. Express 16, 829–840 (2008).

[26] C. Schmidt-Langhorst, and H. G. Weber "Optical sampling techniques" in Optical and Fiber Communication Reports 3, "Ultrahigh-speed optical transmission technology", (H. G. Weber and M. Nakazawa eds), New York: Springer ScienceþBusiness Media, LLC, ISBN-13: 978-3-540- 23878-2, pp. 453–481, 2007.

[27] R.C. Giles and K.C. Reichman, " Optical self-homodyne DPSK transmission at 1-Gbit/s and 2-Gbit/s over 86 km of fiber," Electron. Lett., 23, 1180-1180, 1987.

[28] L. G. Kazovsky, S. Benedetto, and A. E. Willner, Optical Fiber Communication Systems (Artech House, 1996).

[29] T. Okoshi and K. Kikuchi, Coherent Optical Fiber Communications (Springer, 1988).

[30] R. Noe, D. Sandel, M. Yoshida-Dierolf, S. Hinz, V. Mirvoda, A. Schopflin, C. Glingener, E. Gottwald, C. Scheerer, G. Fischer, T. Weyrauch, and W. Haase, "Polarization mode dispersion compensation at 10, 20, and 40 Gb/ s with various optical equalizers," J. Lightwave Technol. 17, 1602– 1616 (1999).

[31] S. J. Savory, G. Gavioli, R. I. Killey, and P. Bayvel, "Electronic compensation of chromatic dispersion using a digital coherent receiver," Opt. Express 15, 2120–2126 (2007).

[32] D. S. Ly-Gagnon, S. Tsukarnoto, K. Katoh, and K. Kikuchi, "Coherent detection of optical quadrature please-shift keying signals with carrier phase estimation," J. Lightwave Technol. 24, 12–21 (2006).

[33] G. Charlet, J. Renaudier, M. Salsi, H. Mardoyan, P. Tran, and S. Bigo, "Efficient mitigation of fiber impairments in an ultra-long haul transmission of 40 Gbit/s polarizationmultiplexed data, by digital processing in a coherent receiver," in Optical Fiber Communication Conference and Exposition and the National Fiber

Optic Engineers Conference, Technical Digest (Optical Society of America, 2007), paper PDP17.

[34] W. Shieh, X. Yi, Y. Ma, and Y. Tang, "Theoretical and experimental study on PMD-supported transmission using polarization diversity in coherent optical OFDM systems," OSA Opt. Express, vol. 15, no. 16, pp. 9936–9947, 2007.

[35] S. L. Jansen, I. Morita, and H. Tanaka, "16×52.5-Gb/s, 50-GHz spaced, POLMUX-COOFDM transmission over 4,160 km of SSMF enabled by MIMO processing KDDI R&D Laboratories," in *Proc. of European Conference on Optical Communications (ECOC)*, Paper PD1.3, Berlin, Germany, 2007.

[36] W. Shieh, X. Yi, and Y. Tang, "Transmission experiment of multi-gigabit coherent optical OFDM systems over 1000 km SSMF fiber," *IEE Electron. Lett.*, vol. 43, no. 3, pp. 183–185, 2007.

[37] E. Ip and J. M. Kahn, "Digital equalization of chromatic dispersion and polarization mode dispersion," J. Lightwave Technol. 25, 2033–2043 (2007).

[38] K. Kikuchi, "Phase-Diversity Homodyne Receiver for Coherent Optical Communications," in Optical Amplifiers and Their Applications/Coherent Optical Technologies and Applications, Technical Digest (CD) (Optical Society of America, 2006), paper CThB3.

[39] M. G. Taylor, "Coherent detection method using DSP for demodulation of signal and subsequent equalization of propagation impairments," IEEE Photon. Technol. Lett., vol. 16, no. 2, pp. 674–676, 2004.

[40] D. McGhan, "Electronic dispersion compensation," presented at the Optical Fiber Commun. Conf., Anaheim, CA, 2006, Paper OWK1.

[41] R. I. Killey, P. M. Watts, M. Glick, and P. Bayvel, "Electronic dispersion

compensation by signal predistortion," presented at the Optical Fiber Commun. Conf., Anaheim, CA, 2006, Paper OWB3.

[42] A. Färbert, "Application of digital equalization in optical transmission systems," presented at the Optical Fiber Commun. Conf., Anaheim, CA, 2006, Paper OTuE5.

[43] F. Ouellette, J. F. Cliche, and S. Gagnon, "All-fiber devices for chromatic dispersion compensation based on chirped distributed resonant coupling," *J. Lightw. Technol.*, vol. 12, no. 10, pp. 1728–1738, Oct. 1994.

[44] D. J. Moss, M. Lamont, S. McLaughlin, G. Randall, P. Colbourne, S. Kiran, and C. A. Hulse, "Tunable dispersion and dispersion slope compensators for 10 Gb/s using all-pass multicavity etalons," IEEE Photon. Technol. Lett., vol. 15, no. 5, pp. 730–732, May 2003.

[45] J. H.Winters and R. D. Gitlin, "Electrical signal procressing techniques in long-haul fiber-optic systems," Trans. Commun., vol. 38, no. 9, pp. 1439–1453, 1990.

[46] H. Bülow and G. Thielecke, "Electronic PMD mitigation – from linear equalization to maximum-likelihood detection," in Proc. Tech. Dig. OFC' 2001, Anaheim, CA, Mar. 10–21, 2001, vol. 3, pp. WAA3–1–WAA3–3.

[47] H. F. Haunstein, K. Sticht, A. Dittrich, M. Lorang, W. Sauer-Greff, and R. Urbansky, "Implementation of near optimum electrical equalization at 10 Gbit/s," in Proc. ECOC 2000,Munich, Germany, Sep. 3–7, 2000, vol. 3, pp. 223–224.

[48] A. Färbert, S. Langenbach, N. Stojanovic, C. Dorschky, T. Kupfer, C. Schulien, J. P. Elbers, H. Wernz, H. Griesser, and C. Glingener, "Performance of a 10.7 Gb/s receiver with digital equalizer using maximum likelihood sequence estimation," in Proc. ECOC, Stockholm, Sweden, 2004, Post deadline, Th4.1.5.

[49] S. Tsukamoto et al., "Coherent demodulation of 40-Gbit/s polarization multiplexed QPSK signals with 16-GHz spacing after 200-km transmission," in Proc. OFC2005, Anaheim, CA, 2005, PDP29.

[50] R. Noé, "Phase noise tolerant synchronous QPSK receiver concept with digital I&Q baseband processing," in Proc. OECC/COIN2004, Yokohama, Japan, Jul. 12–16, 2004, pp. 818–819.

[51] R. Ramaswami and K. N. Sivarajan, Optical Networks: A Practical Perspective, 2nd ed. San Francisco: Morgan Kaufmann Publishers, 2002.

[52] R. Lachance, S. Lelievre, and Y. Painchaud, "50 and 100 GHz multichannel tunable chromatic dispersion slope compensator," in Conf. Optical Fiber Communication (OFC), vol. 1, Mar. 2003, pp. 164–165.

[53] D. Stahl, P. J. Winzer, C. R. Doerr, and S. Chandrasekhar, "Extending the chromatic dispersion tolerance by optical equalization at 43 Gb/s," in Conf. Optical Fiber Communication (OFC), vol. 2, Feb. 2004, ThU5, pp. 3–5.

[54] C. R. Doerr, "Optical compensation of system impairments," in Conf. Optical Fiber Communication (OFC), Mar. 2006, OThL1.

[55] C. R. Doerr, S. Chandrasekhar, P. J. Winzer, A. R. Chraplyvy, A. H. Gnauck, L. W. Stulz, R. Pafchek, and E. Burrows, "Simple multichannel optical equal- izer mitigating intersymbol interference for 40-Gb/s nonreturn-to-zero signals," J. Lightwave Technol., vol. 22, no. 1, pp. 249–256, Jan. 2004.

[56] J. H. Winters and R. D. Gitlin, "Electrical signal processing techniques in long-haul fiber-optic systems," IEEE Trans. Commun., vol. 38, no. 9, pp. 1439–1453, Sept. 1990.

[57] H. B¨ulow, W. Baumert, H. Schmuck, F. Mohr, T. Schulz, F. Kuppers, and M. Weiershausen, “Measurement of the maximum speed of PMD fluctuation in installed field fiber,” in Conf. Optical Fiber Communication (OFC), vol. 2, Feb. 1999, P3.10, pp. 83–85.

[58] H. Rosenfeldt, “Deploying optical PMD compensators,” in Conf. Optical Fiber Communication (OFC), vol. 3, Mar. 2005, OWO1.

[59] H. B¨ulow, “Electronic equalization of transmission impairments,” in Conf. Optical Fiber Communication (OFC), Mar. 2002, TuE4.

[60] A. Ghiasi, A. Momtaz, A. Dastur, F. Chang, G. Noh, B. Gomatam, E. Ibragimov, A. Shanbhag, O. Schreiber, E. Su, K. Conroy, R. Jambunathan, and J. Wood, “Experimental results of EDC based receivers for 2400 ps/nm at 10.7 Gb/s for emerging telecom standards,” in Conf. Optical Fiber Communication (OFC), Mar. 2006, OTuE3.

[61] R. I. Killey, P. M. Watts, V. Mikhailov, M. Glick, and P. Bayvel, “Electronic dispersion compensation by signal predistortion using digital processing and a dual-drive Mach–Zehnder modulator,” IEEE Photon. Technol. Lett., vol. 17, no. 3, pp. 714–716, Mar. 2005

[62] J. McNicol, M. O’Sullivan, K. Roberts, A. Comeau, D. McGhan, and L. Strawczynski, “Electrical domain compensation of optical dispersion [optical fibre communication applications],” presented at the Optical Fiber Commun. Conf., Anaheim, CA, 2005, Paper OThJ3.

[63] McGhan, D., et.al., “5120 km RZ-DPSK transmission over G652 fibre at 10 Gbit/s with no optical dispersion compensation”, Proc OFC 2005, paper PDP-27, (2005)

[64] Bulow, H., Buchali, F.; Klekamp, A., "Electronic Dispersion Compensation," Lightwave Technology, Journal of , vol.26, no.1, pp.158-167, Jan.1, 2008

[65] Griggin, R.A., Busico G. “Laser FM Noise Impact on DCF Free Transmission Utilising Electronic Dispersion Compensation”, proc ECOC 2005, paper Tu 4.2.5 (2005)

[66] Xiang Liu, S. Chandrasekhar, and Andreas Leven, "Digital self-coherent detection," Opt. Express 16, 792-803

[67] J. A. C. Bingham, “Multicarrier modulation for data transmission: An idea whose time has come,” IEEE Commun. Mag., vol. 28, pp. 5–14, 1990.

[68] R. van Nee and R. Prasad, OFDM for Wireless Multimedia Communications. Boston: Artech House, 2000.

[69] W. Y. Zou and Y. Wu, “COFDM: An overview,” IEEE Trans. Broadcasting, vol. 41, pp. 1–8, 1995.

[70] J. H. Stott, “The how and why of COFDM,” EBUTech. Rev., pp. 43–50, 1998.

[71] R. W. Chang, “Orthogonal Frequency Multiplex Data Transmission System,” USA U.S. Patent 3,488,445, 1966.

[72] J. Salz and S. B. Weinstein, “Fourier transform communication system,” in Proc. ACM Symp. Problems Optim. Data Commun. Syst., Pine Mountain, GA, USA, 1969.

[73] A. Peled and A. Ruiz, “Frequency domain data transmission using reduced computational complexity algorithms,” in Proc. ICASSP 80, Denver, CO, USA, 1980, vol. III, pp. 964–967, IEEE.

[74] L. J. Cimini, Jr., “Analysis and simulation of a digital mobile channel using orthogonal frequency division multiplexing,” IEEE Trans. Commun., vol. CM-33, pp. 665–675, 1985.

[75] R. Lassalle and M. Alard, “Principles of modulation and channel coding for digital broadcasting for mobile receivers,” EBU Tech. Rev., pp. 168–190, 1987.

[76] H. C. Bao and W. Shieh, “Transmission of Wavelength-Division-Multiplexed Channels With Coherent Optical OFDM,” Photonics Technol. Lett., 19:12 (2007), 922–924.

[77] F. Buchali, “Sensitivity and Distortion Tolerance of Optical OFDM,” Proc. Eur. Conf. on Optical Commun. (ECOC ‘07) (Berlin, Ger., 2007), Workshop 5, Electronic Signal Processing for Transmission Impairment Mitigation: Future Challenges.

[78] Q. Yang, Y. Ma, and W. Shieh, “107 Gb/s Coherent Optical OFDM Reception Using Orthogonal Band Multiplexing,” Proc. Optical Fiber Commun./National Fiber Optic Engineers Conf. (OFC/NFOEC ‘08) (San Diego, CA, 2008), paper PDP7.

[79] S. L. Jansen, I. Morita, and H. Tanaka, “10×121.9-Gb/s PDM-OFDM Transmission With 2-b/s/Hz Spectral Efficiency Over 1,000km of SSMF,” Proc. Optical Fiber Commun./National Fiber Optic Engineers Conf. (OFC/NFOEC ‘08) (San Diego, CA, 2008), paper PDP2.

[80] Y. Tang and W. Shieh, "Coherent Optical OFDM Transmission up to 1-Tb/s per Channel," *J. Lightwave Technol.*, vol.27, pp.3511-3517, 2009.

[81] Y. Ma, Q. Yang, Y. Tang, S. Chen and W. Shieh , "1-Tb/s Single-Channel Coherent Optical OFDM Transmission with Orthogonal-band Multiplexing and Subwavelength Bandwidth Access,” submitted to the J. Lightwave Technol. , accepted for publication.

[82] F. Buchali and R. Dischler, "Optimized Sensitivity Direct Detection O-OFDM with Multi Level Subcarrier Modulation," Optical Fiber Communication Conference (OFC), San Diego, California, p. paper OMU5, 2008.

[83] E. Yamada, A. Sano, H. Masuda, T. Kobayashi, E. Yoshida, Y. Miyamoto, Y. Hibino, K. Ishihara, Y. Takatori, K. Okada, K. Hagimoto, T. Yamada, and H. Yamazaki, "Novel No-Guard-Interval PDM CO-OFDM Transmission in 4.1 Tb/s (50x 88.8-Gb/s) DWDM Link Over 800km SMF Including 50-GHz Spaced ROADM Nodes," Proc. Optical Fiber Commun./National Fiber Optic Engineers Conf. (OFC/NFOEC '08) (San Diego, CA, 2008), paper PDP8.

[84] Yonenaga, K.; Sano, A.; Yamazaki, E.; Inuzuka, F.; Miyamoto, Y.; Takada, A.; Yamada, T., "100 Gbit/s All-Optical OFDM Transmission Using 4 x25 Gbit/s Optical Duobinary Signals with Phase-Controlled Optical Sub-Carriers," Optical Fiber communication/National Fiber Optic Engineers Conference, 2008. OFC/NFOEC 2008. Conference on , vol., no., pp.1-3, 24-28 Feb. 2008

[85] Z. Tong, Q. Yang, Y. Ma, and W. Shieh, "21.4 Gb/s Coherent Optical OFDM Transmission over 200 km Multi-mode Fiber," Optoelectronics and Communications Conference (OECC), 2008, postdeadline paper PDP 5

[86] A. J. Lowery and J. Armstrong, "10 Gb/s Multimode Fiber Link Using Power-Efficient Orthogonal-Frequency-Division Multiplexing," Optics Express, 13:25 (2005), 10003–10009.

[87] Lee, S.C.J., Breyer, F., Randel, S., Boom, H.P.A. van den, Koonen, A.M.J. (2008). High-speed transmission over multimode fiber using discrete multitone modulation. Journal of Optical Networking, 7(2), 183-196.

[88] Q. Pan and R. J. Green, "Bit-error-rate performance of lightwave hybrid AM/OFDM systems with comparison with AM/QAM systems in the presence of

clipping impulse noise," IEEE Photon. Technol. Lett., vol. 8, pp. 278–280, Feb. 1996.

[89] A. J. Lowery and J. Armstrong, "Orthogonal-frequency-division multiplexing for dispersion compensation of long-haul optical systems," Opt. Expr., vol. 14, pp. 2079–2084, 2006.

[90] E. Giacoumidis, J. L. Wei, X. Q. Jin, and J. M. Tang, "Improved transmission performance of adaptively modulated optical OFDM signals over directly modulated DFB laser-based IMDD links using adaptive cyclic prefix," Opt. Express 16, 9480-9494 (2008).

[91] B.J. Dixon, R.D. Pollard, and S. Iezekeil, "Orthogonal frequency-division multiplexing in wireless communication systems with multimode fiber feeds," IEEE Trans. Microwave Theory Tech. 49, 1404-1409 (2001).

[92] J. M. Kahn and J. R. Barry, "Wireless infrared communications," Proc. IEEE, vol. 85, pp. 265–298, 1997.

[93] O. Gonzalez, R. Perez-Jimenez, S. Rodriguez, J. Rabadan, and A. Ayala, "OFDM over indoor wireless optical channel," IEE Proc.—Optoelectronics, vol. 152, pp. 199–204, 2005.

[94] R. Dischler and F. Buchali, "Experimental Assessment of a Direct Detection Optical OFDM System Targeting 10 Gb/s and Beyond," Proc. Optical Fiber Commun./National Fiber Optic Engineers Conf. (OFC/NFOEC '08) (San Diego, CA, 2008), paper OMI2.

[95] B. J. C. Schmidt, A. J. Lowery, and J. Armstrong, "Experimental Demonstrations of Electronic Dispersion Compensation for Long-Haul Transmission Using Direct-Detection Optical OFDM," J. Lightwave Technol., 26:1 (2008), 196–203.

[96] D. F. Hewitt, “Orthogonal Frequency Division Multiplexing using Baseband Optical Single Sideband for Simpler Adaptive Dispersion Compensation,” in Optical Fiber Communication Conference and Exposition and The National Fiber Optic Engineers Conference, OSA Technical Digest Series (CD) (Optical Society of America, 2007), paper OME7.

[97] W. Peng, X. Wu, V.R. Arbab, B. Shamee, J. Y. Yang, L. C. Christen, K. M. Feng, A. E. Willner, S. Chi, “Experimental Demonstration of 340 km SSMF Transmission Using a Virtual Single Sideband OFDM Signal that Employs Carrier Suppressed and Iterative Detection Techniques,” in Optical Fiber Communication Conference and Exposition and The National Fiber Optic Engineers Conference, OSA Technical Digest Series (CD) (Optical Society of America, 2008), paper OMU1.

[98] Lowery, A.J.; Liang Bangyuan Du; Armstrong, J., "Performance of Optical OFDM in Ultralong-Haul WDM Lightwave Systems," Lightwave Technology, Journal of , vol.25, no.1, pp.131-138, Jan. 2007

[99] B. J. C. Schmidt, A. J. Lowery and J. Armstrong, “Experimental demonstrations of 20 Gbit/s directdetection optical OFDM and 12 Gbit/s with a colorless transmitter”, in Tech. Digest of the Conference on Optical Fiber Communication, (Optical Society of America, 2007), Postdeadline Paper PDP18.

[100] W. R. Peng; X. Wu, V. R. Arbab, B. Shamee, L. C. Christen, J. Y. Yang; K. M. Feng, A. E. Willner, S. Chi, “Experimental Demonstration of a Coherently Modulated and Directly Detected Optical OFDM System Using an RF-Tone Insertion,” Optical Fiber communication Conference, 2008. OFC/NFOEC 2008, paper OMU2,

[101] W. Shieh, X. Yi, and Y. Tang, “Transmission experiment of multi-gigabit coherent optical OFDM systems over 1000 km SSMF fiber,” Electron. Lett., 43, 183-185, 2007.

[102] E. Yamada, A. Sano, H. Masuda, T. Kobayashi, E. Yoshida, Y. Miyamoto, Y. Hibino, K. Ishihara, Y. Takatori, K. Okada, K. Hagimoto, T. Yamada, and H. Yamazaki, “Novel no-guardinterval PDM CO-OFDM transmission in 4.1 Tb/s (50 88.8-Gb/s) DWDM link over 800 km SMF including 50-GHz spaced ROADM nodes” Opt. Fiber Commun. Conf., paper PDP8, San Diego, CA, USA, 2008.

[103] Lei Xu; Junqiang Hu; Dayou Qian; Ting Wang, "Coherent Optical OFDM Systems Using Self Optical Carrier Extraction," Optical Fiber communication/National Fiber Optic Engineers Conference, 2008. OFC/NFOEC 2008. Conference on , vol., no., pp.1-3, 24-28 Feb. 2008

[104] A. D. Ellis and F. C. Garcia Gunning, “Spectral density enhancement using coherent WDM,” IEEE Photon. Technol. Lett., vol. 17, no. 2, pp. 504–506, Feb. 2005.

[105] W. Shieh, H. Bao, and Y. Tang, "Coherent optical OFDM: theory and design," Opt. Express 16, 841-859 (2008).

[106] W. Shieh, “PMD-supported coherent optical OFDM systems,” IEEE Photon.Technol. Lett. 19, 134-136 (2007).

[107] K. Roberts, “Electronic dispersion compensation beyond 10 Gb/s,” in *Technical Digest of IEEE LEOS Summer Topical Meeting*, Paper MA2.3, Portland Oregon, USA, 2007.

[108] J. Sitch, “Implementation aspects of high-speed DSP for transmitter and receiver signal processing,” in *Technical Digest of IEEE LEOS Summer Topical Meeting*, paper MA4.3, Portland Oregon, USA, 2007.

[109] Q. Yang, S. Chen, Y. Ma, and W. Shieh, "Real-time reception of multi-gigabit coherent optical OFDM signals," *OSA Opt. Express*, vol. 17, no. 10, pp. 7985-7992, 2009.

[110] R. W. Chang, "Synthesis of band-limited orthogonal signals for multichannel data transmission," Bell Systems Technical Journal, vol. 46, pp. 1775–1796, December 1966.

[111] M. Zimmermann and A. Kirsch, "The AN/GSC-10/KATHRYN/variable rate data modem for HF radio," IEEE Transactions on Communication Technology, vol. CCM–15, pp. 197–205, April 1967.

[112] S. B. Weinstein and P. M. Ebert, "Data transmission by frequency division multiplexing using the discrete Fourier transform," IEEE Transactions on Communication Technology, vol. COM–19, pp. 628–634, October 1971.

[113] F.Frederiksen and B. Prasad, "An overview of OFDM and related techniques towards development of future wireless multimedia communications," Radio and Wireless Conference, 2002, IEEE RAWCON 2002, USA, pp.19-22, 11-14, August, 2002.

[114] S. B. Weinsten and P. M. Ebert, "Data Transmission by Frquency-Division Multiplexing Using the Discrete Frouer Transform, " IEEE Trans. Commun., vol.19, pp. 628-634, 1971.

[115] R. Ramaswami and K. N. Sivarajan, Optical Networks - A Practical Perspective, Morgan Kaufmann Publishers, 2nd edition, 2002.

[116] Govind P. Agrawal, Fiber-Optic Communication Systems, Third Edition, John Wiley & Sons, Inc., New York, 3rd edition, 2002.

[117] L. Hanzo, M. Munster, B. J. Choi, and T. Keller, OFDM and MC-CDMA for Broadband Multi-User Communications, WLANs and Broadcasting, Wiley, New York, 2003.

[118] S.L Jansen ; I. Morita; T.C.W. Schenk; D. van den Borne; H. Tanaka, "Optical OFDM - A Candidate for Future Long-Haul Optical Transmission Systems," Optical Fiber communication/National Fiber Optic Engineers Conference, 2008. pp.1-3, 2008.

[119] X. Yi, W. Shieh, and Y. Ma, "Phase Noise on Coherent Optical OFDM Systems with 16-QAM and 64-QAM beyond 10 Gb/s," European Conference on Optical Communications, paper 5.2.3, Berlin, Germany (2007).

[120] H. Takahashi, A. A. Amin, S. L. Jansen, I. Morita and H. Tanaka, "8x66.8-Gbit/s Coherent PDM-OFDM Transmission over 640 km of SSMF at 5.6-bit/s/Hz Spectral Efficiency," European Conference on Optical Communications, paper Th.3.E.4, Brussels, Belgium, 2008.

[121] N. Gisin, and B. Huttner, "Combined effects of polarization mode dispersion and polarization dependent losses in optical fibers," Opt. Commun. 142, 119-125 (1997).

[122] T. M. Schmidl and D. C. Cox, "Robust frequency and timing synchronization for OFDM," IEEE Trans. Commun. 45, 1613–1621 (1997).

[123] W. Shieh, X. Yi, Y. Ma and Q. Yang, 'Coherent optical OFDM: has its time come? [Invited]' Journal of Optical Networking, Vol. 7, pp. 234-255, 2008.

[124] S Hara, M Mouri, M Okada, and N Morinaga, "Transmission performance analysis of multi-carrier modulation in frequency selective fast Rayleigh fading channel," Wireless Personal Commun.**, 2**, 335-356 (1996).

[125] X. Yi, W. Shieh, and Y. Tang, "Phase Estimation for Coherent Optical OFDM,"

IEEE Photon. Technol. Lett., vol. 19, pp. 919 – 921, 2007.

[126] W. Shieh, “Maximum-Likelihood Phase and Channel Estimation for Coherent Optical OFDM,”IEEE Photonics Technology Letters, vol. 20, pp. 605 – 607, 2008.

[127] Y. George and O. Amrani, “Bit loading algorithms for OFDM,” in ISIT 2004, Chicago, IL, 2004, p. 388.

[128] B. S. Krongold, K. Ramchandran, and D. L. Jones, “Computationally efficient optimal power allocation algorithms for multicarrier communication systems,” IEEE Trans. Commun., vol. 48, no. 1, pp. 23–27, Jan. 2000.

[129] Qi Yang; Shieh, W.; Yiran Ma, "Bit and Power Loading for Coherent Optical OFDM," Photonics Technology Letters, IEEE , vol.20, no.15, pp.1305-1307, Aug.1, 2008

[130] W. Shieh, Q. Yang, and Y. Ma, "107 Gb/s coherent optical OFDM transmission over 1000-km SSMF fiber using orthogonal band multiplexing," Opt. Express 16, 6378-6386 (2008).

[131] J. Proakis, M.Salehi, *Digital Communications*, 5th edition, McGraw-Hill International edition, 2008

[132] R. C. Alferness, “Titanium-diffused lithium niobatewaveguide devices,” in *Guided-Wave Optoelectronics*, 2 ed, T. Tamir, Ed. Berlin, Germany: Springer-Verlag, 1990, pp. 145–210.

[133] W. K. Burns, M. M. Howerton, R. P. Moeller, R. R. Krähenbühl, R. W. McElhanon, and A. S. Greenblatt, “Low drive voltage, broad-band LiNbO modulators with and without etched ridges,” *J. Lightw. Technol.*, vol. 17, no. 12, pp. 2551–2555, Dec. 1999.

[134] E. L. Wooten, K. M. Kissa, A. Yi-Yan, E. J. Murphy, D. A. Lafaw, P. F. Hallemeier, D. Maack, D. V. Attanasio, D. J. Fritz, G. J. McBrien, and D. E. Bossi, "A review of lithium niobate modulators for fiber-optic communications systems," *IEEE J. Sel. Topics Quantum Electron.*, vol. 6, no. 1, pp. 69–82, Jan.–Feb. 2000.

[135] R. G. Walker, "High-speed electrooptic modulation in GaAs/GaAlAs waveguide devices," J. Lightw. Technol., vol. LT-5, no. 10, pp. 1444–1453, Oct. 1987.

[136] F. J. Leonberger and J. P. Donnelly, "Semiconductor integrated optic devices," in Guided-Wave Optoelectronics, 2 ed, T. Tamir, Ed. Berlin, Germany: Springer-Verlag, 1990, pp. 317–396.

[137] Y. Shi, C. Zhang, H. Zhang, J. H. Bechtel, L. R. Dalton, B. H. Robinson, andW. H. Steier, "Low (sub-1-Volt) halfwave voltage polymeric electrooptic modulator achieved controlling chromophore shape," Science, vol. 288, pp. 119–122, 2000.

[138] A. Liu, R. Jones, L. Liao, D. Samara-Rubio, D. Rubin, O. Cohen, R. Nicolaescu, and M. Paniccia, "A high-speed silicon optical modulator based on a metal semiconductor capacitor," Nature, vol. 427, pp. 615–618, 2004.

[139] B. H .Kolner and D. W. Dolfi, 'Intermodulation distortion and compression in an integrated electrooptic modulator,' Appl. optics, 26, pp.3676.

[140] W. Feller, 'An introduction to probability theory and its apphcations, Vol. II' (I. WiIey & Sons, New York, 1971), 2nd edn.

[141] R. O'Neil and L. N. Lopes, "Envelope variations and spectral splatter in clipped multicarrier signals," Proc. Of IEEE 1995 International Symp. on Personal, Inddor and Mobile Radio Commun., 1995, pp. 71-75.

[142] X. Li and L. J. Cimini Jr., "Effects of clipping and filtering on the performance of OFDM," IEEE Communications Letters, vol. 2, pp. 131-133, 1998.

[143] J. Armstrong, "Peak-to-average power reduction for OFDM by repeated clipping and frequency domain filtering," Electronics Letters, vol. 38, pp. 246-247, 2002.

[144] D. J. G. Mestdagh and P. M. P. Spruyt, " A method to reduce the probability of clipping DMT-based transceivers," IEEE Transaction on Communications, vol. 44, pp. 1234-1238, 1996.

[145] R. W. Bauml, R. F. H. Fischer, and J. B. Huber, "Reducing the peak-to-average power ratio of multicarrier modulation by selected mapping," Electronic Letters, vol. 32, pp. 2056-2057, 1996.

[146] S. H. Muller and J. B. Huber, " A novel peak power reduction scheme for OFDM," in Proc. of IEEE 1997 International Symposium on Personal, Indoor and Mobile Radio Communications, pp. 1090-1094, 1997.

[147] M. Friese, "OFDM signals with low crest-factor," in Proceeding of 1997 IEEE Global Telecommunications conference, pp. 290-294, 1997.

[148] J. Tellado and J. M. Cioffi, "Peak power reduction for multicarrier transmission," in Proc. of 1998 IEEE Global Telecommun. Conf., pp. 219-224, 1998.

[149] B. S. Krongold and D. L. Jones, "PAR reduction in OFDM via active constellation extension," IEEE Transactions on Broadcasting, vol. 49, pp. 258-268, 2003.

[150] R.Van Nee, A. De Wild, 'Reducing the Peak-To-Average Power Ratio of OFDM,' VTC 98. 4fh IEEE, Vol. 3, pp. 2072-2076, May 1998.

[151] Hideki Ochiai, Hideki Imai, 'Performance Analysis of Deliberately Clipped OFDM Signals,' IEEE Trans. On Comm., Vo1.50, No. 1, Jan 2002.

[152] D. J. G. Mestdagh, P. M. P. Spruyt, and B. Biran, 'Effect of amplitude clipping in DMT-ADSL transceivers,' Electron. Lett., vol. 29, pp. 1354 – 1355, 1993.

[153] D. J. G Mestdagh, P. M. P. Spruyt, and B. Biran, “Effect of amplitude clipping in DMT-ADSL transceivers,” Electronics Letters, vol. 29, pp. 1354 – 1355, 1993.

[154] J. Proakis, Digital Communications, WCB/McGraw-Hill, Boston, 1995

[155] L. G. Kazovsky, S. Benedetto, and A. E. Willner, Optical Fiber Communication Systems (Artech House, 1996).

[156] T. Okoshi and K. Kikuchi, Coherent Optical Fiber Communications (Springer, 1988).

[157] L. Kazovsky, “Multichannel coherent optical communications systems,” J. Lightwave Technol. 5, 1095–1102 (1987).

[158] T. Okoshi, “Heterodyne and coherent optical fiber communications: recent progress,” IEEE Trans. Microwave Theory Tech. 82, 1138–1149 (1982).

[159] J. M. Kahn, I. M. I. Habbab, and C. R. Giles, “1 Gbit/s zero-IF DPSK coherent optical system using a single photodetector,” Electron. Lett. 24, 1455–1457 (1988).

[160] N. A. Olsson, “Lightwave systems with optical amplifiers,” J. Lightwave Technol., vol. 7, no. 7, pp. 1071–1082, July 1989.

[161] Douglas M. Baney, Philippe Gallion, and Rodney S. Tucker, “Theory and measurement techniques for the noise figure of optical amplifiers,” Optical Fiber Technology, 6, pp. 122–154, 2000.

[162] Dennis Derickson, Ed., Fiber Optic Test and Measurement, Prentice Hall PTR, Upper Saddle River, New Jersey 07458, 1998.

[163] J. McDonough, "Moving standards to 100 GbE and beyond," IEEE Applications and Practice, pp. 6-9, 2007.

[164] S. Chandrasekhar, L. Xiang, D. Kilper, C. R. Doerr, A. H. Gnauck, E. C. Burrows, and L. L. Buhl, "Terabit Transmission at 42.7-Gb/s on 50-GHz Grid Using Hybrid RZ-DQPSK and NRZ-DBPSK Formats Over 16 × 80 km SSMF Spans and 4 Bandwidth-Managed ROADMs," Lightwave Technology, Journal of, vol. 26, pp. 85-90, 2008.

[165] M. Nakazawa, T. Yamamoto, and K. R. Tamura, "1.28 Tbit/s-70 km OTDM transmission using third- and fourth-order simultaneous dispersion compensation with a phase modulator," Electronics Letters, vol. 36, pp. 2027-2029, 2000.

[166] H. G. Weber, S. Ferber, M. Kroh, C. Schmidt-Langhorst, R. Ludwig, V. Marembert, C. Boerner, F. Futami, S. Watanabe, and C. Schubert, "Single channel 1.28 Tbit/s and 2.56 Tbit/s DQPSK transmission," Electronics Letters, vol. 42, pp. 178-179, 2006.

[167] I. B. Djordjevic, “PMD compensation in fiber-optic communication systems with direct detection using LDPC-coded OFDM,” Opt. Express, vol. 15, pp. 3692-3701, 2007.

[168] T. Kobayash, A. Sano, E. Yamada, “Electro-optically subcarrier multiplexed 110 Gb/s OFDM signal transmission over 80 km SMF without dispersion compensation,” Electron. Lett., vol. 44, pp. 225-226, 2008.

[169] Y. Tang; W. Shieh,; X. Yi; R Evans., "Optimum Design for RF-to-Optical Up-Converter in Coherent Optical OFDM Systems," Photonics Technology Letters, IEEE , vol.19, no.7, pp.483-485, April1, 2007

[170] Djordjevic, I., and Vasic, B.: ‘100-Gbit/s transmission using orthogonal frequency-division multiplexing’, IEEE Photonics Technol. Lett., 2006, 18, pp. 1576–1578.

[171] Bergano, N.S., "Wavelength division multiplexing in long-haul transoceanic transmission systems," Lightwave Technology, Journal of , vol.23, no.12, pp. 4125 4139, Dec. 2005

[172] R.J. Essiambre, P.J. Winzer, and X. Wang, “Electronic predistortion and fiber nonlinearity,” Photon. Technol. Lett. vol.17, pp. 1804 – 1806, 2006.

[173] K. Forozesh, S. L. Jansen, S. Randel, “The influence of the dispersion map in coherent optical OFDM transmission systems,” LEOS Summer Topical Meeting’2008, paper WC2.4.

[174] M. Duelk, “Next generation 100 Gb/s Ethernet,” presented at the ECOC, 2005, Tu3.1.2.

[175] W. Shieh, Q. Yang, and Y. Ma, “107 Gb/s coherent optical OFDM transmission over 1000-km SSMF fiber using orthogonal band multiplexing,” Opt. Exp., vol. 16, pp. 6378–6386, 2008.

[176] H. Sun, K.-T. Wu, and K. Roberts, "Real-time measurements of a 40 Gb/s coherent system," Opt. Express, vol. 16, pp. 873-879, 2008.

[177] I. B. Djordjevic and B. Vasic, "100 Gb/s transmission using orthogonal frequency-division multiplexing," Photon. Technol. Lett, vol. 18, pp. 1576-1578, 2006.

[178] A. D. Ellis and F. C. G. Gunning, “Spectral density enhancement using coherent WDM,” IEEE Photon. Technol. Lett., vol. 17, pp. 504–506, 2005.

[179] A. Sano, E. Yoshida, H. Masuda, T. Kobayashi, E. Yamada, Y. Miyamoto, F. Inuzuka, Y. Hibino, Y. Takatori, K. Hagimoto, T. Yamada, and Y. Sakamaki, “30 □ 100-Gb/s all-optical OFDM transmission over 1300 km SMF with 10 ROADM

nodes," presented at the Eur. Conf. Opt. Commun., Berlin, Germany, 2007, Paper PD 1.7

[180] T. Kobayashi, A. Sano, E. Yamada, Y. Miyamoto, H. Takara, and A. Takada, "Electro-optically subcarrier multiplexed 110 Gb/s OFDM signal transmission over 80 km SMF without dispersion compensation," Electron. Lett., vol. 44, pp. 225–226, 2008.

[181] S. L. Jansen, I. Morita, N. Takeda, and H. Tanaka, "20-Gb/s OFDM transmission over 4,160-km SSMF enabled by RF-Pilot tone phase noise compensation," presented at the Optical Fiber Commun. Conf., Anaheim, CA, 2007, Paper PDP15

[182] B. R. Washburn, S. A. Diddams, N. R. Newbury, J. W. Nicholson, M. F. Yan, and C. G. Jorgensen, "Phaselocked, erbium-fiber-laser-based frequency comb in the near infrared," Opt. Lett., vol. 29, pp. 250–252, 2004.

[183] M.J. Li, "Recent progress in fiber dispersion compensators," in ECOC' 2001, pp. 486 – 489, 2001

[184] W. Shieh, "Coherent optical MIMO-OFDM for optical fibre communication systems," in Proc. Workshop 5, Eur. Conf. Opt. Commun., Berlin, Germany, 2007.

[185] S. L. Jansen, I. Morita, and H. Tanaka, "16×52.5-Gb/s, 50-GHz spaced, POLMUX-CO-OFDM transmission over 4,160 km of SSMF enabled by MIMO processing KDDI R&D Laboratories," presented at the Eur. Conf. Opt. Commun., Berlin, Germany, 2007, Paper PD1.3.

[186] A. Lowery, "Fiber nonlinearity pre- and post-compensation for long-haul optical links using OFDM," Opt. Express 15, 12965-12970, 2007.

[187] M. Nazarathy, J. Khurgin, and R. Weidenfeld, “Phased-array cancellation of nonlinear FWM in coherent OFDM dispersive multi-span links,” Opt. Express, Vol. 16, pp. 15777-15810, 2008.

[188] G. Hart and Z. Mansourati,“The Dynamic Network: Managing Bandwidth and Content on Demand at the Optical Level”, , SCTE Conference on Emerging Technologies, 2004.

[189] Keyworth, B.P., "ROADM subsystems and technologies," Optical Fiber Communication Conference, 2005. Technical Digest. OFC/NFOEC , vol.3, no., pp. 4 pp. Vol. 3-, 6-11 March 2005

[190] B. Pratt, “Strategies for Metro/Regional Optical Networks”, CEF Conference, Prague, 2005.

[191] L. Xiang, "Can 40-gb/s duobinary signals be carried over transparent DWDM systems with 50-GHz channel spacing?," Photonics Technology Letters, IEEE, vol. 17, pp. 1328-1330, 2005.

[192] B. B. Dingel and T. Aruga, "Properties of a novel noncascaded type, easy-to-design, ripple-free optical bandpass filter," Lightwave Technology, Journal of, vol. 17, pp. 1461-1469, 1999.

[193] C. H. Doan, S. Emami, and A. M. Niknejad, "Millimeter-wave CMOS design," J.Solid-state Circuits, vol. 40, pp. 144-155, 2005

[194] A. Sano, E. Yoshida, H. Masuda, T. Kobayashi, E. Yamada, Y. Miyamoto, F. Inuzuka, Y. Hibino, Y. Takatori, K. Hagimoto, T. Yamada, and Y. Sakamaki, "30 x 100-Gb/s all-optical OFDM transmission over 1300 km SMF with 10 ROADM nodes," European Conference on Optical Communications, 2007

Appendix A

Acronyms

ADC	Analog-to-Digital Converters
ADSL	Asynchronous Digital Subscriber Line
AP	Alternative Polarization
ASE	Amplified Spontaneous Emission
AWG	Arbitrary Waveform Generator
BER	Bit Error Ratio
BPSK	Binary Phase-Shift Keying
BS	Beam Splitter
CD	Chromatic Dispersion
CDF	Cumulative Density Function
CMA	Constant Modulus Algorithm
CMOS	Complementary Metal Oxide Semiconductor
CO-FODM	Coherent Optical OFDM
CP	Cyclic Prefix
CPE	Common Phase error
CR	Compensation Ratio
CW	Continuous Wave
DAC	Digital-to-Analog Converter
DC	Direct Current
DCF	Dispersion Compensation Fiber
DDO-OFDM	Direct-Detection Optical OFDM
DEMUX	De-multiplexer
DFE	Decision Feedback Equalizer
DFT	Discrete Fourier Transform
DGD	DGD Differential Group Delay
DPC	Digital Phase Conjugation
DPSK	Differential Phase-Shift Keying
DQPSK	Differential Quadrature Phase-Shift Keying
DSCD	Digital Self-Coherent Detection
DSP	Digital Signal Processing

DUDC	Direct up/down Conversion
DWDM	dense wavelength division multiplexed
EDC	Electronic Dispersion Compensation
EDFA	Erbium Doped Fiber Amplifier
E/O	Electro-Optic
EPEC	Electronic Pre-Compensation
EPOC	Electronic Post-Compensation
EVM	Error Vector Magnitude
FBG	Fiber Bragg grating
FDM	Frequency-division multiplexing
FEC	Forward Error Correction
FFE	Feed-Forward Equalizer
FFT	Fast Fourier Transform
FIR	Finite Impulse Response
GDR	Group Delay Response
GI	Guard Interval
GTR	Gires–Tournois resonator
I	In-phase
IC	Integrated Circuit
ICI	Inter-Carrier Interference
IDFT	Inverse Discrete Fourier Transform
IF	Intermediate frequency
IFFT	Inverse Fast Fourier Transform
IM	Intensity Modulators
IMD	Inter-Modulation Distortion
IM/DD	Intensity Modulation/ Direct Detection
IMOD	Intensity Modulator
IP	Internet Protocol
IPN	Nth Order Intercept point
I/Q	In-phase/Quadrature
ISI	Inter-Symbol Interference
ITU	International Telecommunication Union
Km	Kilometer
LAN	Local Area Networks
LiNbO3	Lithium-Niobate

LO	Local Oscillator
LPF	Low Pass Filter
MCM	Multiple-Carrier Techniques Modulation
MEMS	Microelectro-mechanical Systems
MIMO	Multiple Input Multiple Output
MOD	Modulator
MUX	Multiplexer
MZM	Mach–Zehnder Modulator
No-GI	No-Guard Interval
OA	Optical amplifier
OBM-OFDM	Orthogonal-band-multiplexed OFDM
OBPF	Optical Band Pass Filters
ODI	Optical Delay Interformeters
O/E	Optical-Electrical
OFDM	Orthogonal Frequency-Division Multiplexing
O-OFDM	Optical OFDM
OOK	On-Off Keying
OPLL	Optical Phase Locked Loop
OSNR	Optical Signal NoiseRatio
OSW	Optical Switches
OTDM	Optical Time Division Multiplexing
OTR	Optical to RF
PA	Power Amplifier
PAPR	Peak to Average Power Ratio
PBC	Polarization Beam Combiner
PBS	Polarization Splitter
PDF	Probability Density Function
PDL	Polarization-Dependent loss
PIC	Photonic Integration circuits
PMD	Polarization Mode Dispersion
PRBS	Pseudo-Random Binary Sequence
PSK	Phase Shift Keying
Q	Quadrature
QAM	Quadrature Amplitude Modulation
QPSK	Quadrature Phase-Shift Keying

RF	Radio Frequency
RIN	Relative Intensity Noise
RMS	Root-Mean-Square
ROADM	Reconfigurable Optical Add-Drop Multiplexer
RTO	RF-to-Optical
RZ	Return-to-Zero
SCNR	Signal-to-Clipping Noise Ratio
SISO	Single Input Single Output
SMF	Single Mode Fiber
SNR	Signal to Noise Ratio
SOP	State of Polarization
SP	Same Polarization
SQNR	Signal-to-Quantization Noise
SSB	Single Side Band Se Ratio
SSMF	Standard Single Mode Fiber
TDM	Time Division Multiplexing
TDS	Time Domain-Sampling Scope
TISO	Two Input Single Output
TITO	Two Input two Output
TX	Transmitter
WAN	wide area networks
WB	Wavelength Blocker
WDM	Wavelength-Division Multiplexing
WiMAX	Worldwide interoperability for Microwave Access
WLAN	Wireless Local Area Networks
WSS	Wavelength Selective Switch
WWAN	Wireless Wide Area Networks
XCOFDM	Cross-channel OFDM